Design of Experiments for Nonlinear System Identification

Doctoral Dissertation
Doctoral Program in Computer and Control Engineering (31st cycle)

Design of Experiments for Nonlinear System Identification

Applications of Set Membership Identification for Experiment Design and Fault Detection

Milad Karimshoushtari

* * * * * *

Supervisor

Prof. Carlo Novara

Politecnico di Torino
April 30, 2019

I hereby declare that the contents and organization of this dissertation constitute my own original work and does not compromise in any way the rights of third parties, including those relating to the security of personal data.

. . . . . .

Milad Karimshoushtari

Turin, April 30, 2019

Summary

The topic of this thesis is applications of set membership identification to Design of Experiments (DoE) and fault detection. DoE is a fundamental step in system identification. Regardless of the chosen model structure and identification method, the quality of the DoE determines an upper bound on the accuracy of the identified model. One of the greatest challenges in this context is to design an experiment which gives the maximum information about the dynamics of the system of interest.

The first main contribution of this thesis is a novel DoE algorithm for input-constrained MISO nonlinear systems. A key element to design a proper DoE algorithm is understanding which are the regions of the regressor space where the model is most uncertain. Set membership identification allows us to properly quantify the uncertainty of the identified model in a deterministic manner. Therefore, we formulated the DoE problem in a set membership framework and proposed a quasi-local nonlinear set membership approach that results in less conservative uncertainty bounds compared to the global approach. However, knowing where the model is most uncertain is not sufficient. Since the unknown system is dynamic, the DoE algorithm has to be able to generate an input sequence such that the system moves toward those uncertain regions of the regressor space, in order to take new measurements. For this reason, we propose a novel adaptive Set Membership Predictive Control (SMPC) algorithm to move the system toward the most uncertain regions of the regressor space and take new informative measurements. Finally, a Set Membership DoE (SM-DoE) algorithm for input-constrained MISO nonlinear dynamic systems is proposed which is aimed to minimize the so-called radius of information, a quantity giving the worst-case model error. The proposed SM-DoE algorithm is able to guarantee any desired worst-case error larger than the measurement error in a finite-time experiment. Applications of the proposed method are clearly most useful in areas where experiments are expensive and/or a very accurate model is desired. Two numerical examples and a case study in the automotive field are also presented, showing the effectiveness of the approach and its potential in view of real-world applications.

The second main contribution of this thesis is an innovative approach to fault detection for nonlinear dynamic systems, based on the introduced quasi-local set membership identification method, overcoming some relevant issues proper of the "classical" techniques. The approach is based on the direct identification from experimental data of a suitable filter and related uncertainty bounds. These bounds are used to detect when a change (e.g., a fault) has occurred in the dynamics of the system of interest. The main advantage of the approach compared to the existing methods is that it avoids the utilization of complex modeling and filter design procedures since the filter/observer is directly designed from data. Other advantages are that the approach does not require to choose any threshold (as typically done in many "classical" techniques) and it is not affected by under-modeling problems.

Acknowledgements

I would like to thank my supervisor, Prof. Carlo Novara, for the patient guidance, encouragement and advice he has provided throughout my time as his student.

I would like to thank my parents, my brother and my friends. They were always supporting me and encouraging me with their best wishes.

Contents

List of Tables

List of Figures

Chapter 1

Introduction

In many technological areas, obtaining an accurate model of a dynamic system of interest is a fundamental step for any system analysis and/or design operation. However, building an accurate model using the physical laws governing the system may not be possible in several situations, due to the fact that these laws are not sufficiently well known or they are too complex, requiring a computationally expensive model that may be difficult to analyze or to use for design purposes. In this view, data-driven system identification approaches can be crucial in a wide range of applications.

Data-driven system identification can be seen as the science of building mathematical models of dynamic systems, using data and a "weak" prior physical knowledge. For example, the physical laws governing the system of interest may be not known but some less detailed information may be available, regarding its block structure, the type of involved dynamics, the type of involved nonlinearities, the system order, etc. Typically, the identification process consists of the following main steps (not necessarily in the order reported here): 1) design of experiment (DoE); 2) selection of a suitable parametrized model structure; 3) identification of the model parameters (usually done through an optimization problem); 4) evaluation of the model quality through some validation analysis. In this process, the command input signal is the only means that can be used in the DoE phase to influence the information content of a dataset to be used for identification (this set is called identification dataset or training dataset). Regardless of the chosen model structure and identification method, the quality of the DoE determines the accuracy that can be achieved by any identified method.

The first topic that is addressed in this thesis is designing a DoE algorithm for nonlinear dynamic systems. One of the greatest challenges in this context is to design an experiment giving the maximum information about the system to be identified [22, 36]. Most of the studies carried out so far have mainly focused on linear systems [25, 77, 68, 17, 66] and static systems [14, 64, 28]. On the other side, very few studies regarding nonlinear dynamic systems are available [47, 10, 21, 23]. In fact, nonlinear systems are characterized by a significantly higher complexity than linear systems. While for linear systems the excitation properties of an input signal essentially depend on the signal frequencies, for nonlinear systems they also depend on the signal amplitudes [47]. For example, a white noise input signal is known in general to be appropriate for the identification of a linear system of any order. On the other side, it may not be suitable to allow an accurate exploration of the regressor domain of a nonlinear system, and this may lead to a low model accuracy.

Currently, the most popular DoE methods for nonlinear dynamic systems are classified in two main categories: model-free and model-based methods [10, 76, 9, 24]. The idea of these methods is to parameterize a pre-defined excitation signal, and then optimize the signal parameters, called the design points, according to different criteria. In model-free DoE, no assumptions on the model and/or input structure are made. The typical approach is to distribute the design points in the input domain as much uniformly as possible. This DoE approach is also known as space-filling DoE. In model-based DoE, after assuming a particular model structure, the idea is to distribute the design points in the input domain, in such a way that the estimation of the model parameters is as much insensitive as possible to the measurement noise. In both model-free and model-based DoE, after designing the distribution of the design points in the input space, they are used as the parameter values of the pre-defined excitation signal. However, both methods provide no information about the optimal sequence of the design points. Although these methods are simple and adequate to capture the steady state behavior of a system of interest, they don't take into account the dynamics of the system. Therefore, by using these methods, capturing the nonlinear dynamic behavior of the system in the whole regressor domain is a heuristic/arbitrary process. In general, as far as the authors are aware, no DoE method for nonlinear dynamic systems can be found in the literature, which can ensure the exploration of the relevant regressor domain of a nonlinear system and, consequently, guarantee a desired model accuracy.

Due to the presence of disturbances and measurement noise, in general, no

identification process can result in a model that perfectly corresponds to the true system. Any identified model is always affected by some uncertainty. Understanding which are the regions of the regressor space where the model is most uncertain is a key element to design a proper DoE algorithm. However, knowing where the model is most uncertain is not sufficient. Since the unknown system is dynamic, the DoE algorithm has to be able to generate an input sequence such that the system moves toward those uncertain regions of the regressor space, in order to take new measurements.

The second topic that is addressed in this thesis is fault detection for nonlinear dynamic systems. A "classical" approach to fault detection is to identify a model of the system and to design a filter/observer on the basis of the identified model. The designed filter/observer is then used to generate online a suitable residual signal. The fault is detected when the residual exceeds a given threshold, see e.g. [78, 53, 20, 55, 29, 15, 35, 63, 8, 54]. However, the design of the filter/observer may be hard in the presence of nonlinear and/or uncertain dynamics. Indeed, designing an optimal filter from a nonlinear model is in general not possible, and approximate filters only, such as the extended Kalman filters, can be actually obtained. These kinds of filters may often be inaccurate and not even guarantee the estimation error stability. Moreover, the choice of the threshold may be critical, especially when poor prior information on the system is available. Another relevant issue is that, in real-world applications, the system is unknown and only approximate models can be identified from finite data; evaluating the effects of the modeling error on the estimation error of the filter designed from the approximated model is a largely open problem.

In the last three decades, there has been an increasing interest and research, formulating the identification problem in Set Membership (SM) framework [39, 67, 44, 43, 42, 49, 52, 41, 7]. The main reason is the fact that SM identification allows us to properly quantify the uncertainty of the identified model in a deterministic manner. In SM nonlinear identification, no assumptions on the structure of the unknown system are required. Instead, two basic assumptions are made. An assumption on the regularity of the system, given by bounds on its gradient, and another assumption on the noise boundedness. Then, an optimal estimate, with minimal guaranteed identification error and tight uncertainty bounds, is derived. This nonlinear SM approach does not require any iterative minimization and thus avoids the issue of local minima. Since no optimization problems have to

be solved, nonlinear SM identification is particularly suitable for adaptive identification, making the model more accurate over time by adding new measurements collected online. Because of these features, the applications of SM in robust control, experiment design, and fault detection is a promising research area [67].

1.1 Outline and Contribution

In this thesis, a novel online DoE algorithm for nonlinear dynamic MISO systems is proposed, that is able to reduce the worst-case model error while considering input constraints of the system. The proposed DoE algorithm is able to guarantee any desired worst-case error larger than the measurement error in a finite time experiment. The main contributions are the following. First, a so-called quasi-local nonlinear SM identification method is presented, that is characterized by less conservative bounds with respect to the global version of [39] and is simpler with respect to the local version of [39]. The second contribution is a novel adaptive Set Membership Predictive Control (SMPC) algorithm, that is able to drive the system toward the most uncertain regions of the regressor space. And finally, the third contribution is the online DoE algorithm itself. The effectiveness of the proposed DoE algorithm is illustrated in two simulation examples and compared to other DoE methods taken from the literature.

The increasing demand for higher torque, reduced fuel consumption, and emissions has led to more complex engine and after-treatment system designs with more actuators and sensors which are more difficult to model, calibrate and control. Considering the expensive operating costs of the engine/after-treatment test benches, and increasing demand for accurate dynamic models, DoE plays a critical role in automotive applications. In this thesis, a simulation case study regarding Lean NO_x Trap (LNT) has been performed and a novel approach for regeneration timing control of LNTs is proposed. This approach, named data-driven model predictive control, does not require a physical model of the engine/trap system but is based on a model, directly identified from data. In this way, all problems due to the fact that LNTs are highly complex systems difficult to model are overcome. However, acquiring the data necessary for identification is very challenging due to highly nonlinear dynamics of the after-treatment system. Therefore, we implemented the proposed Set Membership Design of Experiments for the LNT which was able to capture nonlinear behavior of the system in a short experiment. The regeneration timing is

then computed through an optimization algorithm, which uses the identified model to estimate and predict the LNT behavior.

Regarding the second topic of this thesis, an innovative approach to fault detection for nonlinear dynamic systems is proposed, based on the introduced quasi-local set membership identification method, overcoming some relevant issues proper of the "classical" techniques. The approach is based on the direct identification from experimental data of a suitable filter and related uncertainty bounds. These bounds are used to detect when a change (e.g., a fault) has occurred in the dynamics of the system of interest. The main advantage of the approach compared to the existing methods is that it avoids the utilization of complex modeling and filter design procedures since the filter/observer is directly designed from data. Other advantages are that the approach does not require to choose any threshold (as typically done in many "classical" techniques) and it is not affected by under-modeling problems. The set membership fault detection approach can also be made adaptive which is very useful in systems where the dynamics change over time.

This thesis is organized as follows. In Chapter 2 the identification problem is formulated in the nonlinear SM framework and the quasi-local approach is introduced. In Chapter 3, a static DoE algorithm and a SM predictive controller are proposed, which are then used in the dynamic SM-DoE algorithm. Then, the proposed SM-DoE algorithm is tested in two simulation examples. In Chapter 4, a simulation case study has been performed regarding regeneration timing control of the LNT using the proposed SM-DoE algorithm to identify a model of the LNT. Finally, in Chapter 5, following the set membership philosophy, an innovative approach to fault detection for nonlinear dynamic systems is proposed and an experimental study regarding fault detection for a drone actuator is presented to demonstrate the effectiveness of the proposed approach.

Chapter 2

Nonlinear Set Membership Identification

2.1 Introduction

The aim of system identification is to build accurate mathematical model of a dynamic system where the knowledge of the laws governing the system is too complex or not sufficiently known. The usual approach is to consider that the dynamic system belongs to a finitely parameterized set of functions called basis functions. Then, estimate the parameters of the functions using measured data. Proper choice of the parametric family of the functions, which is typically realized by some search on different functional forms (linear, polynomial, sigmoid, wavelet, etc.), may be quite time consuming and the effects of such approximations on identification errors appear at present to be a largely open problem. Another critical point is that the estimate of the parameters is usually obtained by a prediction error method which requires minimization of an error function. This optimization problem is convex with respect to the parameters only if the basis functions are not dependent on tuneable parameters i.e. fixed basis functions. However, it is well known that the fixed basis functions suffer from the "course of dimensionality". In other words, the number of basis functions required for obtaining an approximation increases exponentially with the dimension of the regressor space. On the other side, tuneable basis functions such as neural networks or wavelets, have much powerful approximation properties, requiring only polynomial growth [2, 26]. However, such basis functions are not convex with respect to the parameters, giving rise to

possible deteriorations in approximation, due to trapping in local minima during its minimizations. Other problems also arise in giving a measure of identification error. Under the standard assumption that the noise affecting the measurements is a stochastic process, the measure of the quality of the identification, or in other words, the uncertainty of the identified model is probabilistic.

In order to overcome such problems, In the last three decades, there has been an increasing interest and research formulating the identification problem in Set Membership (SM) framework [39, 67, 44, 43, 42, 49, 52, 41, 7]. The main reason is the fact that SM identification allows us to properly quantify the uncertainty of the identified model in a deterministic manner. In SM nonlinear identification, no assumptions on the structure of the unknown system are required. Instead, two basic assumptions are made. An assumption on the regularity of the system, given by bounds on its gradient, and another assumption on the noise boundedness. Then, an optimal estimate, with minimal guaranteed identification error and tight uncertainty bounds, is derived. which is a bounded identification uncertainty description given by the set of all possible models that are all equally probable. This nonlinear SM approach does not require any iterative minimization and thus avoids the issue of local minima. Since no optimization problems have to be solved, nonlinear SM identification is particularly suitable for adaptive identification, making the model more accurate over time by adding new measurements collected online. Because of these features, the applications of SM in robust control and experiment design is a promising research area [67].

Even though nonlinear set membership is a quite powerful method, in some situations a global constant bound on the gradient of the function is too conservative, resulting in high uncertainty bounds. Computation of uncertainty bounds and radius of information is discussed in detail in [38]. In this chapter a quasi-local Nonlinear Set Membership (NSM) identification method is presented. In this approach, instead of a global constant bound on the gradient of the function, a quasi-local bound is assumed. Therefore, the uncertainty bounds are less conservative. Also unlike the local NSM presented in [39], this quasi-local approach does not require a preliminary estimate of the function. In Chapter 3 this quasi-local approach is used to develop a DoE algorithm. Also in Chapter 5, it is used for set membership fault detection.

This chapter is organized as follows. In section 2.2, the identification problem is formulated in set membership framework, defining the type of assumptions considered, the optimality concept and guaranteed identification error. Section 2.3

and 2.4 are directly taken from [39, 49] and slightly modified for notation consistency and reported here for the ease of the reader. In section 2.5, the quasi-local nonlinear set membership approach is proposed. For estimation of set membership parameters, two algorithms are given in section 2.7. And finally, in section 2.8, an algorithm is presented for adaptive nonlinear set membership models.

2.2 Problem Formulation

Consider a nonlinear discrete-time dynamic system in regression form:

$$\begin{aligned} y^{t+1} &= f_o(w^t) \\ w^t &= [y^t \dots y^{t-n_y+1}\ u^t \dots u^{t-n_u+1}]. \end{aligned} \tag{2.1}$$

where $y^t \in \mathbb{R}$, $u^t \in \mathbb{R}^m$, $f_o : \mathbb{R}^n \to \mathbb{R}$, $n = n_y + mn_u$ and the superscript is used to indicate the time index $t \in \mathbb{Z}$. Suppose that the function f_o is unknown but a set of noise corrupted data called *measurement dataset* generated by the system (2.1) is available.

$$\mathcal{D} \doteq \left\{\widetilde{y}^{t+1}, \widetilde{w}^t\right\}_{t=1}^{T-1} \tag{2.2}$$

Then,

$$\widetilde{y}^{t+1} = f_o(\widetilde{w}^t) + d^t, t = 1, \dots, T. \tag{2.3}$$

where the term d^t accounts for the fact that y and w are not exactly known, due to possible disturbances and noises affecting the system.

The aim is to derive an estimate $\widehat{f}$ of f_o from the available measurements $\mathcal{D}$, using a suitable identification algorithm.

An identification algorithm can be seen as a sequence of operations, providing some estimate $\widehat{f}$ of the unknown function f_o from the available measurements $\mathcal{D}$. Clearly, the algorithm should be chosen to give a small (possibly minimal) identification error $e(\widehat{f}) = \|f_o - \widehat{f}\|_p$, where $\|\cdot\|_p$ is the functional L_p norm, defined as

$$\|f\|_p \equiv \|f(\cdot)\|_p \doteq \begin{cases} [\int_{\mathcal{W}} |f(w)|^p \, dw]^{1/p}, p \in [1, \infty) \\ \operatorname{ess\,sup}_{w \in \mathcal{W}} |f(w)|, p = \infty \end{cases} \tag{2.4}$$

being $\mathcal{W}$ a compact and connected set in $\mathbb{R}^n$.

This error is not known since, from the available data, it is only known that $f_o \in \tilde{\mathcal{F}}$, where $\tilde{\mathcal{F}}$ is the set of all functions that could have generated the data. If no assumptions are made on f_o, this set, even in the case of exact measurements, is unbounded. Whatever identification algorithm is chosen, no information on the identification error can be derived, unless some assumptions are made on the function f_o and the noise d. The typical approach in the literature is to assume

a finitely parameterized structure for f_o (linear, polynomial, neural network, etc.) and a statistical model for the noise, see [65]. In the set membership approach, different and somewhat weaker assumptions are taken, not requiring the choice of the parametric structure for f_o, but related to its regularity. Moreover, the noise sequence $\{d^t\}_{t=1}^T$ is only supposed to be bounded.

Assumption 1. The noise sequence $d = (d^1, d^2, ..., d^T)$ is unknown but bounded:

$$\|d\|_q \leqslant \mu, \tag{2.5}$$

where $\|\cdot\|_q$ is the vector ℓ_q norm. A general formulation is developed in the following, allowing us to deal with the most important cases (i.e. $q = 2, \infty$) in a unified framework. As well known, the ℓ_2 norm is related to the energy of the considered signal, while the ℓ_∞ norm to its amplitude. The choice of this norm can be carried out on the basis of the prior knowledge on the energy or amplitude of the involved noise (if available) or by means of a trial and error procedure.

Differently from [46], where f_o is assumed to be parametrized by a finite set of basis functions, a mild regularity assumption is made here on f_o, not requiring any knowledge on its parametric form. In particular, we assume that the function f_o is Lipschitz continuous on $\mathcal{W}$:

Assumption 2. The function f_o is Lipschitz continuous on $\mathcal{W}$.

$$f_o \in \mathcal{F}(\Gamma) \tag{2.6}$$

for some $\Gamma < \infty$, where

$$\mathcal{F}(\Gamma) \doteq \{f : |f(w) - f(\widehat{w})| \leqslant \Gamma \|w - \widehat{w}\|_2, \forall w, \widehat{w} \in \mathcal{W}\}.$$

In the following sections, the problem of deriving from the available data an approximation $\hat{f}$ of f_o and evaluating tight estimate bounds on f_o is considered. The approximation is required to be accurate on the whole domain $\mathcal{W}$. The accuracy is measured by means of the following approximation error:

$$e(\hat{f}) \doteq \|f_o - \hat{f}\|_p. \tag{2.7}$$

For a given estimate $\widehat{f}$, the related L_p error is given by (2.7). This error cannot

be exactly computed since f_o is not known. It is only known that $f_o \in FFS^T$, where FFS^T is called the *Feasible Function Set*, that is, the set of all possible functions consistent with the available prior information and measured data. The formal definition of FFS^T will be given in the next sections, for three relevant specific cases. This motivates the following definition of identification error, often indicated as worst-case or guaranteed error.

Definition 1. *Worst-case approximation error* of $\widehat{f}$:

$$EN(\widehat{f}) \doteq \sup_{f \in FFS^T} \|f - \widehat{f}\|_p. \qquad \square \tag{2.8}$$

An optimal approximation is defined as a function f_{op} which minimizes the worst-case approximation error.

Definition 2. An approximation f_{op} is *optimal* if

$$EN(f_{op}) = \inf_{\widehat{f}} EN(\widehat{f}) \doteq \mathcal{R}_{\mathcal{I}}.$$

The quantity $\mathcal{R}_{\mathcal{I}}$, called the *radius of information*, gives the minimum worst-case error that can be guaranteed by any estimate, based on the prior and experimental information available up to time T. In other words, $\mathcal{R}_{\mathcal{I}}$ is a measure of the uncertainty associated with the identification process, for the given dataset and prior information. A reduction/minimization of $\mathcal{R}_{\mathcal{I}}$ can be obtained by a suitable experiment design procedure, as shown in Chapter 3. $\square$

Finding optimal approximations may be hard or not convenient, and sub-optimal solutions can be looked for. In particular, approximations called interpolatory are often considered in the literature, see e.g. [71], [44].

Definition 3. An approximation f_I is *interpolatory* if

$$f_I \in FFS^T. \qquad \square$$

A fundamental property of an interpolatory approximation is that it guarantees a worst-case error degradation of at most 2, [71], [44]. An approximation with this property is called almost-optimal.

Definition 4. An approximation f_{ao} is *almost-optimal* if

$$EN\left(f_{ao}\right) \leqslant 2 \inf_{\widehat{f}} EN(\widehat{f}). \qquad \square$$

In this chapter, the following problem is considered.

Problem 1. From the dataset (2.2), find an approximation $\hat{f}$ of f_o
(i) optimal or almost-optimal;
(ii) equipped with tight interval estimates $\overline{f}, \underline{f}$ for f_o. □

Remark 1. In the set membership and approximation theory literature, two optimality concepts are typically considered: local and global optimality, [71, 39]. The worst-case error (2.8) is a local error since it depends also on the function f_o and the data $\mathcal{D}$, i.e. $EN(\widehat{f}) = EN(\widehat{f}, f_o, \mathcal{D})$. A global identification error is also often considered, defined as:

$$EN^g(\widehat{f}) \doteq \sup_{\substack{f_o \in \mathcal{F}(\Gamma) \\ \mathcal{D} \in \{d : \|d\|_q \leqslant \mu\}}} EN(\widehat{f}, f_o, \mathcal{D}).$$

An approximation f_g is called globally optimal if $EN^g(f_g) = \inf_{\widehat{f}} EN^g(\widehat{f})$. This is the optimality concept usually investigated in the set membership context and approximation theory literature, [71]. Note that a locally optimal algorithm f_{op} is globally optimal, but f_g is not in general locally optimal. Therefore, the local optimality concept investigated in this chapter is stronger and thus less conservative than the global optimality concept investigated in the above mentioned literature.

2.3 Global Approach

As mentioned earlier, a key role in set membership framework is played by the *Feasible Function Set*, the set of all functions consistent with prior information and measurement data.

Definition 5. The Feasible Function Set is

$$FFS^T \doteq \left\{ f \in \mathcal{F} : \|\widetilde{y} - f(\widetilde{w})\|_q \leqslant \mu \right\}. \tag{2.9}$$

where $\widetilde{y} = (\widetilde{y}^1, \ldots, \widetilde{y}^T)$ and $f(\widetilde{w}) \doteq (f(\widetilde{w}^1), \ldots, f(\widetilde{w}^T))$. □

The feasible function set FFS^T summarizes all the information on the mechanism generating the data that is available up to time T. If the prior assumptions hold, then $f_o \in FFS^T$, that is an important property for evaluating the accuracy of any estimate.

In the set membership framework, the validation of prior assumptions is a fundamental step. It is usual to introduce the concept of prior assumption validation as consistency with the available data: the prior assumptions are considered validated if at least one estimate consistent with these assumptions and the data exists, i.e. if FFS^T is not empty, see e.g. [44, 7].

Definition 6. Prior assumptions are validated if $FFS^T \neq \emptyset$ □

The following theorem gives a necessary and a sufficient condition for the validation of prior assumptions.

Let us define the following functions:

$$\begin{aligned} \overline{f}(w) &\doteq \min_{t=1,\ldots,T} (\overline{h}^t + \Gamma \|w - \widetilde{w}^t\|_2), \\ \underline{f}(w) &\doteq \max_{t=1,\ldots,T} (\underline{h}^t - \Gamma \|w - \widetilde{w}^t\|_2). \end{aligned} \tag{2.10}$$

where $\overline{h}^t \doteq \widetilde{y}^t + \varepsilon^t$ and $\underline{h}^t \doteq \widetilde{y}^t - \varepsilon^t$.

Necessary and sufficient conditions for checking the validity of the assumptions are now given.

Theorem 1. *(i) A necessary condition for prior assumptions to be validated is:* $\overline{f}(\widetilde{w}^t) \geqslant \underline{h}^t$, $\underline{f}(\widetilde{w}^t) \leqslant \overline{h}^t$, $t = 1, \ldots, T$.

(ii) A sufficient condition for prior assumptions to be validated is: $\overline{f}(\widetilde{w}^t) > \underline{h}^t$,$\underline{f}(\widetilde{w}^t) < \overline{h}^t$, $t = 1, \ldots, T$.

Proof. See [39]. □

Note that the fact that prior assumptions are validated, i.e., that they are consistent with the present data, does not exclude that they may be invalidated by future data. In the remainder of the chapter, it is assumed that the sufficient condition hold. If not, values of the constants appearing in the assumptions on function f_o and on the noise d^t have to be suitably modified. The above validation theorem can be used for assessing the values of such constants so that sufficient conditions holds.

Now let the function f_c be defined as:

$$f_c(w) \doteq \frac{1}{2}[\underline{f}(w) + \overline{f}(w)]. \tag{2.11}$$

where $\underline{f}(w)$ and $\overline{f}(w)$ are given in (2.10). The next result shows that the estimate f_c is optimal according to Definition 2 for any L_p norm.

Theorem 2. *Assume that:*
(i) The noise affecting the measurements $\mathcal{D}$ is bounded according to (2.5).
(ii) The function f_o is Lipschitz continuous according to (2.6).
Then, for $q = \infty$ and for any $p \in [1, \infty]$:
(i) The approximation f_c defined in (2.11) is optimal.
(ii) The worst-case approximation error of f_c is given by

$$E(f_c) = \frac{1}{2}\|\overline{f} - \underline{f}\|_p = \inf_{\widehat{f}} EN(\widehat{f}) = \mathcal{R}_{\mathcal{I}}. \tag{2.12}$$

Proof. See [39]. □

2.3.1 Interval estimates

The interval estimates $\overline{f}, \underline{f}$ of the unknown function f_o are now given for the cases where the noise is bounded in ℓ_∞ norm (i.e. $q = \infty$ in (2.5)). Indeed, from

the FFS^T definition, it follows that $f_o(x)$ is bounded as

$$\underline{f}(w) \leqslant f_o(w) \leqslant \overline{f}(w), \forall w \in \mathcal{W} \tag{2.13}$$

where

$$\begin{aligned} \overline{f}(w) &= \sup_{f_o \in FFS^T} f(w), \\ \underline{f}(w) &= \inf_{f_o \in FFS^T} f(w). \end{aligned} \tag{2.14}$$

Theorem 3. *Assume that:*
(i) The noise affecting the measurements $\mathcal{D}$ is bounded according to (2.5).
(ii) The function f_o is Lipschitz continuous according to (2.6).
Then, for $q = \infty$ and for any $w \in \mathcal{W}$, $f_o(w)$ is tightly bounded as

$$\underline{f}(w) \leqslant f_o(w) \leqslant \overline{f}(w). \tag{2.15}$$

Proof. See [39]. □

$\overline{f}$ and $\underline{f}$ are also called *optimal bounds* since they are tightest upper and lower bounds of f_o.

2.4 Local Approach

Suppose that a preliminary approximation f_* of the function f_o has been obtained using any method. This approximation is of the form

$$f_*(x) = \sum_{i=1}^{N} a_i \phi_i(w) \tag{2.16}$$

where $\phi_i : \mathcal{W} \to \mathbb{R}$ are Lipschitz continuous basis functions and $a_i \in \mathbb{R}$ are parameters identified by means of some suitable algorithm (two algorithms will be presented in Section 2.4.2). The choice of the basis functions ϕ_i is clearly an important step of the identification process, see e.g. [65, 28, 51]. In several cases of practical interest, the basis functions are known a priori to belong to some "large" set of functions, see e.g. the example presented in [46]. The sparse approximation algorithms presented below can be applied in these cases to select within this "large" set the functions which are important for providing an accurate description of the system under investigation. In other cases, the basis functions are not known a priori and their choice can be carried out considering the numerous options available in the literature (e.g. gaussian, sigmoidal, wavelet, polynomial, trigonometric). See [65] for a discussion on the main features of the most used basis functions and for indications for their choice.

Define the following *residue function*:

$$f_\Delta(w) \doteq f_o(w) - f_*(w). \tag{2.17}$$

From (2.6) and from the Lipschitz continuity of ϕ_i, it follows that f_Δ is Lipschitz continuous over the set $\mathcal{W}$:

$$f_\Delta \in \mathcal{F}(\Gamma_\Delta). \tag{2.18}$$

for some $\Gamma_\Delta < \infty$. Note that the Lipschitz constant Γ_Δ can be estimated by means of the algorithm presented in Section 2.7.

Remark 2. The inclusion (2.18) corresponds to assume a *global* maximum rate of variation for f_Δ but a *local* maximum rate of variation for f_o. Indeed, for every $w, \widehat{w} \in \mathcal{W}$, the following inequalities hold:

$$-\Gamma_\Delta \leqslant \frac{f_\Delta(w) - f_\Delta(\widehat{w})}{\|w - \widehat{w}\|_2} \leqslant \Gamma_\Delta$$

$$\frac{f_*(w) - f_*(\widehat{w})}{\|w - \widehat{w}\|_2} - \Gamma_\Delta \leqslant \frac{f_o(w) - f_o(\widehat{w})}{\|w - \widehat{w}\|_2} \leqslant \frac{f_*(w) - f_*(\widehat{w})}{\|w - \widehat{w}\|_2} + \Gamma_\Delta.$$

We can observe that, as expected, the maximum rate of variation of f_Δ is constant and equal to Γ_Δ for any $\hat{w} \in \mathcal{W}$. Instead, the maximum rate of variation of f_o is Γ_Δ plus a quantity that depends locally on the point $\hat{w}$. For this reason, when $f_* = 0$ and thus $f_\Delta = f_o$, the approach is called *global set membership approach* which was discussed in Section 2.3. Otherwise, the approach is called *local set membership approach*.

Under the above assumptions and, in particular, under (2.5) and (2.18), we have that $f_o \in FFS^T$, where FFS^T is the Feasible Function Set defined as follows.

Definition 7. The *Feasible Function Set* is

$$FFS \doteq \{f : f = f_* + f_\Delta,\ f_\Delta \in \mathcal{F}(\Gamma_\Delta), \|\widetilde{y} - f(\widetilde{w})\|_q \leqslant \mu\}.$$

where $\widetilde{y} = (\widetilde{y}^1, \ldots, \widetilde{y}^T)$ and $f(\widetilde{w}) \doteq (f(\widetilde{w}^1), \ldots, f(\widetilde{w}^T))$. □

According to this definition, FFS^T is the set of all functions consistent with the prior assumptions and data. In the set membership framework, the validation of prior assumptions is a fundamental step. It is usual to introduce the concept of prior assumption validation as consistency with the available data: the prior assumptions are considered validated if at least one estimate consistent with these assumptions and the data exists, i.e., if FFS^T is not empty, see, e.g., [44, 7].

Definition 8. The prior assumptions are validated if $FFS^T \neq \emptyset$. □

The following theorem gives a necessary and sufficient condition for the validation of prior assumptions.

Theorem 4. *$FFS^T \neq \emptyset$ if and only if the optimization problem (2.29) is feasible.*

Proof. See [49]. □

The following theorem shows that the approximation f_* in (2.16) is interpolatory (and thus almost-optimal). The theorem also provides an explicit bound on the worst-case approximation error.

Let us define the following functions:

$$\begin{aligned} \overline{f}_\Delta(w) &\doteq \min_{t=1,\ldots,L} \left(\delta^t(a^*) + \varepsilon^t + \Gamma_\Delta \|w - \widetilde{w}^t\|_2\right), \\ \underline{f}_\Delta(w) &\doteq \max_{t=1,\ldots,L} \left(\delta^t(a^*) - \varepsilon^t - \Gamma_\Delta \|w - \widetilde{w}^t\|_2\right). \end{aligned} \tag{2.19}$$

$$\begin{aligned} \overline{f}(w) &= f_*(w) + \overline{f}_\Delta(w), \\ \underline{f}(w) &= f_*(w) + \underline{f}_\Delta(w). \end{aligned} \tag{2.20}$$

where $\delta^t(a^*) = \widetilde{y}^t - f_*(\widetilde{w}^t)$ (see (2.30)) and $\widehat{\varepsilon}^t \geqslant 0$, $t = 1, \ldots, T$.

Theorem 5. *Assume that:*
(i) The noise affecting the measurements $\mathcal{D}$ is bounded according to (2.5).
(ii) The function f_o is Lipschitz continuous according to (2.6).
Then, for $q = 2, \infty$ and for any $p \in [1, \infty]$:
(i) The approximation f_* defined in (2.16) is interpolatory (and thus almost-optimal).
(ii) The worst-case approximation error of f^* is bounded as

$$EN(f_*) \leqslant \max_{\substack{\|\widehat{\varepsilon}\|_q \leqslant \mu \\ \|\widehat{\boldsymbol{\epsilon}}\|_q \leqslant \mu}} \left\| \overline{f}_\Delta(\cdot, \widehat{\varepsilon}) - \underline{f}_\Delta(\cdot, \widehat{\boldsymbol{\epsilon}}) \right\|_p = 2 \inf_{\widehat{f}} EN(\widehat{f}). \tag{2.21}$$

Proof. See [49]. □

Suppose that $\widehat{\varepsilon}^* = \widehat{\boldsymbol{\epsilon}}^* = \varepsilon$, where $\varepsilon = (\varepsilon^1, \ldots, \varepsilon^T)$ is obtained as described in Section 2.4.1. Now let the function f_c be defined as

$$f_c(w) \doteq f_*(w) + \frac{1}{2}\left[\overline{f}_\Delta(w, \varepsilon) + \underline{f}_\Delta(w, \varepsilon)\right]. \tag{2.22}$$

where $\overline{f}_\Delta, \underline{f}_\Delta$ are given in (2.19). The following result shows that this function f_c is an optimal approximation of f_o.

Theorem 6. *Assume that:*
(i) The noise affecting the measurements $\mathcal{D}$ is bounded according to (2.5).
(ii) The function f_o is Lipschitz continuous according to (2.6).
Then, for $q = 2, \infty$ and for any $p \in [1, \infty]$:
(i) The approximation f_c defined in (2.22) is optimal.
(ii) The worst-case approximation error of f_* is given by

$$EN(f_c) = \frac{1}{2}\left\| \overline{f}_\Delta(\cdot, \varepsilon) - \underline{f}_\Delta(\cdot, \varepsilon) \right\|_p = \inf_{\widehat{f}} EN(\widehat{f}). \tag{2.23}$$

Proof. See [39]. □

In summary, we have shown that the function $f_*(w)$ is an almost-optimal approximation, whereas the function $f_c(w) \doteq f_*(w) + [\overline{f}_\Delta(w,\varepsilon) + \underline{f}_\Delta(w,\varepsilon)]/2$ is an optimal approximation of f_o. The correction term $[\overline{f}_\Delta(w,\varepsilon)+\underline{f}_\Delta(w,\varepsilon)]/2$ can be useful to check how close is f_* to the optimum: The two approximations can be be evaluated off-line on a set of data not used for identification. If the errors of the two approximations on these data are similar, it can be concluded that f_* is practically optimal. Otherwise, this comparison allows us to quantify the suboptimality level of f_* with respect to f_c.

Remark 3. A subcase of the general theory presented here is when $f_* = 0$, in which we have the so-called *global set membership approach*, previously presented. Otherwise, if $f_* \neq 0$, we have the so-called *local set membership approach*. See also Remark 2 for an explanation of this terminology.

2.4.1 Interval estimates

Interval estimate on the unknown function f_o are now derived. A general formulation is developed, allowing us to deal with the cases where the noise is bounded in ℓ_2 or ℓ_∞ norm (i.e. $q = 2$ or $q = \infty$ in (2.5)).

Noise bounded in ℓ_2 norm

Theorem 5 does not allow the evaluation of interval estimates since the assumption that the noise sequence $d = (d^1, d^2, \ldots, d^T)$ is bounded in ℓ_2 norm gives no information on how the single elements d^t are bounded. In order to overcome this issue, some additional assumption has to be made on the element-wise boundedness of the noise sequence d. This kind of assumption can be obtained as follows.

Since f_* is an almost-optimal approximation of f_o, we have that $f_*(\widetilde{w}^t) \cong f_o(\widetilde{w}^t)$ and, consequently, that $d^t = \widetilde{y}^t - f_o(\widetilde{w}^t) \simeq \widetilde{y}^t - f_*(\widetilde{w}^t) \doteq \delta^t(a^*)$. It is then reasonable to assume the following relative plus absolute error bound:

$$\left|d^t\right| \leqslant \varepsilon^t \doteq \varepsilon^r \left|\delta^t(a^*)\right| + \varepsilon^a, \quad t = 1, \ldots, T. \tag{2.24}$$

where the term $\varepsilon^r |\delta^t(a^*)|$ accounts for the fact that $d^t \simeq \delta^t(a^*)$ and ε^a accounts for the fact that d^t and $\delta^t(a^*)$ are not exactly equal. The parameters $\varepsilon^r, \varepsilon^a \geqslant 0$

have to be taken such that $\varepsilon^r \mu + \varepsilon^a \sqrt{T} \leqslant \mu$. Indeed, if this inequality is satisfied, (2.24) is consistent with (2.5): $\|d\|_2 \leqslant \varepsilon^r \mu + \varepsilon^a \sqrt{T} \leqslant \mu$. Following this indication, ε^r and ε^a (together with Γ_Δ) can be chosen by means of the procedure presented in [39].

In order to satisfy the assumption (2.24), the following additional constraints have to be inserted in Algorithm 1 (in particular, in (2.29) and on line 5 of (2.31)):

$$\left| \widetilde{y}^t - \Phi^t \left(\widetilde{w}^t \right) a \right| \leqslant \varepsilon^t, \quad t = 1, \ldots, T. \tag{2.25}$$

where $\Phi^t \left(\widetilde{w}^t \right)$ is the t-th row of the matrix Φ. □

Noise bounded in ℓ_∞ norm

If the noise is bounded in ℓ_∞ norm, the required interval estimates can be obtained without introducing any further assumption. Indeed, in this case,

$$\left| d^t \right| \leqslant \varepsilon^t \doteq \mu, \quad t = 1, \ldots, T. \tag{2.26}$$

□

The following theorem, holding for both the ℓ_2 and ℓ_∞ cases, provides tight point-wise interval estimates for $f_o(w)$ and gives an expression of the worst-case error bound computable for any dimension n_x (a computationally tractable algorithm for this computation is presented in [38]).

Theorem 7. *Assume that:*
(i) The noise affecting the measurements $\mathcal{D}$ is bounded according to (2.24) or (2.26).
(ii) The function f_o is Lipschitz continuous according to (2.6).
Then, for $q = 2, \infty$ and for any $p \in [1, \infty]$:
(i) The worst-case approximation error of f_* is bounded as

$$EN(f_*) \leqslant \left\| \overline{f}_\Delta(\cdot, \varepsilon) - \underline{f}_\Delta(\cdot, \varepsilon) \right\|_p = 2 \inf_{\widehat{f}} EN(\widehat{f}).$$

(ii) For any $w \in \mathcal{W}$, $f_o(w)$ is tightly bounded as

$$\underline{f}(w, \varepsilon) \leqslant f_o(w) \leqslant \overline{f}(w, \varepsilon). \tag{2.27}$$

Proof. See [49]. □

2.4.2 Local Approach - identification algorithms

In this section, two algorithms for the identification of the parameters a_i in (2.16) are proposed.

In order to ensure suitable regularity properties of the approximation, limiting well-known issues such as overfitting and the curse of dimensionality, we require the vector $a = (a_1, a_2, \dots, a_N) \in \mathbb{R}^N$ of the coefficients in (2.16) to be sparse. Hence, under the assumption (2.5), a solution to the identification Problem 1 could be found by solving the following optimization problem:

$$\begin{aligned} a^0 &= \arg\min_{a \in \mathbb{R}^N} \|a\|_0 \\ &\text{subject to} \quad \left\|\widetilde{y} - \Phi a\right\|_q \leqslant \mu. \end{aligned} \tag{2.28}$$

where

$$\begin{aligned} \widetilde{y} &\doteq (\widetilde{y}^1, \dots, \widetilde{y}^T) \\ \Phi &\doteq \begin{bmatrix} \phi_1(\widetilde{w}^1) & \cdots & \phi_N(\widetilde{w}^1) \\ \vdots & \ddots & \vdots \\ \phi_1\left(\widetilde{w}^T\right) & \cdots & \phi_N\left(\widetilde{w}^T\right) \end{bmatrix} \\ &= \begin{bmatrix} \phi_1(\widetilde{w}) & \cdots & \phi_N(\widetilde{w}) \end{bmatrix}, \end{aligned}$$

$\phi_1(\widetilde{w}) \doteq (\phi_1(\widetilde{w}^1), \dots \phi_1(\widetilde{w}^T))$, and $\|a\|_0$ is the ℓ_0 quasi-norm of a, defined as the number of non-zero components of a. In fact, minimizing the ℓ_0 quasi-norm of a vector corresponds to minimizing the number of its non-zero elements, i.e. to maximizing its sparsity. On the other hand, the constraint $\left\|\widetilde{y} - \Phi a\right\|_q \leqslant \mu$ ensures that the identified coefficient vector is consistent with the measured data (2.2) and the prior assumption on noise (2.5).

However, the optimization problem (2.28) cannot be easily solved, since the ℓ_0 quasi-norm is a non-convex function and its minimization is an NP-hard problem. The classical approach to overcome this issue is to replace the ℓ_0 quasi-norm with its convex envelope, i.e. the ℓ_1 norm, see e.g. [18], [72], [12]. The identification Problem 1 can thus be solved efficiently by means of the following convex optimization problem.

Algorithm 1 Function Identification 1

$$\begin{aligned} a^* &= \arg\min_{a\in\mathbb{R}^N} \|a\|_1 \\ \text{subject to} \quad & \left\|\widetilde{y} - \Phi a\right\|_q \leqslant \mu \end{aligned} \tag{2.29}$$

where μ can be chosen as a positive number slightly larger than μ^{min}, the minimum value for which the problem is feasible (this choice is theoretically motivated by the validation Theorem 4). Provided that $\mu > \mu^{min}$, the value of μ can be tuned to suitably manage the trade-off between accuracy and sparsity.

Another interesting ℓ_1 algorithm, completely based on convex optimization, is now presented. As discussed below, this algorithm provides sparser solutions with respect to the standard algorithm (2.29), which is based on simple ℓ_1-norm minimization.

Without loss of generality, assume that the columns of Φ are normalized: $\|\phi_i(\widetilde{w})\|_2 = 1$, $i = 1,2,\ldots,N$. Define the following quantity:

$$\xi(a) \doteq \frac{|\delta(a)|_1 + |\delta(a)|_{K_0}}{\underline{\sigma}^2(\Phi)}$$

where $K_0 \doteq 2\|a\|_0$, $\underline{\sigma}(\Phi)$ is the minimum non-zero singular value of Φ and

$$\begin{aligned} \delta(a) &\doteq \widetilde{y} - \Phi a \\ |w|_K &\doteq \sqrt{\sum_{i\in I_K} \left(w^T \phi_i(\widetilde{x})\right)^2}, \end{aligned} \tag{2.30}$$

being I_K the set of the K largest inner products $\left|w^T\phi_i(\widetilde{x})\right|$. Let card$(\cdot)$ denote the set cardinality.

Algorithm 2 Function Identification 2

1. Solve the optimization problem (2.29) and set $a^1 := a^*$.

2. Let $r(a^1) \doteq \left\{i_1, \ldots, i_j : \xi\left(a^1\right) > |a^1_{i_1}| \geqslant \ldots \geqslant |a^1_{i_j}|\right\}$ and let $r_\lambda(a^1)$ denote the subset of $r(a^1)$ with indices in λ. Compute the coefficient vector a^* as follows:

$$
\begin{array}{l}
\text{for } k = 1 : \text{card}(r(a^1)) \\
\qquad c^k = \arg\min\limits_{a \in \mathbb{R}^N} \|\widetilde{y} - \Phi a\|_q \\
\qquad \text{subject to} \quad a_i = 0, \ \forall i \in r_\lambda(a^1) \\
\qquad\qquad\qquad\quad \lambda = \{k, \ldots, \text{card}(r(a^1))\} \\
\qquad \text{if } \left\|\widetilde{y} - \Phi c^k\right\|_q \leqslant \mu \\
\qquad\qquad a^* := c^k \\
\qquad\qquad \text{break} \\
\qquad \text{end} \\
\text{end}
\end{array}
\tag{2.31}
$$

The rationale behind Algorithm 2 can be explained as follows: In step 1, an optimization problem similar to (2.28) is solved, where the ℓ_0 quasi-norm is replaced by the ℓ_1 norm. The ℓ_1 norm is the convex envelope of the ℓ_0 quasi-norm, and its minimization yields a sparse vector a^1 [18], [72], [12]. However, it is not guaranteed that all the non-zero elements of a^1 are necessary to have $\|\widetilde{y} - \Phi a^1\|_q \leqslant \mu$. In step 2, only the elements of a^1 larger than $\xi\left(a^1\right)$ are kept (indeed, $\xi\left(a^1\right)$ discriminates between "important" and "less important" vector components, [46]), while the remaining ones, ordered by decreasing amplitude, are progressively included to form the vector a^*. The algorithm stops when $\|\widetilde{y} - \Phi c^k\|_q \leqslant \mu$. The solution provided by step 2 is thus a vector a^* where the number of non-zero elements is further reduced with respect to the initial sparse solution a^1. The sparse approximation is given by (2.16), with $a_i = a_i^*$, $\forall i$.

2.5 Quasi-Local Approach

In this section, the so-called quasi-local nonlinear set membership approach is presented, capturing the advantages of the global and local approaches of Section 2.3, 2.4 and avoiding some drawbacks of these two. On one hand, the quasi-local approach allows the derivation of significantly less conservative uncertainty bounds with respect to the global approach of Section 2.3. On the other hand, the quasi-local approach does not require to choose a suitable parametric form for the filter, as done in the local approach of Section 2.4. The filter is obtained directly from the data in a non-parametric closed form.

Based on Assumption 2, we can define the following quantity, called the *quasi-local Lipschitz parameter*:

$$\gamma(w) \doteq \sup_{\widehat{w}\in\mathcal{W},\widehat{w}\neq w} \frac{|f_o(w) - f_o(\widehat{w})|}{\|w - \widehat{w}\|_2}. \tag{2.32}$$

Obviously, the Lipschitz constant of f on $\mathcal{W}$ is given by

$$\Gamma = \sup_{w\in\mathcal{W}} \gamma(w). \tag{2.33}$$

Lemma 1. For any $w \in \mathcal{W}$, a $\gamma(w)$ exists, such that

$$|f_o(w) - f_o(\widehat{w})| \leqslant \gamma(w) \, \|w - \widehat{w}\|_2 \,, \ \forall \widehat{w} \in \mathcal{W}.$$

Proof. The statement follows directly from (2.32). □

Let us now suppose that the quasi-local Lipschitz parameters $\gamma(\widetilde{w}^t)$, $t = 1, \ldots, T$, are known or can be estimated (a method for performing such an estimation is given in Section 2.7). Assume also that the noise is bounded in ℓ_∞ norm according to (2.5), with $q = \infty$ and $\varepsilon \doteq \mu$. On the basis of this information, we can define the following function set:

$$\mathcal{F}_{ql} \doteq \{f : \left|f(w) - f(\widehat{w}^t)\right| \leqslant \gamma(\widehat{w}_t) \left\|w - \widehat{w}^t\right\|_2, \forall w \in \mathcal{W}, \ t = 1, \ldots, T\}. \tag{2.34}$$

This allows us to define the *Feasible Function Set* as follows.

Definition 9. The *Feasible Function Set* is

$$FFS^T \doteq \left\{ f \in \mathcal{F}_{ql} : \|\widetilde{y} - f(\widetilde{w})\|_q \leqslant \mu \right\}. \tag{2.35}$$

where $\widetilde{y} = (\widetilde{y}^1, \ldots, \widetilde{y}^T)$ and $f(\widetilde{w}) \doteq (f(\widetilde{w}^1), \ldots, f(\widetilde{w}^T))$. □

As discussed in Section 2.4, FFS^T is the set of all functions consistent with the prior assumptions and data. The prior assumptions are considered validated if at least one estimate consistent with these assumptions and the data exists, i.e. if FFS^T is not empty, see e.g. [44, 7].

Definition 10. The prior assumptions are validated if $FFS^T \neq \emptyset$. □

The following theorem gives a necessary and a sufficient condition for the validation of prior assumptions.

Let us define the following functions:

$$\begin{aligned} \overline{f}(w) &\doteq \min_{t=1,\ldots,T} (\overline{h}^t + \gamma(\widetilde{w}^t)\|w - \widetilde{w}^t\|_2), \\ \underline{f}(w) &\doteq \max_{t=1,\ldots,T} (\underline{h}^t - \gamma(\widetilde{w}^t)\|w - \widetilde{w}^t\|_2). \end{aligned} \tag{2.36}$$

where $\overline{h}^t \doteq \widetilde{y}^t + \varepsilon^t$ and $\underline{h}^t \doteq \widetilde{y}^t - \varepsilon^t$.

Theorem 8. *(i) A necessary condition for prior assumptions to be validated is* $\overline{f}(\widetilde{w}^t) \geqslant \underline{h}^t$,$\underline{f}(\widetilde{w}^t) \leqslant \overline{h}^t$, $t = 1, \ldots, T$.
(ii) A sufficient condition for prior assumptions to be validated is $\overline{f}(\widetilde{w}^t) > \underline{h}^t$,$\underline{f}(\widetilde{w}^t) < \overline{h}^t$, $t = 1, \ldots, T$.

Proof. (i) we have to prove that if prior assumptions are validated, i.e. $FFS^T \neq \emptyset$, then, $\overline{f}(\widetilde{w}^t) \geqslant \underline{h}^t$, $t = 1, \ldots, T$.
Let $f \in C^1(w)$. From Lemma 1, it follows that for every $w \in \mathcal{W}$, and for each $t = 1, \ldots, T$, a $\gamma(\widetilde{w}^t)$ exist such that $f(w) \leqslant f(\widetilde{w}^t) + \gamma(\widetilde{w}^t)\|w - \widetilde{w}^t\|$. From $f \in FFS^T$ we have $f(\widetilde{w}^t) \leqslant \widetilde{y}^{t+1} + \varepsilon^t$. Then,

$$f(w) \leqslant \widetilde{y}^{t+1} + \varepsilon^t + \gamma(\widetilde{w}^t)\|w - \widetilde{w}^t\|.$$

This holds for $\forall w \in \mathcal{W}$ and $t = 1, \ldots, T$. Then, from (2.36) we have

$$f(w) \leqslant \overline{f}(w), \forall w \in \mathcal{W}. \tag{2.37}$$

Similarly, it can be proven that:

$$f(w) \geqslant \underline{f}(w), \forall w \in \mathcal{W}. \tag{2.38}$$

From (2.37),(2.38) it follows that $\overline{f}(\widetilde{w}^t) \geqslant \underline{f}(\widetilde{w}^t)$, $t = 1, \ldots, T$, and from (2.36) it follows that $\underline{f}(\widetilde{w}^t) \geqslant \underline{h}^t, t = 1, \ldots, T$, then $\overline{f}(\widetilde{w}^t) \geqslant \underline{h}^t, t = 1, \ldots, T$.
The proof that $\underline{f}(\widetilde{w}^t) \leqslant \overline{h}^t$ is similar.
(ii) Suppose that $\overline{f}(\widetilde{w}^t) > \underline{h}^t$,$\underline{f}(\widetilde{w}^t) < \overline{h}^t$, $t = 1, \ldots, T$. We have to prove that $FFS^T \neq \emptyset$, i.e. that a function $f \in \mathcal{F}$ can be found such that $|\widetilde{y}^{t+1} - f(\widetilde{w}^t)| \leqslant \varepsilon, t = 1, \ldots, T$. For a given $w \in \mathcal{W}$, let $\bar{t}$ and $\underline{t}$ be such that $\bar{t} = \arg\min_t(\overline{h}^t + \gamma(\widetilde{w}^t)\,\|w - \widetilde{w}^t\|)$ and $\underline{t} = \arg\max_t(\underline{h}^t + \gamma(\widetilde{w}^t)\,\|w - \widetilde{w}^t\|)$. From (2.36) we have: $\overline{f}(w) - \underline{f}(w) = \overline{h}^{\bar{t}} - \underline{h}^{\underline{t}} + \gamma(\widetilde{w}^{\bar{t}})\|w - \widetilde{w}^{\bar{t}}\| + \gamma(\widetilde{w}^{\underline{t}})\|w - \widetilde{w}^{\underline{t}}\|$.
If $\gamma(\widetilde{w}^{\bar{t}}) > \gamma(\widetilde{w}^{\underline{t}})$ we have: $\overline{f}(w) - \underline{f}(w) \geqslant \overline{h}^{\bar{t}} - \underline{h}^{\underline{t}} + \gamma(\widetilde{w}^{\underline{t}})\|\widetilde{w}^{\bar{t}} - \widetilde{w}^{\underline{t}}\| \geqslant \overline{f}(\widetilde{w}^{\underline{t}}) - \underline{h}^{\underline{t}} > 0$
If $\gamma(\widetilde{w}^{\underline{t}}) > \gamma(\widetilde{w}^{\bar{t}})$ we have: $\overline{f}(w) - \underline{f}(w) \geqslant \overline{h}^{\bar{t}} - \underline{h}^{\underline{t}} + \gamma(\widetilde{w}^{\bar{t}})\|\widetilde{w}^{\bar{t}} - \widetilde{w}^{\underline{t}}\| \geqslant -\underline{f}(\widetilde{w}^{\bar{t}}) + \overline{h}^{\bar{t}} > 0$.
Since w is an arbitrary point of $\mathcal{W}$, Then

$$\underline{f}(w) < \overline{f}(w), \forall w \in \mathcal{W}. \tag{2.39}$$

By defining $f_c(w) = \frac{1}{2}[\underline{f}(w) + \overline{f}(w)]$, this inequality implies that

$$\underline{f}(w) < f_c(w) < \overline{f}(w), \forall w \in \mathcal{W}. \tag{2.40}$$

On the other hand, from (2.36) it follows $\overline{f}(\widetilde{w}^t) \leqslant \widetilde{y}^{t+1} + \varepsilon^t$, $\underline{f}(\widetilde{w}^t) \geqslant \widetilde{y}^{t+1} - \varepsilon^t$, $\forall t$, which, together with (2.40), implies $\widetilde{y}^{t+1} - \varepsilon^t \leqslant \underline{f}(\widetilde{w}^t) < f_c(\widetilde{w}^t) < \overline{f}(\widetilde{w}^t) \leqslant \widetilde{y}^{t+1} + \varepsilon$, $\forall t$ and then $|\widetilde{y}^{t+1} - f_c(\widetilde{w}^t)| < \varepsilon^t, t = 1, \ldots, T$. □

Let us now define the function

$$f_c(w) \doteq \frac{1}{2}[\underline{f}(w) + \overline{f}(w)]. \tag{2.41}$$

where $\underline{f}(w)$ and $\overline{f}(w)$ are given in (2.36). The next result shows that the approximation f_c is optimal for any L_p norm. The theorem also provides an explicit bound on the worst-case approximation error.

Theorem 9. *Assume that:*
(i) The noise affecting the measurements $\mathcal{D}$ is bounded according to (2.5).
(ii) The function f_o is Lipschitz continuous according to (2.6).
Then, for $q = \infty$ and for any $p \in [1, \infty]$:
(i) The approximation f_c defined in (2.41) is optimal.

(ii) The worst-case approximation error of f_c is bounded as

$$EN(f_c) = \frac{1}{2}\left\|\overline{f} - \underline{f}\right\|_p = \inf_{\widehat{f}} EN(\widehat{f}) \doteq \mathcal{R}_{\mathcal{I}}. \tag{2.42}$$

Proof. The proof can be obtained by minor modifications of the proof of Theorem 7 in [39]. □

2.5.1 Interval estimates

The interval estimates of the unknown function f_o are now given for the cases where the noise is bounded in ℓ_∞ norm (i.e. $q = \infty$ in (2.5)).

Theorem 10. *Assume that:*
(i) The noise affecting the measurements $\mathcal{D}$ is bounded according to (2.5).
(ii) The function f_o is Lipschitz continuous according to (2.6).
Then, for $q = \infty$ and for any $w \in \mathcal{W}$, $f_o(w)$ is tightly bounded as

$$\underline{f}(x) \leqslant f_o(w) \leqslant \overline{f}(w). \tag{2.43}$$

Proof. For a given $w \in \mathcal{W}$, let $\bar{t} = \arg\min_{t=1,\dots,T}(\widetilde{y}^{t+1} + \varepsilon^t + \gamma(\widetilde{w}^t)\|w - \widetilde{w}^t\|)$. From Lemma 1 we have $f(w) \leqslant f(\widetilde{w}^{\bar{t}}) + \gamma(\widetilde{w}^{\bar{t}})\|w - \widetilde{w}^{\bar{t}}\|$. Also let $f \in FFS^T$. Then we have $f(\widetilde{w}^{\bar{t}}) \leqslant \widetilde{y}^{\bar{t}+1} + \varepsilon^{\bar{t}}$. Therefore,
$\sup f(w) = \sup f(\widetilde{w}^{\bar{t}}) + \gamma(\widetilde{w}^t)\|w - \widetilde{w}^t\| = \widetilde{y}^{\bar{t}+1} + \varepsilon^{\bar{t}} + \gamma(\widehat{w}^t)\|w - \widetilde{w}^{\bar{t}}\| = f_u(w)$
This holds for all $w \in \mathcal{W}$. Then, $f_u(w) = \sup_{f \in FFS^T} f(w) = \overline{f}(w)$.
The proof that $f_l(w) = \inf_{f \in FFS^T} f(w) = \underline{f}(w)$ is similar. □

Remark 4. The point-wise bounds (2.43) provide an interval estimate of the unknown value $f_o(w)$. Interval estimates allow us to quantify the uncertainty associated with the identification process, and are thus important in system and control applications. Indeed, these estimates can be used e.g. for robust control design, [59, 57], prediction interval evaluation, [40], and fault detection, see the following chapters.

Remark 5. A study on the relation between the representativeness and length of the available data and the quality of the approximation can be found in [38]. This study relies on the computation of the radius of information $\mathcal{R}_{\mathcal{I}}$ (see Definition 2), representing the minimum worst-case error that can be achieved from the available

prior and experimental information. Based on this concept, a methodology is proposed in [38], where $\mathcal{R}_{\mathcal{I}}$ is used to evaluate the "level of information" provided by a given dataset and to obtain precise indications on the quality of the approximation that can be obtained.

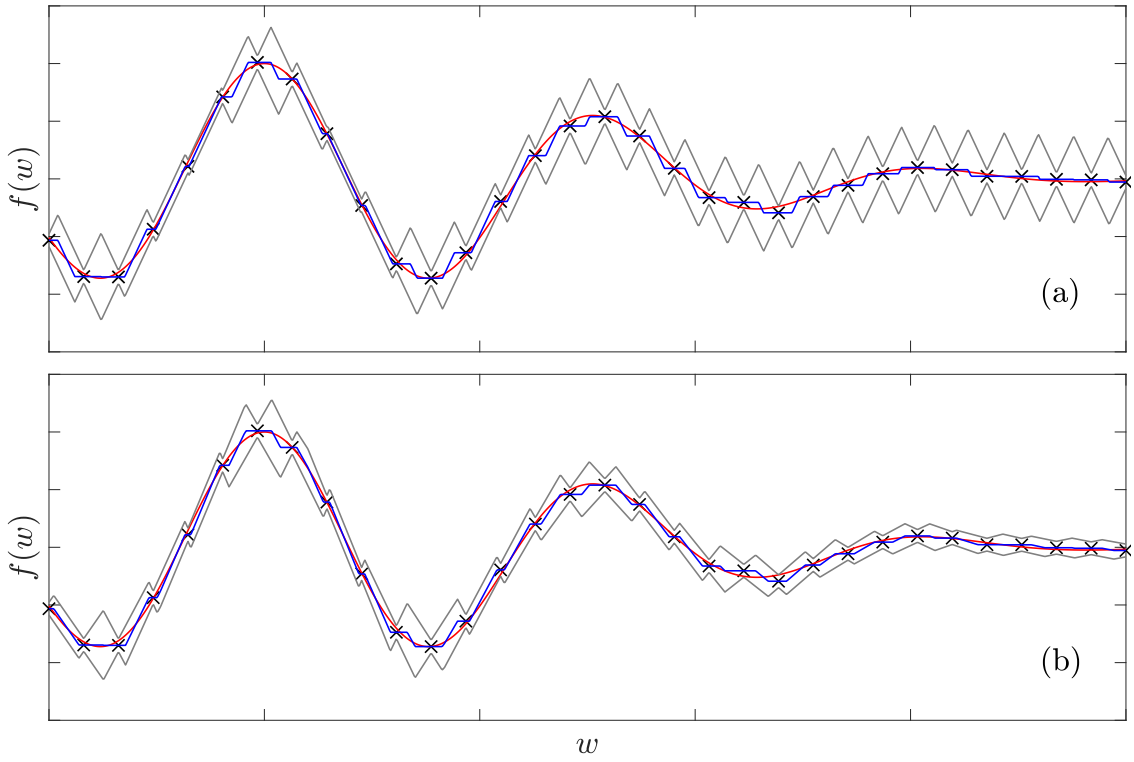

Figure 2.1: Optimal bounds: (a) global bound, (b) quasi-local bound, $f_o(w)$ red line, measurements black cross, $f_c(w)$ blue line, $\overline{f}(w), \underline{f}(w)$ grey line.

Figure 2.1 shows the comparison between the global and quasi-local set membership bounds for a nonlinear function. In Figure 2.1(a), a global Lipschitz constant Γ was assumed for the function f_o. In Figure 2.1(b), a quasi-local Lipschitz parameter $\gamma(w)$ was assumed. It can be noted that the resulting uncertainty bounds are clearly tighter in the quasi-local case, especially in regions where the function is relatively "flat".

2.6 Radius of Information

Let us define the following error function:

$$f_e(w, \mathcal{D}) \equiv f_e(w) \doteq \frac{1}{2}[\overline{f}(w) - \underline{f}(w)]. \tag{2.44}$$

where $\mathcal{D}$ is the identification dataset (2.2). Here, the dependence on $\mathcal{D}$ is explicited, in order to emphasize the fact that the function f_e is constructed from the identification dataset. This function allows us to write the radius of information as

$$\mathcal{R}_{\mathcal{I}}^{p} = \|f_e(\cdot, \mathcal{D})\|_p. \tag{2.45}$$

The analytical computation of $\|f_e\|_p$ is not feasible since f_e is a quite "complex" nonlinear function, defined over a multi-dimensional domain. Hence, following a standard approach, we compute numerically the norm, evaluating f_e on a finite set of points w^k and then approximating the norm as

$$\|f\|_p \simeq \widehat{\|f\|}_p = \begin{cases} \left[\sum_{k=1}^{m} a_k \left|f(w^k)\right|^p\right]^{1/p}, p \in [1, \infty) \\ \max\limits_{k=1,\ldots,m} \left|f(w^k)\right|, p = \infty \end{cases} \tag{2.46}$$

where a_k are suitably chosen coefficients. For $a_k = 1/m$ we have the widely used quasi-Monte Carlo algorithms [38].

The expression of $\mathcal{R}_{\mathcal{I}}^{p}$ given in (2.45) and computed according to (2.46) will be used in the next chapters, in order to develop our DoE algorithms.

2.7 Parameter Estimation

Estimates of the noise bound μ, Lipschitz constant Γ, and the quasi-local Lipschitz parameter $\gamma(w)$ such that the assumptions are validated can be obtained by means of two algorithms given in [13] and reported in the following. Algorithm 1 is directly taken from [13], while Algorithm 2 is a generalization of the corresponding one in [13].

Algorithm 3 Noise Bound Estimation μ

1. Choose a "small" $\rho > 0$. for example:
   $\rho = 0.01 \max_{t,k=1,\dots,T-1} \|\widetilde{w}^t - \widetilde{w}^k\|$.
2. Find the set of indexes: $I_t \doteq \left\{k : \|\widetilde{w}^t - \widetilde{w}^k\| \leqslant \rho\right\}$. if $I_t = \emptyset$ for all $t = 1, \dots, T-1$, go to step 1 and choose a larger ρ.
3. For $t = 1, \dots, T-1$ compute $\delta\widetilde{y}^{t+1} = \max_{i \in I_t} |\widetilde{y}^{t+1} - \widetilde{y}^{i+1}|$. If $I_t = \emptyset$, set $\delta\widetilde{y}^{t+1} = \infty$.
4. Obtain the estimate $\widehat{\mu}$ of the noise bound μ as
   $\widehat{\mu} = \frac{1}{2N} \sum_{t \in Q} \delta\widetilde{y}^{t+1}$
   where $Q \doteq \{t \in \{1, \dots, T-1\} : \delta\widetilde{y}^{t+1} < \infty\}$ and $N \doteq \mathrm{card}(Q)$.

Algorithm 4 Lipschitz Parameter Estimation Γ, Γ_Δ, γ

1. For $t, k = 1, \dots, T-1$ and $\widetilde{w}_k \neq \widetilde{w}_t$, compute

$$\widehat{\Gamma} = \max_{t,k=1,\dots,T-1} \begin{cases} \frac{\left|\widetilde{y}^{t+1} - \widetilde{y}^{k+1}\right| - 2\widehat{\mu}}{\|\widetilde{w}^t - \widetilde{w}^k\|_2} & \text{if } \left|\widetilde{y}^{t+1} - \widetilde{y}^{k+1}\right| > 2\widehat{\mu} \\ 0 & \text{otherwise} \end{cases} \tag{2.47}$$

2. For $t, k = 1, \dots, T-1$ and $\widetilde{w}_k \neq \widetilde{w}_t$, compute

$$\widehat{\Gamma}_\Delta = \max_{k,t=1,\dots,T-1} \begin{cases} \frac{\left|\widetilde{\delta}^k - \widetilde{\delta}^t\right| - 2\widehat{\mu}}{\|\widetilde{w}^k - \widetilde{w}^t\|_2} & \text{if } \left|\widetilde{\delta}^k - \widetilde{\delta}^t\right| > 2\widehat{\mu} \\ 0 & \text{otherwise.} \end{cases} \tag{2.48}$$

3. For $t = 1, \dots, T-1$ and $\widetilde{w}^t \neq \widetilde{w}^k$, compute

$$\widehat{\gamma}(\widetilde{w}^t) = \max_{k=1,\dots,T-1} \begin{cases} \frac{\left|\widetilde{y}^{t+1} - \widetilde{y}^{k+1}\right| + 2\widehat{\mu}}{\|\widetilde{w}^t - \widetilde{w}^k\|_2} & \text{if } \left|\widetilde{y}^{t+1} - \widetilde{y}^{k+1}\right| > 2\widehat{\mu} \\ 0 & \text{otherwise} \end{cases} \tag{2.49}$$

The following theorems show that, under reasonable density conditions on the noise, the estimates given by these two algorithms converge to the corresponding true values.

Theorem 11. *(Theorem 2 of [13]) Let the set* $\{\widetilde{w}^t, d^t\}_{t=1}^T$ *appearing in (2.1) be dense on* $\mathcal{W} \times B_\mu$ *as* $T \to \infty$*. Then,*

$$\lim_{T\to\infty} \widehat{\mu} = \mu. \qquad \square$$

Theorem 12. *(Theorem 3 of [13]) Let the set* $\{\widetilde{w}^t, d^t\}_{t=1}^T$ *appearing in (2.1) be dense on* $\mathcal{W} \times B_\mu$ *as* $T \to \infty$*. Then,*

$$\lim_{T\to\infty} \widehat{\Gamma} = \Gamma. \qquad \square$$

2.8 Adaptive Set Membership Model

In many applications, it may happen that the dynamics of the system changes over time or the model is not accurate enough in the whole regressor domain $\mathcal{W}$. One of the advantages of nonlinear set membership (global and quasi-local approach) is that it can be easily made adaptive since no optimization problem needs to be solved online.

In the set membership framework, the model accuracy is defined by the radius of information and it can be computed in a deterministic way [38]. In the global and quasi-local approaches, the model is basically defined by the measurement dataset $\mathcal{D}$, noise bound μ and Lipschitz parameters Γ or $\gamma(x)$. Therefore, the model can be made adaptive by updating online the measurement dataset and the Lipschitz parameters.

Suppose that a model with a desired radius of information $\mathcal{R}_d$ is looked for, where $\mathcal{R}_d < \mathcal{R}_\mathcal{I}$. If, at time instant t, $f_e(w^t) > \mathcal{R}_d$, it means that the model error in that point (w^t) is larger than the desired radius. Therefore, the new measurement can be added to the dataset $\mathcal{D}$ in order to increase the model accuracy.

In the case where the dynamics of the system changes over time, a time label can be assigned to each element of the dataset $\mathcal{D}$ as $\mathcal{D}(T) = \left\{\widetilde{y}^k, \widetilde{w}^k, t^k\right\}_{k=1}^{T-1}$ where t^k indicates the time each measurement was taken. Then, since the model is running online, at each time instant t, we can eliminate the measurements which were taken at $t - \delta t$, where δt is a desired value which depends on the system dynamics variation.

Algorithm 5 Adaptive Set Membership Model

1. Define the measurement dataset $\mathcal{D}$ as $\mathcal{D}(T) = \left\{\widetilde{y}^k, \widetilde{w}^k, t^k\right\}_{k=1}^{T-1}$.

2. At time step t+1, compute the vector w^t and measure the system output y^{t+1}.

3. If $f_e(w^t) > \mathcal{R}_d$. Then,

$$\begin{aligned} &\mathcal{D}(T+1) = \mathcal{D}(T) \cup \left\{\widetilde{y}^{t+1}, \widetilde{w}^t, t+1\right\} \\ &T = T+1. \end{aligned} \tag{2.50}$$

4. Find the set of indexes $I^k = \left\{k : t^k \in \mathcal{D}, t^k < t - \delta t\right\}$. Then,

$$\begin{aligned} &\mathcal{D}(T-N) = \mathcal{D}(T) \setminus \left\{\widetilde{y}^k, \widetilde{w}^k, t^k\right\}_{k \in I^k} \\ &T = T - N \end{aligned} \tag{2.51}$$

   where $N \doteq \text{card}(I^k)$.

5. If $\mathcal{D}$ is changed, update the model Lipschitz parameters according to Algorithm 4.

2.9 Conclusions

In this chapter, a quasi-local nonlinear set membership identification method was presented. In this approach, instead of a global constant bound on the gradient of the function Γ, a quasi-local bound γ is assumed. Therefore, the uncertainty bounds are less conservative. Also unlike the local nonlinear set membership, this quasi-local approach does not require a preliminary estimate of the function.

Chapter 3

Set Membership Design of Experiments

3.1 Introduction

As mentioned in Chapter 1, one of the greatest challenges in system identification context is to design an experiment giving the maximum information about the system to be identified [22, 36]. Most of the studies carried out so far have mainly focused on linear systems [25, 77, 68, 17, 66, 61, 33] and static systems [14, 64, 28]. On the other side, very few studies regarding nonlinear dynamic systems are available [47, 10, 21, 23]. In fact, nonlinear systems are characterized by a significantly higher complexity than linear systems. While for linear systems the excitation properties of an input signal essentially depend on the signal frequencies, for nonlinear systems they also depend on the signal amplitudes [47]. For example, a white noise input signal is known in general to be appropriate for the identification of a linear system of any order. On the other side, it may not be suitable to allow an accurate exploration of the regressor domain of a nonlinear system, and this may lead to a low model accuracy.

Currently, the most popular DoE methods for nonlinear dynamic systems are classified into two main categories: model-free and model-based methods [10, 76, 9, 24]. The idea of these methods is to parameterize a pre-defined excitation signal, and then optimize the signal parameters called the design points, according to

different criteria. For example, a widely applied excitation signal in industrial identification tasks is the amplitude modulated pseudo random binary signal (APRBS). The APRBS signal is a sequence of N fixed steps with associated hold times T_{h_i} and amplitudes $a_i \in [u_{min}\ u_{max}]$ $i = 1, ..., N$. Since the values of the amplitudes are free design parameters in the following they are called design points. In Figure 3.1, a schematic APRBS signal in the time domain is plotted. Given the length T of the signal, the hold time T_{h_i} determines the number of steps and thus influences the frequency characteristics of the signal. It's important to choose an appropriate minimum hold time $T_{h_{min}}$ to assure that the system has a reasonable time to settle. If not, only operating conditions around $(u_{max} - u_{min})/2$ will be covered and a model identified from such data will not be able to describe the static behavior well. Besides the minimum hold time, the distribution of the design points a_i $i = 1, \ldots, N$ is essential for the quality of the excitation signal.

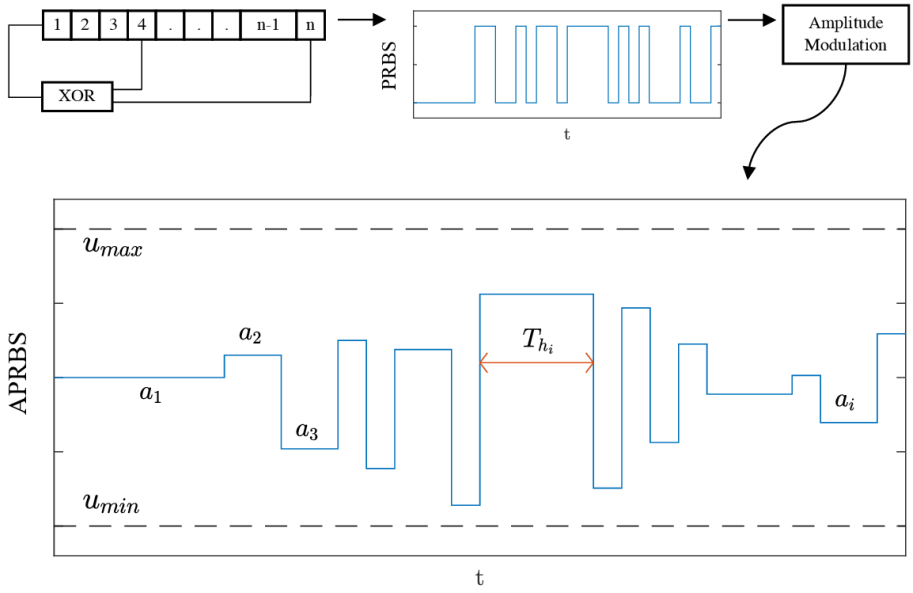

Figure 3.1: APRBS signal in time domain.

In model-free DoE, no assumptions on the model structure are made. The typical approach is to distribute design points in the input domain as much uniformly as possible. This DoE approach is also known as space-filling DoE. The most popular space-filling DoE technique is based on the Latin Hypercube (LHC) distribution. To calculate an LHC distribution, the input space is divided into N intervals. In every column and row, only one design point is placed. Figure 3.2(b) shows an example of the LHC distribution of 50 design points for a two-dimensional

input space.

In model-based DoE, after assuming a particular model structure, the idea is to distribute the design points in the input domain, in such a way that the estimation of the model parameters is as much insensitive as possible to the measurement noise. The most popular model-based DoE is the D-optimal distribution technique. Figure 3.2(c) shows an example of the D-optimal distribution technique with 50 design points based on a polynomial model of the third order.

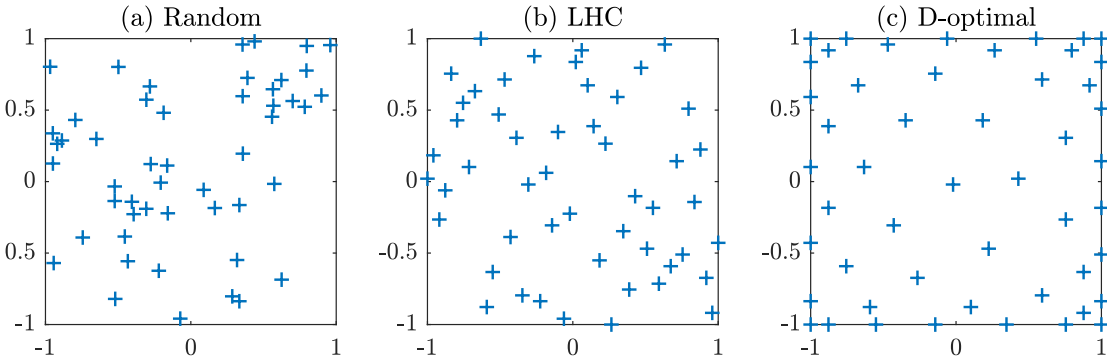

Figure 3.2: Distribution of 50 design points for a two-dimensional input space.

After designing the distribution of the points in the input space, they are used for a parameterized excitation signal, like the above mentioned APRBS signal. Both model-free and model-based DoEs do not take into account the dynamics of the system and do not provide any indication about the optimal sequence of the design points. Although these methods are simple and adequate to capture the steady state behavior of a system of interest, they don't take into account the dynamics of the system. Therefore, by using these methods, capturing the nonlinear dynamic behavior of the system in the whole regressor domain is a heuristic/arbitrary process. In general, as far as the authors are aware, no DoE method for nonlinear dynamic systems can be found in the literature, which can ensure the exploration of the relevant regressor domain of a nonlinear system and, consequently, guarantee a desired model accuracy.

In the last three decades, there has been an increasing interest and research formulating the identification problem in Set Membership (SM) framework [39, 67, 44, 43, 42, 49, 52, 41, 7]. The main reason is the fact that SM identification allows us to properly quantify the uncertainty of the identified model in a deterministic manner. As described in Chapter 2, In SM nonlinear identification, no assumptions

on the structure of the unknown system are required. Instead, two basic assumptions are made. An assumption on the regularity of the system, given by bounds on its gradient, and another assumption on the noise boundedness. Then, an optimal estimate, with minimal guaranteed identification error and tight uncertainty bounds, is derived. which is a bounded identification uncertainty description given by the set of all possible models that are all equally probable. This nonlinear SM approach does not require any iterative minimization and thus avoids the issue of local minima. Since no optimization problems have to be solved, nonlinear SM identification is particularly suitable for adaptive identification, making the model more accurate over time by adding new measurements collected online. Because of these features, the applications of SM in robust control and experiment design is a promising research area [67].

Due to the presence of disturbances and measurement noise, in general, no identification process can result in a model that perfectly corresponds to the true system. Any identified model is always affected by some uncertainty. Understanding which are the regions of the regressor space where the model is most uncertain is a key element to design a proper DoE algorithm. However, knowing where the model is most uncertain is not sufficient. Since the unknown system is dynamic, the DoE algorithm has to be able to generate an input sequence such that the system moves toward those uncertain regions of the regressor space, in order to take new measurements.

In this chapter, a novel online DoE algorithm for nonlinear dynamic MISO systems is proposed, that is able to reduce the worst-case model error while considering input constraints of the system. The proposed DoE algorithm is able to guarantee any desired worst-case error larger than the measurement error in a finite time experiment. In the next chapter, the proposed DoE algorithm is used for a simulation case study in the automotive field to design a data-driven controller for Lean NO_x Trap regeneration.

This chapter is organized as follows. In section 3.2, the DoE problem is formulated in set membership framework. In section 3.3, a static DoE algorithm is proposed that is able to guarantee any desired radius of information for a static nonlinear system. In section 3.4.1, a set membership predictive controller is proposed for nonlinear dynamic systems which is able to move the system toward the most uncertain regions of the regressor space. And finally, in section 3.4, a dynamic Set Membership DoE (SM-DoE) algorithm is proposed. In section 3.5, the proposed SM-DoE algorithm is tested on two simulation examples to illustrate the

effectiveness of the proposed algorithm and compared to other DoE methods.

3.2 Problem Formulation

Let us consider a multiple input single output (MISO) nonlinear system described by (2.1). The system is unknown and the output is corrupted by noise. Let Assumptions 1 and 2 hold. And, let $U_t^T \doteq \left\{u^k\right\}_{k=t}^{T-1}$ be an input sequence from time t to time $T-1$. The problem considered in this section is the following.

Problem 2. Design an input sequence U_1^T that, applied to the nonlinear system (2.1), yields a minimal radius of information $\mathcal{R}_{\mathcal{I}}^p = \|f_e(w)\|_p$. □

Ideally, a solution to this problem is given by

$$\begin{aligned} U_1^{*T} = \arg\min_{U_1^T} \quad & \|f_e(\cdot, \mathcal{D})\|_p \\ \text{subject to} \quad & \widetilde{y}^{t+1} = f_o(\widetilde{w}^t) + d^t, t = 1, \dots, T-1 \\ & \mathcal{D} = \left\{\widetilde{y}^{t+1}, \widetilde{w}^t\right\}_{t=1}^{T-1} \end{aligned} \tag{3.1}$$

where $d^t, t = 1, \dots, T-1$ is the actual noise sequence.

However, for several reasons, this optimization problem cannot be used for DoE in real applications: 1) it requires to know f_o and the complete noise sequence $\{d^t\}_{t=1}^{T-1}$; 2) even assuming that f_o is known and the noise can be measured, the optimization problem can only be solved at time $T-1$, since at previous time instants $t < T-1$, the noise samples d^k are not known for $k > t$; 3) even in the case that f_o and the complete noise sequence are known, the optimization problem is highly nonlinear and non-convex, and thus hard to solve analytically. Nevertheless, in the simulations studies that will be presented in the paper, the problem (3.1) will be solved numerically (without guarantees of finding a global minimum) and the obtained estimate of the "ideal" optimal input sequence U_1^{*T} will be used as a term of comparison, to indicate the maximum performance that can be achieved by any DoE algorithm.

The approach to DoE that we propose can actually be applied in real situations, without knowing a-priori the true function and noise sequence. A key feature is that the approach is sequential: at each time step, on the basis of the current and past measured data, the approach individuates what is the next point of the regressor domain that the system has to visit, in order to maximally reduce the radius of information. In the case where the system is a static function of the input - i.e.,

where $w^t = u^t$ - the optimal input is obviously chosen equal to the individuated next point. In the general case of a dynamic system, it may be not possible to visit the desired point, since the system future regressor depends not only on the current input but also on the past input and output values. Hence, once the next point to visit has been found, a model predictive control (MPC) strategy is used to drive the system toward that point. The proposed MPC strategy is based on a nonlinear set membership model identified from the past data and updated at each time step on the basis of the new measurement.

The cases of static and dynamic systems are treated in the next two sections, respectively.

3.3 Static Set Membership DoE

Consider a static nonlinear system of the form

$$z^t = f_o(w^t),\ w^t = u^t \in \mathcal{W}. \tag{3.2}$$

In this case, solving the experiment design problem is easier with respect to the general case, since the system trajectory depends only on the current input and not on the past input and output values. Hence, it is possible to obtain a measurement of the function f_o at any desired point of the regressor domain $\mathcal{W}$. The static Set-Membership DoE algorithm that we propose is the following.

Algorithm 6 Static Set Membership DoE

1. Choose the initial regressor w^1 (e.g., the center of the regressor domain $\mathcal{W}$);
   Measure $\tilde{z}^1 = f_o(w^1)$;
   Define the measurement dataset $\mathcal{D} = \{\tilde{z}^1, w^1\}$.

2. While $t < T$, solve the optimization problem

$$\begin{aligned} w_M^t &= \arg\max_{w \in \mathcal{W}} f_e^t(w, \mathcal{D}); \\ w^t &\in w_M^t \end{aligned} \tag{3.3}$$

   Evaluate $\tilde{z}^t = f_o(w^t)$;
   Add $\tilde{z}^t$ and w^t to the dataset $\mathcal{D} := \mathcal{D} \cup \{\tilde{z}^t, w^t\}$;
   Set $t := t + 1$.

The vector w^t is any point in w_M^t and f_e^t is the error function (2.44) computed at time instant t.

The algorithm is iterative. At each iteration, a point in the regressor domain where the uncertainty is maximum is considered. The optimization problem (3.3) is nonlinear and non-convex. However, as discussed in section 2.6, we evaluate f_e on a finite set of points in the domain $\mathcal{W}$, making the computation easy (thus obtaining, in general, a sub-optimal solution). The following result holds for Algorithm 6.

Theorem 13. *Let T be the number of steps in Algorithm 6 and $\mathcal{R}_{\mathcal{I}}(t)$ be the radius of information computed at time t. Then, there exists a T such that $\mathcal{R}_{\mathcal{I}}(t) \leqslant \mu$, $\forall t \geqslant T$.*

Proof. Let us define the following set:

$$w_e^t = \left\{ w \in \mathcal{W} : \Gamma \|w - w^t\|_2 < f_e(w) - \mu \right\}. \tag{3.4}$$

The following inequalities hold at each iteration of the algorithm:

$$f_e^{t+1}(w) < f_e^t(w) \quad \forall w \in w_e^t, \tag{3.5}$$

$$f_e^{t+1}(w) = f_e^t(w) \quad \forall w \in \mathcal{W} \setminus w_e^t. \tag{3.6}$$

If $w_M^t \subseteq w_e^t$, we have $f_e^t(w) < f_e^t(w^t) \quad \forall w \in \mathcal{W} \setminus w_e^t$ and from (3.6) we can write $f_e^{t+1}(w) < f_e^t(w^t) = \mathcal{R}_\mathcal{I}(t) \quad \forall w \in \mathcal{W} \setminus w_e^t$. From (3.5) we have $f_e^{t+1}(w) < \mathcal{R}_\mathcal{I}(t) \quad \forall w \in w_e^t$,. Therefore, $f_e^{t+1}(w) < \mathcal{R}_\mathcal{I}(t) \quad \forall w \in \mathcal{W}$. which also means

$$\mathcal{R}_\mathcal{I}(t+1) < \mathcal{R}_\mathcal{I}(t). \tag{3.7}$$

If $w_M^t \nsubseteq w_e^t$, from (3.5), at each iteration we have

$$w_M^{t+1} = w_M^t \setminus w_e^t. \tag{3.8}$$

Since $w^t \in w_e^t, w^t \in w_M^t$ it is evident that $w_M^t \cap w_e^t \neq \emptyset$. Therefore, $w_M^{t+1} \subset w_M^t$ which means w_M is shrinking at each time step therefore in a finite n_i steps we have $w_M^{t+n_i} \subseteq w_e^{t+n_i}$. Thus from (3.7) we have,

$$\mathcal{R}_\mathcal{I}(t+n_i+1) < \mathcal{R}_\mathcal{I}(t). \tag{3.9}$$

$\mathcal{R}_\mathcal{I}$ is a positive definite function and $\mathcal{R}_\mathcal{I} \leqslant \mu$ if $\mathcal{D} = \mathcal{W}$. Also from (3.7),(3.9) we can say $\mathcal{R}_\mathcal{I}$ is a decreasing function. Therefore, as $t \to \infty$, Then $\mathcal{R}_\mathcal{I}(t) \leqslant \mu$.

□

3.4 Dynamic Set Membership DoE

Now Suppose that the DoE has to be carried out for a nonlinear dynamic system, written in the general regression form (2.1). Unlike the static case (3.2), it is not possible to evaluate the regression function at any desired point w, since the system regressor depends not only on the current input but also on the past input and output values. The idea that we propose is to use an algorithm similar to Algorithm 6 to generate desired reference points w^r in combination with an MPC controller making the dynamic system visit the desired point w^r. The MPC approach that we propose is novel and is called set membership model predictive control (SMPC).

3.4.1 Set Membership Model Predictive Control

In recent years, there has been an increasing interest in set membership predictive control laws, designed from experimental data [4, 5, 62, 67]. However, such approaches, implicitly or explicitly, assume that a sufficiently informative set of data is available and do not consider the problem of experiment design. In this section, we propose a novel MPC approach, called SMPC, able to perform together experiment design and controller design.

To formulate the SMPC approach, a state-space-like representation of the plant (2.1) and related models is needed. To this aim, we introduce the following pseudo-state:

$$\begin{aligned} x^t &= [y^t \dots \; y^{t-n_y+1} \quad u^{t-1} \dots \; u^{t-n_u+1}] \\ &= [x^t_{(1)} \dots \; x^t_{(n_y)} \quad x^t_{(n_y+1)} \dots \; x^t_{(n_y+n_u)}] \end{aligned} \tag{3.10}$$

where $\mathcal{W}$ and $\mathcal{X}$ are bounded sets in $\mathbb{R}^n$ and $\mathbb{R}^{n-m}$, respectively. In other words, $x^t \in \mathcal{X}$ is equal to $w^t \in \mathcal{W}$ without the input sample at time t:

$$w^t = [x^t_{(1)} \dots \; x^t_{(n_y)} \quad u^t \quad x^t_{(n_y+1)} \dots \; x^t_{(n_y+n_u)}].$$

The state space representation of the plant and the one-step prediction of the model are given by

$$\begin{aligned} &x^{t+1} = f_o(x^t, u^t) \\ &f_o(x^t, u^t) \doteq [f_o(w^t) \quad x^t_{(1)} \dots \; x^t_{(n_y-1)} \quad u^t \dots \; x^t_{(n_y+n_u-1)}]. \end{aligned} \tag{3.11}$$

$$\begin{aligned} &\widehat{x}^{t+1}_c = f_c(x^t, u^t) \\ &f_c(x^t, u^t) \doteq [f_c(w^t) \quad x^t_{(1)} \dots \; x^t_{(n_y-1)} \quad u^t \dots \; x^t_{(n_y+n_u-1)}]. \end{aligned} \tag{3.12}$$

In the notation above, $f(x^t, u^t)$ returns a vector of pseudo-states, while $f(w^t)$ returns a scalar. f_c is the central estimate of set membership model and $\widehat{\cdot}$ represents the estimate given by the model. From (3.11) and (3.12), it follows that

$$x^{t+1} = f_o(x^t, u^t) = f_c(x^t, u^t) + [e^t \quad 0 \; \dots \; 0]. \tag{3.13}$$

where the model uncertainty is described in terms of additive perturbation e^t, which

is known to be bounded as

$$\left|e^t\right| \leqslant f_e(w^t) \leqslant \mathcal{R}_I^\infty \quad \forall w \in \mathcal{W}. \tag{3.14}$$

The sequence of inputs $\{u^i\}_{i=t}^{t+k-1}$, starting from a generic time instant t, up to a time instant $t+k-1$, is indicated with U_t^k. The state of the plant at time $t+k$ obtained starting from a generic "initial" state x^t and applying the input sequence U_t^k is defined as

$$\begin{aligned} \mathcal{S}_o(x^t, U_t^k) \doteq x^{t+k} : \\ x^{t+n+1} = f_o(x^{t+n}, u^{t+n}) \quad \forall n \in [0, k-1]. \end{aligned} \tag{3.15}$$

The set of all possible plant state values at time $t+k$ that originate from a generic "initial" state x^t by applying the input sequence U_t^k to the system (3.13) is defined as

$$\begin{aligned} \mathcal{S}(x^t, U_t^k) = \{\, \widehat{x}^{t+k} : \\ \widehat{x}^{t+n+1} = f_c(\widehat{x}^{t+n}, u^{t+n}) + [e^{t+n} \quad 0 \ \dots \ 0], \\ \left|e^{t+n}\right| \leqslant f_e(\widehat{w}^{t+n}), \forall n \in [0, k-1] \,\}\,. \\ \widehat{w}^{t+n} = [\widehat{x}_{(1)}^{t+n} \dots \ \widehat{x}_{(n_y)}^{t+n} \quad u^{t+n} \quad \widehat{x}_{(n_y+1)}^{t+n} \dots \ \widehat{x}_{(n_y+n_u)}^{t+n}]. \end{aligned} \tag{3.16}$$

Note that this set is generated by all possible sequences $\{e^{t+n}\}_{n=0}^{k-1}$ such that $|e^{t+n}| \leqslant f_e(\widehat{w}^{t+n}), \forall n \in [0, k-1]$. Clearly, it holds that $\mathcal{S}_o(x^t, U_t^k) \in \mathcal{S}(x^t, U_t^k)$. It is also true that if $\mathcal{R}_I^\infty = 0$ then $\mathcal{S}_o(x^t, U_t^k) = \mathcal{S}(x^t, U_t^k)$. The size of the set $\mathcal{S}(x^t, U_t^k)$ can be interpreted as the uncertainty of the state at time $t+k$. In other words, the uncertainty of the trajectory points, when a certain input sequence U_t^k is applied to the system.
Recalling the idea behind our approach from section 3.2, the aim is to reduce the radius (or diameter) of information by collecting measurements where the uncertainty is maximum. Thus, suppose that we want to take a measurement at a point w^r, or its equivalent (x^r, u^r), where the uncertainty amplitude is $f_e(w^r)$. Our approach consists in using an SMPC controller (to be defined later) to drive the plant state x^t to a neighborhood of x^r, called the reference set $\mathcal{X}_r \subset \mathbb{R}^{n-m}$, defined as

$$\mathcal{X}_r \doteq \{x : \Gamma \left\|x - x^r\right\|_2 + \mu < \lambda f_e(w^r), \lambda \in (0,1]\}\,. \tag{3.17}$$

This set is a ball of radius $\frac{\lambda f_e(w^r) - \mu}{\Gamma}$, centered at x^r; λ is a design parameter, allowing us to change the size of the reference set. When the state of the system x^t is inside $\mathcal{X}_r$ i.e. $x^t \in \mathcal{X}_r$, by applying u^r as input to the system and adding the new

measurement to the dataset $\mathcal{D}$, the uncertainty $f_e(w^r)$ will be reduced by at least a factor of λ.

Assumption 3. For any "initial" state x^t and reference state x^r, there exists a control sequence U_t^k that moves the state from x^t to x^r:

$$\begin{aligned} \forall x^t, x^r \in \mathcal{X},\ \exists K < \infty,\ \exists U_t^k \in \mathcal{U} :\\ \mathcal{S}_o(x^t, U_t^k) = x^r \text{ for } k < K. \end{aligned} \tag{3.18}$$

Assumption 4. For any input sequence U_t^k, the state of the system (3.11) remains inside the compact set $\mathcal{X}$:

$$\forall U_t^k \in \mathcal{U}, \forall t \geqslant 0, k \geqslant 1 : \quad x^t \in \mathcal{X}. \tag{3.19}$$

Assumption 3 is a quite standard controllability assumption. Assumption 4 is a mild boundedness assumption, just requiring that the system trajectory does not tend to infinity.

Let us define the set of potential trajectory horizons from x^t to x^r as follows:

$$\mathcal{I}(x^t, x^r) \doteq \{i \in \mathbb{N} : i < K,\ \exists U_t^i \text{ such that } x^r \in \mathcal{S}(x^t, U_t^i)\}. \tag{3.20}$$

For each element of the set $\mathcal{I}(x^t, x^r)$, there exists an input sequence such that $x^r \in \mathcal{S}(x^t, U_t^i)$. Assumption 3 ensures that this set is non-empty and finite for any initial and reference states.

The optimization problem solved in the SMPC approach is:

$$\begin{aligned} J^*(x^t, x^r, i) &= \max_{U_t^i} J(x^t, x^r, U_t^i) \\ &\text{subject to } U_t^i \in \mathcal{U} \\ &\qquad x^r \in \mathcal{S}(x^t, U_t^i) \\ J(x^t, x^r, U_t^i) &= \sum_{n=1}^{i} \operatorname{diam}(\mathcal{S}(x^t, U_t^n)) \end{aligned} \tag{3.21}$$

where $i = \min\{\mathcal{I}(x^t, x^r)\}$ and $\operatorname{diam}(\mathcal{S})$ is the diameter of the set $\mathcal{S}$.

The controller is implemented according to a receding horizon strategy. The control law, indicated as $u^t = \mathcal{K}(x^t, x^r)$, means solving (3.21) and applying the first element of the maximizer U_t^{i*} as the control action u^{t*} to the system, and adding the new measurement to the dataset $\mathcal{D}$ ($\mathcal{D} := \mathcal{D} \cup \{\widetilde{y}^{t+1}, \widetilde{w}^t\}$). Then, repeating these operations at each time t. The resulting control sequence, starting from a generic time instant t up to another instant k is denoted as $\mathcal{K}_t^k$.

Theorem 14. *Let Assumptions 3 and 4 hold. Starting from any initial state $x^t \in \mathcal{X}$, the state of the system controlled by the feedback law $\mathcal{S}_o(x^t, \mathcal{K}_t^k)$, will visit a point inside the reference set $\mathcal{X}_r$ in finite time. That is,*

$$\begin{aligned} &\forall x^t, x^r \in \mathcal{X},\ \exists K < \infty : \\ &\qquad \mathcal{S}_o(x^t, \mathcal{K}_t^k) \in \mathcal{X}_r \quad \textit{for some} \quad k < K. \end{aligned}$$

Proof. Assumption 3 ensures that the set $\mathcal{I}$ is not empty and the optimization problem (3.21) is always feasible for all $i \in \mathcal{I}$. From the definition of the cost function, the following inequality holds for all feasible solutions.

$$\begin{aligned} &\forall U_t^i \quad \text{such that} \quad U_t^i \in \mathcal{U}, x^r \in \mathcal{S}(x^t, U_t^i) : \\ &\operatorname{diam}(\mathcal{S}(x^t, U_t^i)) \leqslant J^*(x^t, x^r, i) \end{aligned} \tag{3.22}$$

From (3.22) and the fact that $\mathcal{X}_r$ is a ball centered at x^r we can conclude that if $J^*(x^t, x^r, i) \leqslant \operatorname{diam}(\mathcal{X}_r)/2$, then the set $\mathcal{S}(x^t, U_t^i)$ is inside $\mathcal{X}_r$. i.e. $\mathcal{S}_o(x^t, U_t^i) \in \mathcal{S}(x^t, U_t^i) \subset \mathcal{X}_r$. This holds for all feasible solutions which means the state of the real system will be inside $\mathcal{X}_r$ in i steps. Therefore, in order to prove the theorem, we have to prove that

$$\forall \mu > 0, \exists K \quad \text{such that} \quad J_k^* < \mu \quad \text{for} \quad k < K. \tag{3.23}$$

where J_k^* is the cost computed at time instant k. At each time step, we solve (3.21) and apply the first element of the maximizer U_t^{i*} as control action u^{t*} and add a new measurement to the dataset $\mathcal{D}$. The following inequalities hold when a new measurement is added

$$\operatorname{diam}(\mathcal{S}_{k+1}(x^t, u^{t*})) = 2 f_e(w^t) < 2\mu \tag{3.24}$$

$$\mathcal{S}_{k+1}(x^t, u^{t*}) \subset \mathcal{S}_k(x^t, u^{t*}) \tag{3.25}$$

$$\operatorname{diam}(\mathcal{S}_{k+1}(x^t, u^{t*})) < \operatorname{diam}(\mathcal{S}_k(x^t, u^{t*})) \tag{3.26}$$

where the subscript $k+1$ indicates a measurement is added to the dataset $\mathcal{D}$, which happens at each time step.

When a new measurement is added to the dataset $\mathcal{D}$, the uncertainty of the successive predicted states might also be reduced

$$\mathcal{S}_{k+1}(x^t, U_t^n) \subseteq \mathcal{S}_k(x^t, U_t^n) \quad \forall n \in [2, i] \tag{3.27}$$

From (3.27), since the size of the predicted states might be reduced, two things could happen.
If $x^r \in \mathcal{S}_{k+1}(x^t, U_t^{i*})$, from (3.26) we have

$$J_{k+1}^*(x^t, x^r, i_{k+1}) < J_k^*(x^t, x^r, i_k) \quad , \quad i_{k+1} = i_k \tag{3.28}$$

If $x^r \notin \mathcal{S}_{k+1}(x^t, U_t^{i*})$, which means U_t^{i*} is no longer a feasible solution. In such conditions, from the definition of the optimization problem, one of the following inequalities hold

$$\text{card}(\mathcal{I}_{k+1}) \leqslant \text{card}(\mathcal{I}_k), \quad i_{k+1} > i_k \tag{3.29}$$

or

$$J_{k+1}^*(x^t, x^r, i_{k+1}) < J_k^*(x^t, x^r, i_k), \quad i_{k+1} = i_k \tag{3.30}$$

Now consider the following function

$$v(x^t, x^r) = \sum_{i \in \mathcal{I}(x^t, x^r)} J^*(x^t, x^r, i) \tag{3.31}$$

From (3.28), (3.29), (3.30) and (3.31) we have

$$\begin{aligned} v_{k+1}(x^t, x^r) &< v_k(x^t, x^r) \\ v_{k+2}(x^{t+1}, x^r) &< v_{k+1}(x^{t+1}, x^r) \\ v_{k+3}(x^{t+2}, x^r) &< v_{k+2}(x^{t+2}, x^r) \\ &\dots \end{aligned} \tag{3.32}$$

Finally, consider the integral of the function v over the compact set $\mathcal{X}$

$$V(x^r) = \int_{x \in \mathcal{X}} v(x, x^r) dx \tag{3.33}$$

From (3.31), (3.33) we can say $V(x^r)$ is a positive definite function $V(x^r) \geqslant 0$ since $J^* \geqslant 0$ and $V(x^r) = 0$ if and only if $\mathcal{R}_{\mathcal{I}}^{\infty} = 0$. From (3.32), (3.33) it holds that

$$V_{k+1}(x^r) - V_k(x^r) < 0 \quad \forall k > 0 \tag{3.34}$$

Therefore $\lim_{k\to\infty} V_k(x^r) = 0$ which is true if and only if $\lim_{k\to\infty} J_k^* = 0$.

□

Algorithm 7 Dynamic Set Membership DoE

1. Select a reference regressor w^r to be visited which has a high uncertainty and its equivalent pseudo-state x^r is close to the estimated state:

$$w^r, x^r = \arg \min_{w^r \in \mathcal{W}, x^r \in \mathcal{X}} (\left\| \widehat{x}^{t+1} - x^r \right\|_2 + \frac{\delta}{f_e(w^r)}). \tag{3.35}$$

2. Compute $\mathcal{X}_r$ according to (3.17) with a suitable λ.

3. Apply the following criterion:

$$\begin{array}{ll} \text{if} & \widehat{x}^{t+1} \in \mathcal{X}_r \\ \text{then} & u^t = u^r \in w^r \\ \text{else} & u^t = \mathcal{K}(x^r, x^t). \end{array}$$

4. Evaluate $\widetilde{y}^{t+1} = f_o(\widetilde{w}^t) = f_o(x^t, u^t)$.

5. Add $\widetilde{y}^{t+1}$ and $\widetilde{w}^t$ to the dataset $\mathcal{D} := \mathcal{D} \cup \{\widetilde{y}^{t+1}, \widetilde{w}^t\}$.

6. Update γ and Γ according to Algorithm 4.

7. Set $t := t + 1$ and go to step (1).

The dynamic set membership DoE is implemented in Algorithm 7. The Algorithm is iterative: at each iteration, a reference regressor w^r is computed to be visited. Ideally this reference should be where f_e is maximum (similarly to Algorithm 6). However, if the reference is close to the estimated state, it can be visited more quickly. Equation (3.35) combines these two objectives. In step 2, the reference set $\mathcal{X}_r$ is computed. In step 3, if the central estimate is inside the reference set, the input is generated according to the corresponding u^t of the vector w^r. Otherwise, the input is generated by the SMPC controller $\mathcal{K}$. Finally, at each iteration, a new measurement is taken and added to the measurement dataset $\mathcal{D}$

and the Lipschitz bounds γ, Γ are updated. To compute f_e in step 1 and 2, a global bound Γ is used and a quasi-local bound γ is used in step 3.

Corollary 1. For any desired radius of information $\mathcal{R}_d \geqslant \mu$, there exist a finite number of steps T of Algorithm 4 such that $\mathcal{R}_{\mathcal{I}}(t) \leqslant \mathcal{R}_d$, $\forall t \geqslant T$.

According to Theorem 13, it is shown that if the system is static, which means it is possible to take a measurement anywhere in the regressor domain $\mathcal{W}$, then, Algorithm 6 can reach any desired radius of information. Also, according to Theorem 14, it is shown that for a dynamic system the SMPC controller can visit any desired point in the regressor domain. Algorithm 7 is the combination of Algorithm 6 and the SMPC controller assuming a large value δ in equation (3.35). Thus, we can conclude that Algorithm 7 can reach any desired radius of information in a finite time experiment.

3.5 Simulation Results

In this section, we present two simulation studies to illustrate the SM-DoE algorithm. The first example is concerned with a simulated nonlinear system, previously studied in [47]. The input signals obtained by the SM-DoE approach are compared with other input signals and with the optimal one, discussed in section 3.2. The second example also studied in [10], is a nonlinear dynamic system with a static nonlinearity, where we compare the SM-DoE approach with three other DoE methods, taken from the literature.

3.5.1 Example 1:

This section is concerned with the DoE for the following nonlinear dynamic system:

$$y^{t+1} = 0.88\, y^t - 0.12 \tanh(15\, y^t) + 0.06\, u^t. \tag{3.36}$$

Assuming the initial condition $y^1 = 0$. Three inputs signals have been considered:

$$\begin{aligned} U_{(1)} &= \{3\sin(0.2t), t = 1,2,...,T\} \\ U_{(2)} &= \left\{3\sin(0.0009t^2), t = 1,2,...,T\right\} \\ U_{(3)} &= \{WN(0,4,t), t = 1,2,...,T\}\,. \end{aligned} \tag{3.37}$$

where $WN(0,4,t)$ is a white gaussian noise of mean 0 and variance 4. For each of these signals, a simulation of the system (3.36) with length $T = 300$ was performed. The output signal was corrupted by a uniform random noise with amplitude $\leqslant 0.01$. The corresponding radius of information $\mathcal{R}_{\mathcal{I}}$ was computed. The involved regressor is

$$w^t = [y^t\ u^t].$$

The regressor domain of interest $\mathcal{W}$ is the rectangular region indicated in Figure 3.4 and defined by

$$\mathcal{W} \doteq \{w : w_1 \leq 0.35, w_1 \geq -0.35, w_2 \leq 3.5, w_2 \geq -3.5\}\,. \tag{3.38}$$

The values $\mu = 0.01$ and $\gamma(\widetilde{w})$ were computed according to Algorithm 3,4. The ideal optimal input sequence $U_{Optimal}$ was computed according to (3.1), using Matlab® Global Optimization Toolbox, providing the minimum possible radius of information. Finally, a fifth input signal U_{SM-DoE} was obtained, using the proposed SM-DoE algorithm. For each of the five input signals, a dataset was obtained. Figure 3.3 shows the five input sequences.

In order to assess the quality of each dataset, a quasi-local set membership model was identified. Then, the prediction accuracy was validated on a 100×100 grid in the rectangular region defined in (3.38). The following accuracy indexes were considered to evaluate the model accuracy:

$$\begin{aligned} \text{RMSE} &= \|\widetilde{y} - \hat{y}\|_2 / \sqrt{N} \\ \text{FIT} &= 100\left(1 - \frac{\|\widetilde{y} - \hat{y}\|_2}{\|\widetilde{y} - \text{mean}(\widetilde{y})\|_2}\right) \end{aligned} \tag{3.39}$$

where $\widetilde{y}$ indicates the measured output vector and $\hat{y}$ is the predicted output vector and N is the length of these two vectors.

Table 3.1 shows the radius of information and the accuracy on the validation set of the identified set membership models for each input signal.

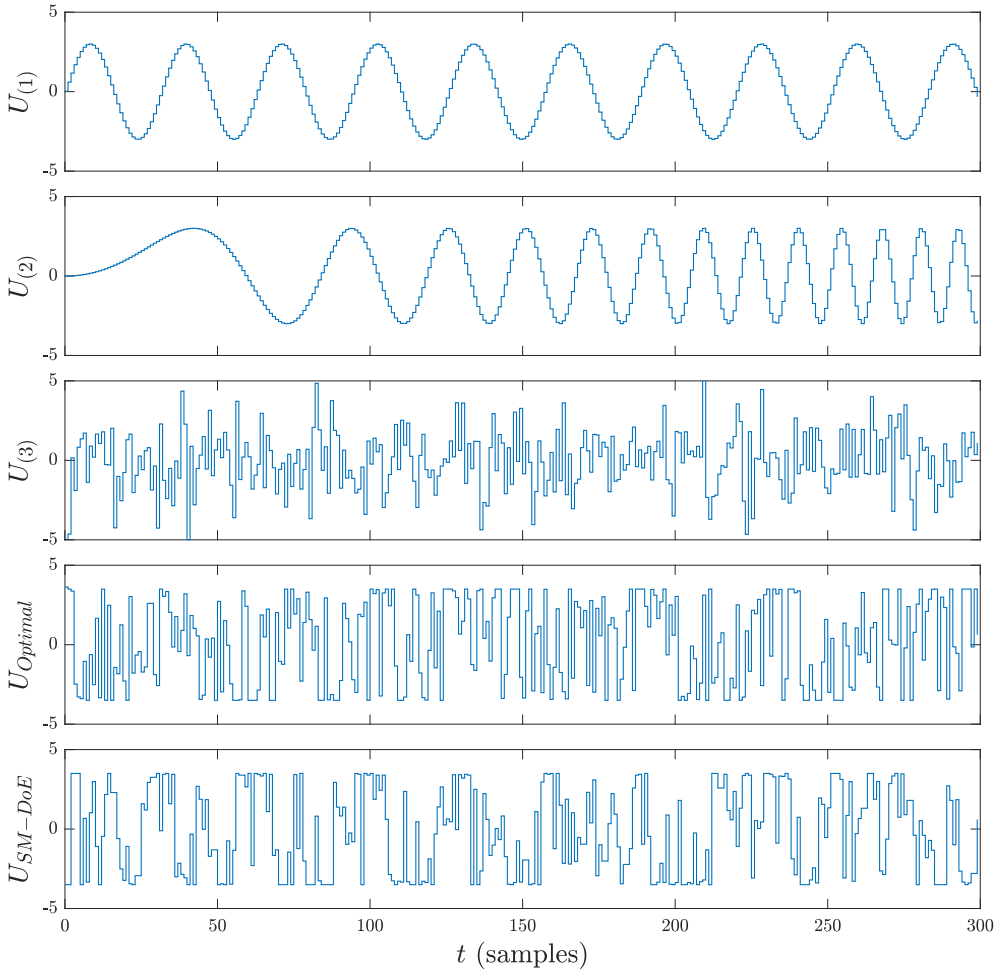

Figure 3.3: Input sequences.

Table 3.1: Radius of information and set membership model accuracy corresponding to the input sequences.

Inputs	$U_{(1)}$	$U_{(2)}$	$U_{(3)}$	$U_{Optimal}$	$U_{SM\text{-}DoE}$
$\mathcal{R}_{\mathcal{I}}^{\infty}$	0.568	0.536	0.209	0.053	0.055
$\mathcal{R}_{\mathcal{I}}^{2}$	0.210	0.177	0.055	0.030	0.033
RMSE	0.0391	0.0350	0.0214	0.0061	0.0062
FIT	0.69	0.72	0.85	0.96	0.96

It can be noted from Table 3.1 that the optimal input sequence and the SM-DoE sequence provide much lower radius of information compared to the sinusoidal and random inputs. The fact that the data generated from $U_{Optimal}$ and U_{SM-DoE} provides lower radius of information, and consequently a higher identification accuracy, is related to the more effective exploration of the regressor domain $\mathcal{W}$. This can be observed in Figure 3.4, where the "measured" regressors are shown for the five simulations.

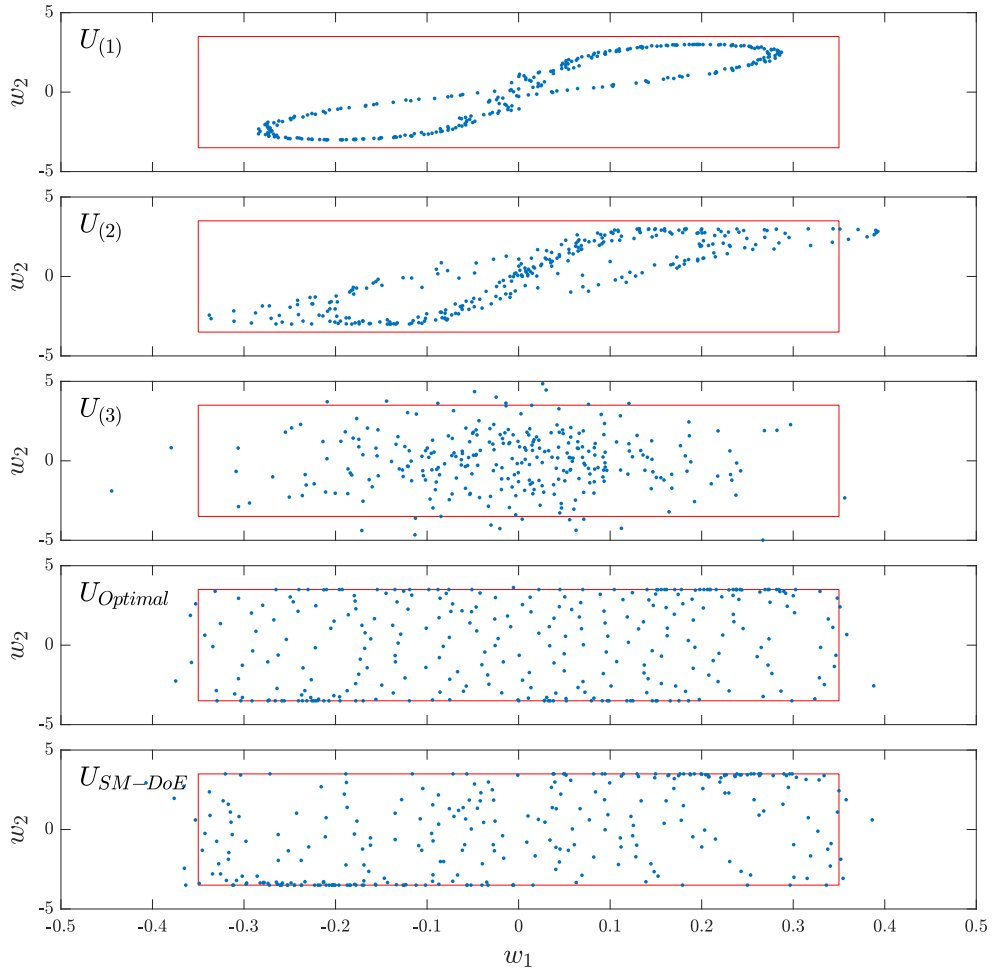

Figure 3.4: Measured regressor $\{\widetilde{y}^t, \widetilde{u}^t\}_{t=1}^{300}$ for different input sequences.

Figure 3.5 shows the radius of information and model accuracy during the SM-DoE process. It can be seen that only half of the experiment was enough to derive an accurate model. It is also evident that reducing the radius of information directly leads to increasing the model accuracy.

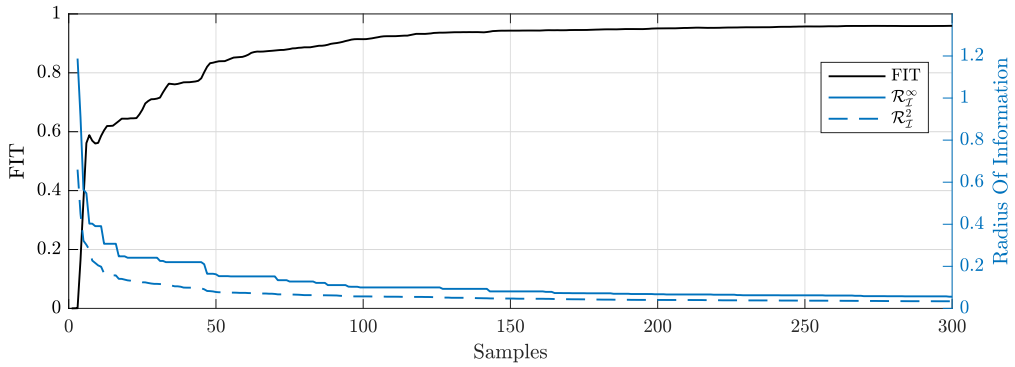

Figure 3.5: Radius of information and model accuracy during SM-DoE experiment.

3.5.2 Example 2:

To evaluate the performance of proposed SM-DoE compared to other DoE methods, a simulation study was performed considering a nonlinear dynamic system previously investigated by [10]. In this example, three different DoE methods, as well as the SM-DoE algorithm, were tested. The system under investigation is the following:

$$\dot{y} = g(y, x) = 2x/(2.4\cos(10x + 4) - 0.5y + 3.3). \tag{3.40}$$

where

$$\begin{aligned} x = f(u_1, u_2) = \cos(9\sqrt{u_1^2 + u_2^2} + 2) + 0.5\cos(11u_1 + 2) \\ + 15((u_1 - 0.4)^2 + (u_2 - 0.4)^2)^2. \end{aligned} \tag{3.41}$$

This system was discretized using forward Euler method with a sampling time of 0.5 s. The system has two inputs, and the single output of the system is corrupted by a uniform bounded noise of amplitude $\leqslant 0.025$. An illustration of the scaled functions of the system is shown in Figure 3.6. The function g of the discretized system is different from that of the continuous-time system.

Three different DoE strategies were used in order to compare with the SM-DoE algorithm, which are mentioned in section 3.1 and are discussed more in detail in [10]. Three distributions (random, LHC and D-optimal) were constructed with 50 design points that are shown in Figure 3.2. For each distribution, 10 different APRBS signals were constructed with a random sequence of the design points with

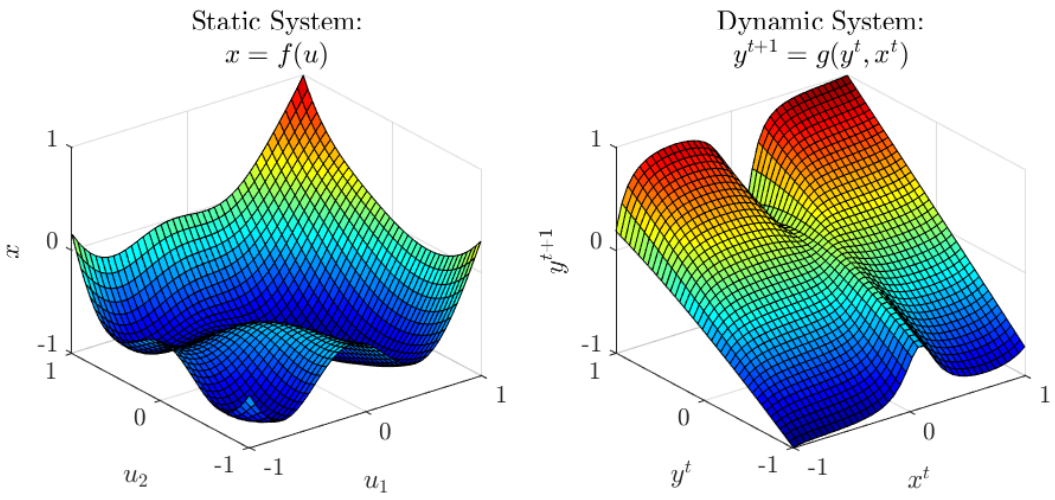

Figure 3.6: Nonlinear Dynamic System.

$T_{h_{min}} = 6s$ and duration of $T = 560s$. (a total of 30 input sequences). $T_{h_{min}}$ was chosen by trial and error which gave the best results.

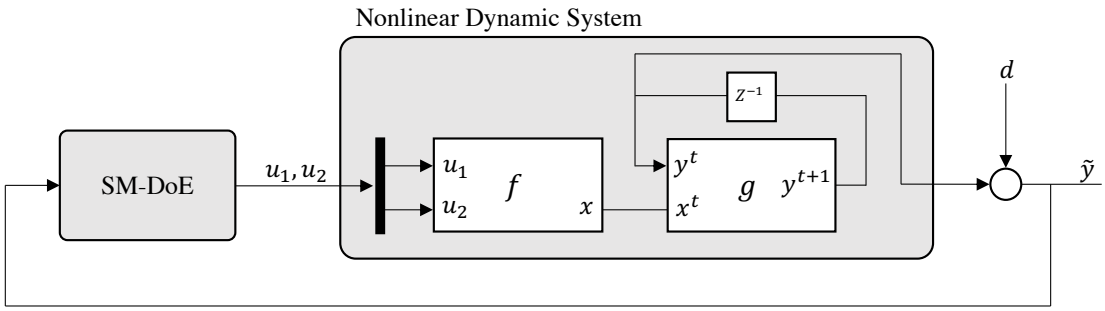

Figure 3.7: Set Membership DoE scheme.

In the SM-DoE algorithm, the regressor has been defined as $w^t = [y^t\ u_1^t\ u_2^t]$, and values $\mu = 0.05$ and $\Gamma = 10, \gamma(\tilde{w})$ were computed according to Algorithm 3,4. Algorithm 7 has been applied to the system according to Figure 3.7, with $\delta = 0.25$, $\lambda = 0.5$ and duration of $T = 560s$.

For each set of data generated by the considered input sequences, a Neural-Network model has been identified with 18 sigmoid neurons. Table 3.2 shows the identified model accuracy for each DoE method. This table shows that the accuracy of the model derived from SM-DoE data is significantly higher.

Table 3.2: Model accuracy mean and standard deviation.

Inputs	FIT	RMSE
Random	0.69 ± 0.03	0.149 ± 0.017
LHC	0.68 ± 0.04	0.155 ± 0.022
D-Optimal	0.76 ± 0.01	0.115 ± 0.008
SM-DoE	0.91	0.043

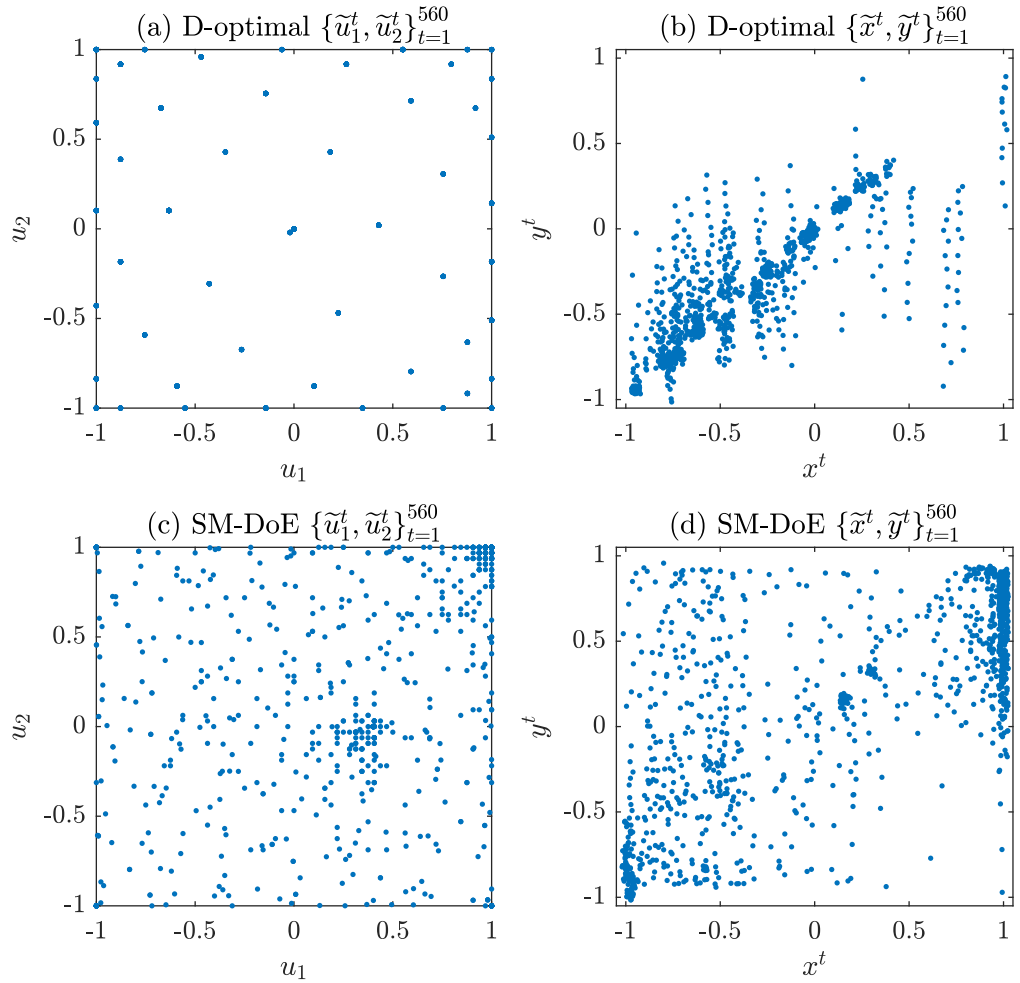

Figure 3.8: Measured regressor. D-optimal design (a),(b). SM-DoE (c),(d)

The measured regressors of the D-optimal design and the SM-DoE approach are shown in Figure 3.8. The domain is the same as the one in Figure 3.6. Both

the experiments have the same duration. In the D-optimal case, although the input space is covered very well (In Fig. 3.8(a), the design points are on top of each other due to the nature of the APRBS signal), we can see that the most nonlinear regions of the dynamic system are not explored (Fig. 3.8(b)), and the measurements are more concentrated around the diagonal which represents the steady state behavior of this system. Thus, the dynamic system nonlinearities are not captured by the data. On the other hand, the SM-DoE was able to better explore the whole regressor domain (Fig.3.8(c), 3.8(d)).

3.6 Conclusions

The aim of this chapter was to develop a systematic DoE method for nonlinear dynamic systems. We formulated the problem in a set membership framework and proposed a quasi-local nonlinear set membership approach that results in less conservative uncertainty bounds compared to the global approach. Then, we proposed a SM-DoE algorithm for input-constrained MISO nonlinear dynamic systems. The algorithm uses a novel SMPC controller to move the system toward the most uncertain regions of the regressor space and take new informative measurements. The proposed SM-DoE algorithm minimizes the worst-case model error. Thus, it is able to guarantee any desired worst-case error larger than the measurement error in a finite-time experiment. Applications of the proposed method are clearly most useful in areas where experiments are expensive and/or a very accurate model is desired. The DoE approach presented in this paper may also be of interest for future studies on adaptive data-driven nonlinear control design.

Chapter 4

From Design of Experiments to Data-Driven Control Design for Lean NO_x Trap Regeneration

4.1 Introduction

Diesel engines are widely used in passenger cars due to their high efficiency. However, diesel engines have higher emissions compared to spark-ignition (SI) engines, and these emissions should be reduced in order to increase the air quality and to meet the constraints imposed by government regulations. After-treatment systems are widely used for this aim. One important issue of these systems is NO_x reduction: since diesel engines usually operate in lean mode, they emit large quantities of NO_x. Indeed, during lean engine operations, the fuel is burned with an excess of air (the air-fuel ratio is leaner than stoichiometric), and this leads to an over-production of NO_x. On the contrary, in rich mode, the engine operates at an almost stoichiometric air-fuel ratio, implying a reduced NO_x production.

Lean NO_x Trap (LNT) is one of the most effective after-treatment technologies used to reduce NO_x emissions of diesel engines. The basic concept of LNT is to store NO_x during lean conditions and release the stored NO_x in rich conditions to react with the available reductants (HC and CO). Like any trapping system, LNTs have a finite capacity. Therefore, the engine must create rich exhaust conditions at given time intervals to regenerate the catalyst, which releases the stored NO_x and

converts it to nitrogen. A method for providing the necessary rich condition for LNT regenerations is using the engine control unit to create a rich air-fuel mixture ratio. This is an attractive approach since it uses actuators already available in the engine.

As shown in Figure 4.1, there are two main operating conditions for LNTs. In the first phase, called adsorption or storage phase, the engine works in a lean condition and the exhaust gas NO_x is chemically stored in the catalyst. In the second phase, called purge or regeneration, by injecting extra fuel in the cylinder, the engine moves to a rich condition and the NO_x is released from the catalyst to react with components of the rich exhaust gas, such as carbon monoxide (CO), hydrocarbons (HC) and hydrogen (H_2), to form nitrogen.

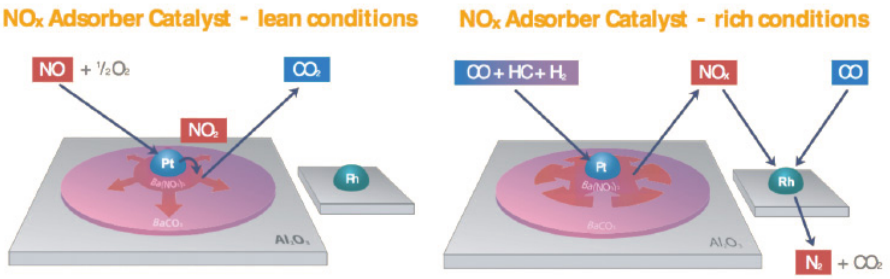

Figure 4.1: LNT storage and purge reactions.

Regeneration timing control plays a vital role in NO_x emission reduction with minimum fuel possible. One of the greatest challenges in this context is deriving an accurate model, able to describe the highly nonlinear dynamics of an LNT. Several studies have documented different approaches for modeling and control of the LNT. One approach is modeling the LNT based on chemical-physical processes [19, 34]. This approach in general yields accurate dynamic models. However, the derived models are complex from a computational point of view and thus they can be suitable for simulation but not for control. Other studies focus on control-oriented modeling [74, 31, 32, 6, 73]. Indeed, most of the control-oriented models proposed in the literature have been validated on stationary engine operating points and this raises questions about their accuracy, as they may show a poor performance in transient conditions. Moreover, the dynamics of newly developed LNT technologies may not be accurately described by the equations of the previous studies. Clearly, a controller designed from a non-accurate model may work well when applied to the model itself [27] but may lead to a very bad performance when applied to the plant of interest. Another approach is black box modeling using system identification. In [75] , a nonlinear autoregressive with exogenous input (NARX) model is used

to describe the LNT. This is an interesting approach since the model is simple and accurate enough for control. However, another fundamental problem is that, even in the rare cases where an accurate model can be found, designing an effective LNT control strategy using this model is difficult, due to the high complexity of the LNT process and to its strongly nonlinear behavior. These problems have led to threshold-based control strategies [31, 45], that are widely used thanks to their simplicity. However, since diesel engines are gaining more and more attention in light-duty applications, there is a need for more efficient algorithms to meet the emission regulations [30]. In other words, a nonlinear MIMO (Multiple Input Multiple Output) control design problem has to be solved, where the goal is to minimize on-line the fuel penalty, while keeping the NO_x emissions under a given level.

In this chapter, a novel approach for regeneration timing control of LNTs is proposed, allowing us to overcome all the issues discussed above. This approach, named data-driven model predictive control (D^2-MPC), does not require a physical model of the engine/trap system but is based on a neural network model, directly identified from data. In this way, all problems due to the fact that LNTs are highly complex systems difficult to model are overcome. However, acquiring the data necessary for identification is very challenging due to the expensive operating costs of the engine/after-treatment test benches and highly nonlinear dynamics of the after-treatment system. Therefore, we propose a Set-Membership Design of Experiments for the LNT which is able to capture nonlinear behavior of the system in a short experiment. The regeneration timing is computed through an optimization algorithm, which uses the identified model to estimate and predict the LNT behavior.

The proposed D^2-MPC approach is tested in a co-simulation study, where the plant is represented by a detailed LNT model, built using the well-known commercial tool AMEsim, and the controller is implemented in Matlab®/Simulink. The control strategy is then compared with other control approaches: The first one is an MPC strategy where a perfect knowledge of the plant is assumed so that the model used for prediction and optimization is the exact plant model. Clearly, this is an ideal strategy that can never be applied in a real situation. In our study, this ideal strategy is important to individuate the maximum performance that can be reached. The second one is an MPC strategy taken from the literature. The third one is a simple threshold-based strategy. This simulation study shows that the proposed D^2-MPC strategies provide very efficient regenerations with a minimum

fuel penalty. In particular, the provided values for these two performance indexes are very close to those provided by the ideal strategy, based on the exact model. On the other hand, the other two strategies provide fairly efficient regenerations, at the expense of quite high fuel penalties.

This chapter is organized as follows. In section 4.2, we present the outline of the D^2-MPC approach. In section 4.3, the engine and the after-treatment system model is described. In section 4.4, the SM-DoE method of Chapter 3 is implemented on the engine/after-treatment system and a neural network model is identified for the LNT. In section 4.5, the D^2-MPC for regeneration timing control of the LNT is presented. And finally, simulation results are given in section 4.6.

4.2 Outline of the Data-Driven Model Predictive Control Approach

In this section, the data-driven MPC approach is briefly outlined. Within this approach, a novel strategy will be developed in the following sections, aimed at LNT regeneration timing control.

Consider a nonlinear discrete-time MIMO system in regression form:

$$\begin{aligned} y^{t+1} &= g\left(\boldsymbol{u}^t, \boldsymbol{y}^t, \boldsymbol{v}^t, \boldsymbol{\xi}^t\right) \\ \boldsymbol{u}^t &= (u^t, \dots, u^{t-n+1}) \\ \boldsymbol{y}^t &= (y^t, \dots, y^{t-n+1}) \\ \boldsymbol{v}^t &= (v^t, \dots, v^{t-n+1}) \\ \boldsymbol{\xi}^t &= (\xi^t, \dots, \xi^{t-n+1}) \end{aligned} \tag{4.1}$$

where $u^t \in U \subset \mathbb{R}^{n_u}$ is the control input, $y^t = (y_1^t, \dots, y_{n_y}^t) \in \mathbb{R}^{n_y}$, with $y_i^t \in \mathbb{R}$, is the output, $v^t \in V \subset \mathbb{R}^{n_v}$ is a measured disturbance, $\xi^t \in \Xi \subset \mathbb{R}^{n_\xi}$ is an unmeasured disturbance, and n is the system order. U, V and Ξ are compact sets. In particular, $U \doteq [\underline{u}, \overline{u}]$ accounts for input saturation. The notation $(\dots, \dots, \dots)$ is used to indicate a column vector.
Suppose that the system (4.1) is unknown, but a set of measurements is available:

$$\mathcal{D} \doteq \left\{\tilde{u}^t, \tilde{y}^t, \tilde{v}^t\right\}_{t=1-L}^{0} \tag{4.2}$$

where $\tilde{u}^t$, $\tilde{v}^t$ and $\tilde{y}^t$ are bounded for all $t = 1-L, \dots, 0$. The tilde is used to indicate the input and output samples of the data set (4.2).
Let $\mathcal{Y}^0 \subseteq R^n$ be a set of initial conditions of interest, $R \subset \mathbb{R}^{n_y}$ a compact set, $\mathcal{R} \doteq \{\boldsymbol{r} = (r^1, r^2, \dots) : r^t \in R, \forall t\}$ a set of output sequences of interest, and $\mathcal{V} \doteq \{\boldsymbol{v} = (v^1, v^2, \dots) : v^t \in V, \forall t\}$ and $\Xi \doteq \{\boldsymbol{\xi} = (\xi^1, \xi^2, \dots) : \xi^t \in \Xi, \forall t\}$ the sets of all possible disturbance sequences.

The problem is to control the system (4.1) such that, for any $\boldsymbol{v} = (v^1, v^2, \dots) \in \mathcal{V}$ *and* $\boldsymbol{\xi} = (\xi^1, \xi^2, \dots) \in \Xi$*, and for any initial condition* $y^0 \in \mathcal{Y}^0$*, the output sequence* $\boldsymbol{y} = (y^1, y^2, \dots)$ *of the controlled system tracks any reference sequence* $\boldsymbol{r} = (r^1, r^2, \dots) \in \mathcal{R}$*.*

To solve this problem, we propose a data-driven model predictive control (D^2-MPC) approach. The first step of this approach is to identify from the data (4.2)

a prediction model for the system (4.1) of the form

$$\begin{aligned} \hat{y}_i^{t+k} &= f_i^k\left(\boldsymbol{u}^t, \boldsymbol{y}^t, \boldsymbol{v}^t\right) \equiv f_i^k\left(\boldsymbol{q}^t, u^t\right) \\ \boldsymbol{q}^t &= (u^{t-1}, \ldots, u^{t-n+1}, y^t, \ldots, y^{t-n+1}, v^t, \ldots, v^{t-n+1}) \end{aligned} \tag{4.3}$$

where u^t, v^t and y^t are the system inputs and output, $\hat{y}_i^{t+k}$ is the ith predicted output, $i = 1, \ldots, n$ indicates the output component, and $k = 1, \ldots, k_M$ is the prediction horizon. For simplicity, this model is supposed of the same order as the system (4.1) but this is not mandatory. See [50, 16, 48] for indications on the order choice. The following parametric structure is taken for the model functions f_i^k:

$$\begin{aligned} f_i^k\left(u^t, \boldsymbol{q}^t, \theta\right) &= \sum_{j=1}^{N} \alpha_j \phi_j\left(u^t, \boldsymbol{q}^t, \beta_j\right) \\ \theta &= [\alpha_1, \ldots, \alpha_N\, \beta_{11}, \ldots, \beta_{Nq}], \beta_j \in \mathbb{R}^q \end{aligned} \tag{4.4}$$

where ϕ_j are basis functions and θ are parameters to be identified. The basis function choice is in general a crucial step, [65, 28, 51]. In the present D^2-MPC approach, one-hidden layer sigmoidal neural networks are used.
The identification of the parameter vectors θ_i^k can be carried out as follows. Define

$$\tilde{\boldsymbol{y}}_i^k \doteq (\tilde{y}_i^{t_1+k}, \ldots, \tilde{y}_i^{t_2+k})$$

$$\Phi \doteq \begin{bmatrix} \phi_1\left(\tilde{u}^{t_1}, \tilde{\boldsymbol{q}}^{t_1}, \beta_1\right) & \cdots & \phi_N\left(\tilde{u}^{t_1}, \tilde{\boldsymbol{q}}^{t_1}, \beta_N\right) \\ \vdots & \ddots & \vdots \\ \phi_1\left(\tilde{u}^{t_2}, \tilde{\boldsymbol{q}}^{t_2}, \beta_1\right) & \cdots & \phi_N\left(\tilde{u}^{t_2}, \tilde{\boldsymbol{q}}^{t_2}, \beta_N\right) \end{bmatrix}$$

where $t_1 \doteq 1-L+n$, $t_2 \doteq -k_M$, $\tilde{\boldsymbol{q}}^t = (\tilde{u}^{t-1}, \ldots, \tilde{u}^{t-n+1}, \tilde{y}^t, \ldots, \tilde{y}^{t-n+1}, \tilde{v}^t, \ldots, \tilde{v}^{t-n+1})$, and $\tilde{u}^t$, $\tilde{y}^t$ and $\tilde{v}^t$ are the input-output measurements of the data set (4.2). The parameter vector θ_i^k is obtained solving the following optimization problem:

$$\theta_i^k = \arg\min_{\theta} \left\| \tilde{\boldsymbol{y}}_i^k - \Phi\alpha \right\|_2 \tag{4.5}$$

Once a model of the form (4.3) has been identified, the command action u^{t*} of the D^2-MPC controller is obtained solving on-line the optimization problem

$$\begin{aligned} u^{t*} \quad = \quad & \arg\min_{\mathfrak{u} \in U} J\left(\mathfrak{u}, f\left(\boldsymbol{q}^t, \mathfrak{u}\right)\right) \\ & \text{subject to} \;\; C\left(\mathfrak{u}, f\left(\boldsymbol{q}^t, \mathfrak{u}\right)\right) \leq 0 \end{aligned} \tag{4.6}$$

where J is a suitable objective function, C is a function defining the constraints of the optimization problem and $f = (f_1^1, \ldots, f_1^{k_M}, \ldots, f_n^1, \ldots, f_n^{k_M})$. The objective function and constraints will be specified below for the LNT control problem considered in this chapter.

4.3 After-treatment System Model

4.3.1 Lean NO_x Trap Dynamics

As outlined in the introduction, LNTs work in storage and purge modes. When the engine is working in lean conditions the emitted NO_x are chemically stored in the LNT. The simplified chemical reactions are the following:

Storage:

$$\mathrm{NO} + \tfrac{1}{2}\,\mathrm{O_2} \longrightarrow \mathrm{NO_2}$$
$$2\,\mathrm{NO_2} + \mathrm{BaCO_3} + \tfrac{1}{2}\,\mathrm{O_2} \longrightarrow \mathrm{Ba(NO_3)_2} + \mathrm{CO_2}$$

Since the storage capacity is limited, the trap needs to be regenerated periodically. In the purge mode, by injecting extra fuel in the cylinder, a rich condition is created. In this mode, the stored NO_x is released from the trap and then converted to nontoxic gases such as N_2 by the available reductants. The simplified chemical reactions are the following:

Purge:

Release:

$$\mathrm{Ba(NO_3)_2} \longrightarrow \mathrm{BaO} + 2\,\mathrm{NO_2} + \tfrac{1}{2}\,\mathrm{O_2}$$
$$\mathrm{BaO} + \mathrm{CO_2} \longrightarrow \mathrm{BaCO_3}$$

Conversion:

$$\mathrm{NO_2} \longrightarrow \mathrm{NO} + \tfrac{1}{2}\,\mathrm{O_2}$$
$$\mathrm{NO} + \mathrm{CO} \longrightarrow \mathrm{CO_2} + \tfrac{1}{2}\,\mathrm{N_2}$$
$$(2\,\mathrm{m} + \mathrm{n}/_2)\mathrm{NO} + \mathrm{CmHn} \longrightarrow \mathrm{mCO_2} + (\mathrm{m} + \mathrm{n}/_4)\mathrm{N_2} + \mathrm{n}/_2\mathrm{H_2O}$$
$$\mathrm{NO} + \tfrac{5}{2}\,\mathrm{H_2} \longrightarrow \mathrm{NH_3} + \mathrm{H_2O}$$

More realistically, there are dozens of chemical reactions occurring at the same

time. Therefore, building a model that accurately captures the NO_x storage and release dynamics is very difficult. As far as the authors are aware, all the existing methods for modeling the LNT strongly rely on simplistic physical descriptions of the system dynamics [31, 6, 32]. Such approaches suffer from two main drawbacks: 1) The effects due to simplifying assumptions for the exhaust gas composition and reaction dynamics; 2) the dynamics of the LNT changes with aging.

In this chapter, according to the D^2-MPC approach described in Section 4.2, we control the regeneration timing of the LNT using a prediction model derived from data, thus avoiding any under-modeling issue. One advantage of our approach is that it can be relatively simply made adaptive: by using the sensors that exist on the vehicle, data can be collected in order to tune on-line the prediction model, in order to account for the LNT changes with aging. In industrial applications, the required data are typically generated by a physical plant, through various experiments. In the present work, a real engine/after-treatment is not available and a detailed model is used instead. Future activities will focus on the application of our control approach to a real diesel engine with after-treatment system.

4.3.2 AMEsim Model

A detailed lean burn engine model with after-treatment system was build in AMEsim, a standard commercial software for modeling, simulation, and analysis of multi-domain systems. In the AMEsim software, there exist a number of libraries dedicated to powertrain analysis. In particular, IFP-Drive library is used that is developed for simulation and analysis of fuel consumption, emissions and vehicle performance [37]. As it is shown in Figure 4.2, the after-treatment system model is coupled with a vehicle model that includes a model for a 2L engine, transmission, powertrain, and driver. The model can be tuned with real engine/after-treatment data and thus can be considered as a faithful representation of a real plant.

In this chapter, the AMEsim detailed model represents the "true" plant to control. It will be used to generate the data necessary for D^2-MPC design and also to test all the designed controllers. In particular, the controller tests will be carried out in AMEsim/Matlab® co-simulation, to reproduce a real-world scenario in which the plant and the controller are "physically separated". It is important to remark that the control design procedure presented below can be applied without significant modifications also when the plant to control is a real engine and not a

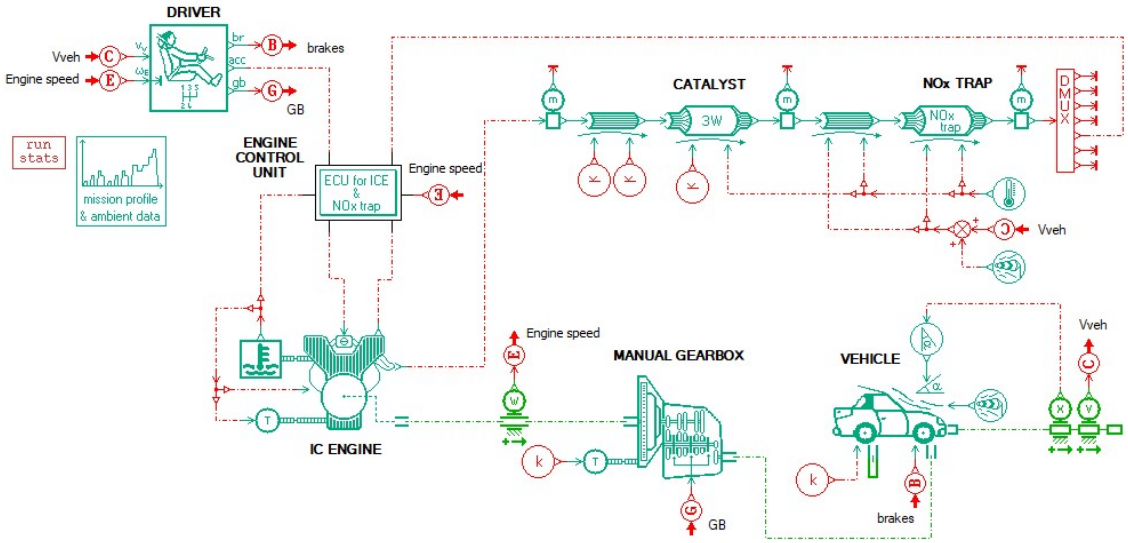

Figure 4.2: AMEsim vehicle model with after-treatment system.

simulation model.

4.4 Design of Experiments for Lean NO_x Trap

The regeneration control strategy that we propose in section 4.5 is based on the estimation of the amount of NO_x stored in the LNT. In order to have efficient regenerations, the control algorithm predicts the amount of NO_x stored in the LNT and then decides if a regeneration is necessary via optimization. For this reason, we need to identify a model of the LNT. The first step to identify a model is to acquire data from the plant. The goal here is to apply the Set Membership DoE algorithm (SM-DoE) of Chapter 3 in order to minimize the experimental effort and acquire a rich dataset for identification by capturing the nonlinear behavior of the LNT in the whole working domain of the system. It is worth mentioning that the DoE algorithm was implemented with special attention to be as close as possible to a real scenario, therefore it can easily be applied in a real engine/after-treatment test bench.

4.4.1 Simulation Setup

According to Figure 4.3, an engine test bench with after-treatment system is simulated in AMEsim software. The engine is connected to a dynamometer which can run the engine to any desired speed. The inputs are the engine speed command to the dynamometer ($u_{V_{eng}}$), the load command to the ECU (u_{Load}) and a regeneration command to the ECU (u_{Regen}) which is a binary signal that changes the combustion mode of the engine to a rich mode with fuel-air equivalence ratio $\phi = 1.2$. The outputs that can be measured by the available sensors in the test bench are LNT wall temperature, fuel-air equivalence ratio (ϕ), exhaust gas flow rate ($\dot{m}_{EG}$) and exhaust NO_x flow rate ($\dot{m}_{NO_x}$). Note that the NO_x stored quantity in the LNT cannot be measured directly. However, it can be computed from exhaust gas composition in the test bench.

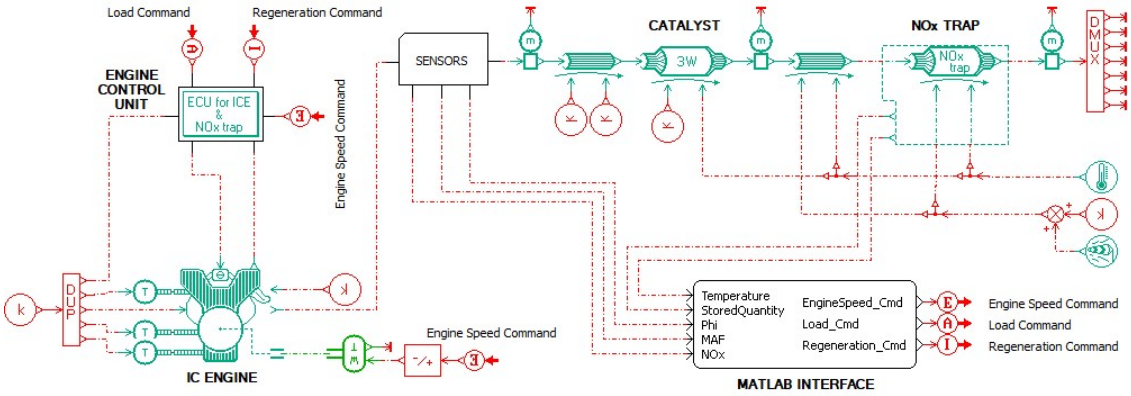

Figure 4.3: Test bench simulation setup - AMEsim/Matlab® co-simulation.

4.4.2 Set Membership Design of Experiments

In this section, we implement the set membership design of experiment algorithm which is discussed in Chapter 3.

The goal is to build a simulation model of the NO_x stored quantity in the LNT. Thus, the DoE aim is to acquire a rich dataset for building such model with possibly low experimental effort. The model is of the form 2.1, with

$$
\begin{aligned}
y^{t+1} &= f(y^t, u^t) \\
u &= [u_{Temp} \quad u_\phi \quad u_{\dot{m}_{EG}} \quad u_{\dot{m}_{NO_x}}]
\end{aligned}
$$

$$
\begin{aligned}
y &: \quad \text{NO}_\text{x} \text{ stored quantity} \\
u_{Temp} &: \quad \text{LNT wall temperature} \\
u_\phi &: \quad \text{fuel-air equivalence ratio} \\
u_{\dot{m}_{EG}} &: \quad \text{exhaust gas flow rate} \\
u_{\dot{m}_{NO_x}} &: \quad \text{exhaust NO}_\text{x} \text{ flow rate}
\end{aligned}
\tag{4.7}
$$

As mentioned in section 4.4.1, the test bench inputs that can be manipulated are $u_{V_{eng}}$, u_{Load}, u_{Regen}. Thus, none of the model inputs u can be manipulated directly as it is required by the DoE algorithm. However, the three inputs u_ϕ, $u_{\dot{m}_{EG}}$, $u_{\dot{m}_{NO_x}}$ are functions of engine speed, load command and combustion mode which are available from the engine lookup tables. Three sets of data is available for this engine for three combustion modes; stoichiometric $\phi = 1$, lean $\phi < 1$ and rich $\phi = 1.2$ modes.

$$
\begin{aligned}
T_{eng} &= f_T(V_{eng}, L_{cmd}, C_{mode}) \\
\phi &= f_\phi(V_{eng}, T_{eng}, C_{mode}) \\
\dot{m}_{EG} &= f_{\dot{m}_{EG}}(V_{eng}, T_{eng}, C_{mode}) \\
\dot{m}_{NO_x} &= f_{\dot{m}_{NO_x}}(V_{eng}, T_{eng}, C_{mode})
\end{aligned}
\tag{4.8}
$$

where V_{eng} is the engine speed, T_{eng} is the engine torque, L_{cmd} is the load command to the ECU and C_{mode} is the combustion mode. Therefore, by generating $u_{V_{eng}}$, u_{Load}, u_{Regen} we can directly manipulate inputs of the model (4.7).
The SM-DoE algorithm is performed on the system according to the scheme shown in Figure. 4.4, 4.3.

The regressor domain of interest $\mathcal{W}$ and the pseudo-state is constructed as following

$$
\begin{aligned}
w^t =& [y^t \quad u^t_{Temp} \quad u^t_{\phi} \quad u^t_{\dot{m}_{EG}} \quad u^t_{\dot{m}_{NO_x}}].\\
x^t =& [y^t \quad u^t_{Temp}].\\
\mathcal{W} \doteq& \{w_1, w_2 : 0 \leqslant w_1 \leqslant 2.5, \quad 20 \leqslant w_2 \leqslant 430,\\
& \quad w_3, w_4, w_5 : 700 \leqslant u_{V_{eng}} \leqslant 4000, \quad 0 \leqslant u_{Load} \leqslant 100, \quad u_{Regen} \in \{0,1\}\}.\\
\mathcal{X} \doteq& \{x_1, x_2 : 0 \leqslant x_1 \leqslant 2.5, \quad 20 \leqslant x_2 \leqslant 430\}.
\end{aligned}
\tag{4.9}
$$

w_1, x_1 is the NO_x stored quantity which can be between 0 and 2.5 grams, w_2, x_2 is the LNT temperature which can be between $20°C$ and $430°C$. The other three inputs can have specific values depending of the engine speed, load and regeneration command according to the engine maps eq.(4.8).

Please note that regardless of the DoE method, the first input that is the temperature of the LNT cannot be manipulated. Once we start an experiment with an initial LNT temperature and an initial NO_x stored quantity in the LNT, it is impossible to reach some regions of the regressor domain (Assumption 3 is not satisfied). For example, imagine the experiment is started with the LNT temperature equal to the ambient temperature and NO_x stored quantity equal to zero. i.e. $x^t = [0 \quad 30]$. It takes a certain amount of time for the LNT to store NO_x, and in the meanwhile, the LNT temperature will rise. Thus, it is impossible to take any measurement where the LNT temperature is equal to the ambient temperature and NO_x stored quantity other than zero e.g. $x^r = [1 \quad 30]$.

In order to overcome this issue, one solution is to split the DoE into multiple experiments, and each experiment starts with an initial LNT temperature and initial NO_x stored quantity which has the maximum radius of information at the end of the previous experiment. Therefore, we can be sure all the regressor domain is somehow reachable. This is also possible to be applied in a real test bench where we can wait for the LNT to cool down between experiments.

The SM-DoE is applied to the system according to Figure 4.4 and Algorithm 7 of Chapter 3 which is repeated here as Algorithm 8 for the ease of the reader.

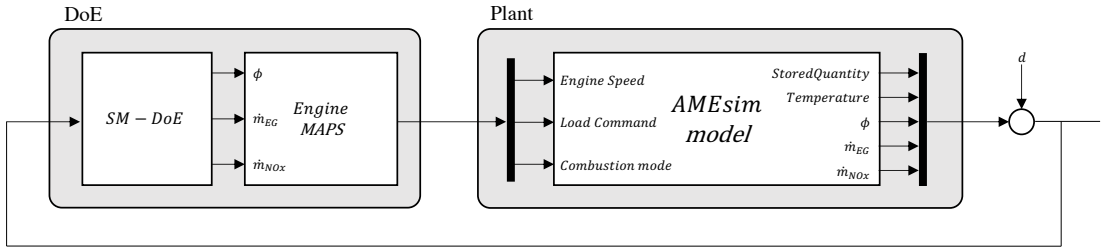

Figure 4.4: Set Membership Design of Experiments for LNT.

Algorithm 8 Dynamic Set Membership DoE for LNT

1. Select a reference regressor w^r to be visited which has a high uncertainty and its equivalent pseudo-state is close to the estimated state.

$$w^r, x^r = \arg \min_{w^r \in \mathcal{W}, x^r \in \mathcal{X}} (\left\| \widehat{x}^{t+1} - x^r \right\|_2 + \frac{\delta}{f_e(w^r)}) \tag{4.10}$$

2. Compute $\mathcal{X}_r$ according to (3.17) with a suitable λ.

3. Apply the following criterion:

$$\begin{aligned} &\text{if} && \widehat{x}^{t+1} \in \mathcal{X}_r \\ &\text{then} && u^t = u^r \in w^r \\ &\text{else} && u^t = \mathcal{K}(x^r, x^t) \end{aligned}$$

4. Apply the input to the plant and take the measurement i.e. $\widetilde{y}^{t+1} = f_o(\widetilde{w}^t) = f_o(x^t, u^t)$

5. Add $\widetilde{y}^{t+1}$ and $\widetilde{w}^t$ to the dataset $\mathcal{D} := \mathcal{D} \cup \{\widetilde{y}^{t+1}, \widetilde{w}^t\}$.

6. Update γ and Γ according to Algorithm 4.

7. Set $t = t + 1$ and go to step (1).

In step three the control law indicated as $u^t = \mathcal{K}(x^t, x^r)$ means solving (3.21) and applying the first element of the maximizer U_t^{i*} as control action u^{t*}. Implementing this SMPC controller is computationally expensive therefore in this example we propose the following controller that is more computationally tractable.

$$u^t = \mathcal{K}(x^r, x^t) = \arg\min_{u \in \mathcal{U}} (\|\hat{x}^{t+k} - x^r\|_2 - \alpha \sum_{\tau=1}^{k} f_e(\hat{w}^{t+\tau})). \tag{4.11}$$

where $\hat{x}^{t+k}, \hat{w}^{t+\tau}$ are the multi-step central estimate according to Equation (3.12), k is the prediction horizon and α is a tuning variable.

In the next section, a neural network model for the LNT has been identified using the data generated by the SM-DoE algorithm. For comparison, another set of data was also generated as follows. 20 experiments each one for a duration of 500 seconds starting with a random initial LNT temperature and initial NO_x stored quantity. For inputs $u_{V_{eng}}$, u_{Load}, two APRBS signals with a random distribution of the design points were used. And for the input u_{Regen} 10 random regenerations were performed for each experiment. (A total of 20000 samples data including 200 regenerations).

Table 4.1 shows the radius of information of the data generated by the SM-DoE algorithm and the data generated by the APRBS-Random strategy. Despite the fact that the duration of the SM-DoE experiment is much shorter i.e. much less experimental effort, the radius of information is much lower. Therefore, we can expect the model identified from SM-DoE data to be much more accurate which is shown in the next section.

Table 4.1: Radius of information of the data generated by SM-DoE and APRBS-Random input sequence.

Inputs	Duration (Samples)	$\mathcal{R}_{\mathcal{I}}^{\infty}$	$\mathcal{R}_{\mathcal{I}}^{2}$
APRBS-Random	20000	1.03	0.22
SM-DoE	3000	0.36	0.07

4.4.3 NO_x Stored Quantity Estimation Model

Two neural network NARX models were identified using the set of data generated by the SM-DoE algorithm and the data generated by APRBS-Random strategy. The model is of the form (4.3), with

- $\hat{y}^{t+k}$: predicted amount of NO_x stored in the LNT,

- $v^t = (u^t_{Temp} \quad u^t_{\phi} \quad u^t_{\dot{m}_{EG}} \quad u^t_{\dot{m}_{NO_x}})$: measured inputs,
- $\boldsymbol{y}^t = (\hat{y}^t, \ldots, \hat{y}^{t-n+1})$, where the $(\,\hat{\cdot}\,)$ indicates the output values predicted by the model in the previous time steps,
- $k = k_M = 1$.
- $n = 1$,
- sampling time = 0.5 s.

Note that the model uses the output values predicted in the previous time steps by the model itself, and thus works in simulation. As mentioned earlier, the reason is that we assume y^t cannot be measured in normal operating conditions, as it happens in standard LNT configurations.

In order to assess the quality of each model, the models were validated on another set of data not used for identification. The validation dataset was generated as follows. 10 set of data each one with a duration of 1180 seconds during the NEDC driving cycle with random initial LNT temperature and random initial NO_x stored quantity and 10 random regenerations (A total of 23600 samples including 100 regenerations). The following accuracy indexes were considered to evaluate the models accuracy:

$$\begin{aligned} \text{RMSE} &= \|\tilde{y} - \hat{y}\|_2 / \sqrt{N} \\ \text{FIT} &= 100 \left(1 - \frac{\|\tilde{y} - \hat{y}\|_2}{\|\tilde{y} - \text{mean}(\tilde{y})\|_2}\right) \end{aligned} \tag{4.12}$$

where $\tilde{y}$ indicates the measured output sequence and $\hat{y}$ is the simulated output sequence and N is the length of these two sequences.

As it is shown in Table 4.2, the model that is identified from SM-DoE data is significantly more accurate with much less amount of data.

Table 4.2: Accuracy of the models identified from SM-DoE and APRBS-Random data.

Inputs	Duration (Samples)	RMSE	FIT	$\mathcal{R}^{\infty}_{\mathcal{I}}$	$\mathcal{R}^{2}_{\mathcal{I}}$
APRBS-Random	20000	0.11 ± 0.12	0.65 ± 0.49	1.03	0.22
SM-DoE	3000	0.03 ± 0.007	0.90 ± 0.03	0.36	0.07

In the remaining of this chapter the model is referred to the one that is identified form SM-DoE data. Figure 4.5, shows the simulation accuracy of the model validated using the NEDC driving cycle with zero initial NO_x stored quantity, $30°C$ initial LNT temperature, and 10 random regenerations. The obtained model FIT is 93% with a root-mean-square error (RMSE) of 0.03.

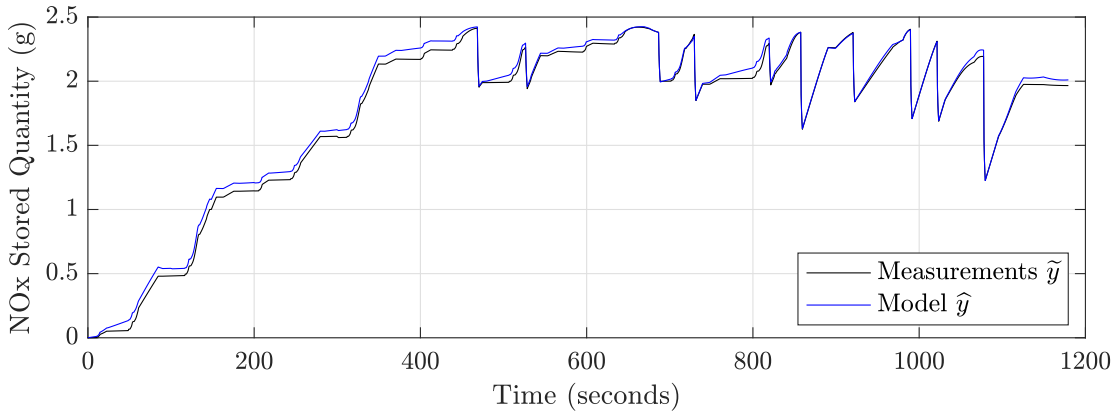

Figure 4.5: Validation of the NO_x stored quantity simulation model during the NEDC driving cycle.

4.5 Regeneration Timing Control: Data-Driven Model Predictive Control

In order to regenerate the LNT, extra fuel is injected in the cylinder to create a rich condition, and this causes a higher fuel consumption. A great challenge is to determine the best timing for regeneration in order to reduce the fuel consumption and the NO_x emissions. To accomplish this task, we consider the following criteria:

- Reducing the amount of extra fuel used for the regeneration of the LNT;
- Maximizing the amount of NO_x removed from the trap in each regeneration;
- Keeping the tailpipe NO_x emissions below a given level (defined on the basis of the government regulation holding in the country of interest).

To formalize these criteria, we first need to specify the form of the LNT command input u^t. As explained above, this command is the LNT regeneration trigger,

i.e., a binary variable enabling the regeneration when equal to 1 and disabling it when equal to 0 (changing the combustion mode of the engine to a rich mode). Hence, u_t can be defined as

$$u^t = \begin{cases} 0 & t < t_1, t > t_2 \\ 1 & t_1 \leq t \leq t_2 \end{cases} \tag{4.13}$$

where t_1 and t_2 are the regeneration start and stop times, respectively. These times determine the regeneration timing and are the control variables to choose at each time step in order to satisfy the above three criteria.

The first criterion is as follows. The amount of extra fuel used for the regeneration of the LNT is said the *fuel penalty* and is defined as

$$\begin{aligned} FP(t_1, t_2) = \quad & \sum_{t=t_1}^{t_2} \left(\phi^t_{reg} - \phi^t_{eng}\right) \frac{\dot{m}^t_{EG}}{AFR_{stoich}} \\ \dot{m}^t_{EG}: \quad & \text{mass air flow rate (g/s)} \\ AFR_{stoich}: \quad & \text{stoichiometric air fuel ratio} \\ \phi^t_{reg}: \quad & \text{fuel-air equivalence ratio during regeneration} \\ \phi^t_{eng}: \quad & \text{fuel-air equivalence ratio without regeneration} \end{aligned} \tag{4.14}$$

The first criterion thus consists in minimizing, at each time t, $FP(t_1, t_2)$ with respect to (t_1, t_2).

Note that as discussed later in this section, the control algorithm predicts the fuel penalty of a regeneration. Since $\dot{m}^t_{EG}$ and ϕ^t are known functions of engine speed and engine torque (4.8), this prediction is done by assuming linear trend models for engine speed and engine torque as shown in equation (4.15).

$$\begin{aligned} V^{t+k}_{eng} &= V^t_{eng} + k(V^t_{eng} - V^{t-1}_{eng}), \\ T^{t+k}_{eng} &= T^t_{eng} + k(T^t_{eng} - T^{t-1}_{eng}). \end{aligned} \tag{4.15}$$

Then, $\dot{m}^t_{EG}$ and ϕ^t in the receding horizon are obtained as functions of V^t_{eng} and T^t_{eng} by the engine maps that are available on the ECU (4.8).

The second criterion can be formalized as follows. Using the prediction model identified in section 4.4.3 for the NO_x stored quantity, the amount of NO_x that is

removed from the trap is estimated by the following quantity:

$$\hat{y}^{t+t_1} - \hat{y}^{t+t_2} \tag{4.16}$$

The second criterion is thus maximizing, at each time t, $\hat{y}^{t+t_1} - \hat{y}^{t+t_2}$ with respect to (t_1, t_2). Note that, as explained in Section 4.4.3, the prediction model for y^t works in simulation. Hence, the multi-step prediction in (4.16) is obtained via simulation.

The first and second criteria can be combined to have a unique criterion, that is minimizing with respect to (t_1, t_2) the following objective function:

$$J(t_1, t_2) \equiv J(t, t_1, t_2) = \frac{FP(t_1, t_2)}{\hat{y}^{t+t_1} - \hat{y}^{t+t_2}}. \tag{4.17}$$

The third criterion can be addressed by imposing a constraint on the cost function $J(t_1, t_2)$, which gives a tradeoff between fuel penalty and tailpipe NO_x emissions.

The final regeneration command is obtained by Algorithm 9.

Algorithm 9 LNT Regeneration Timing Control

1: Compute V_{eng}^{t+k} , T_{eng}^{t+k} for $k \in [0, K_M]$ according to (4.15).
2: Solve optimization problem:

$$(t_1^*, t_2^*) = \arg \min_{0 \le t_1 < t_2 \le k_M} J(t_1, t_2) \tag{4.18}$$

by computing ϕ^{t+k}, $\dot{m}_{EG}^{t+k}$, $\dot{m}_{NOx}^{t+k}$ according to (4.8) that is a function of V_{eng}^{t+k}, T_{eng}^{t+k}, t_1 and t_2. And, by simulating the LNT model starting from $\hat{y}^t$ to $\hat{y}^{t+k}$.
3: **if** $J(t_1^*, t_2^*) \leqslant$ Threshold **then**
4: $u^* = u_t$
5: **else**
6: $u^* = 0$
7: **end if**
8: Set $t = t + t_s$ and go to step (1).

where Threshold is a bound imposed to have not too high values of the objective function. In practice, the Threshold is a design parameter tunable to achieve the

desired performance. As it is shown in Figure 4.8.

The prediction horizon $k_M = 5$ seconds was chosen by means of a trial and error procedure: it was observed that larger values of k_M do not provide a better performance and require a bigger computational effort. The control sampling time is $t_s = 0.5$ second, implying that the optimization problem (4.18) is solved every 0.5 second. Note that this task can be accomplished quite easily, since both t_1 and t_2 can assume only 10 values and $t_2 > t_1$, so that the maximum number of function/constraint evaluations needed at each time step to find the global solution is non-larger than 55. The D^2-MPC and the plant scheme is shown in Figure 4.6, 4.7.

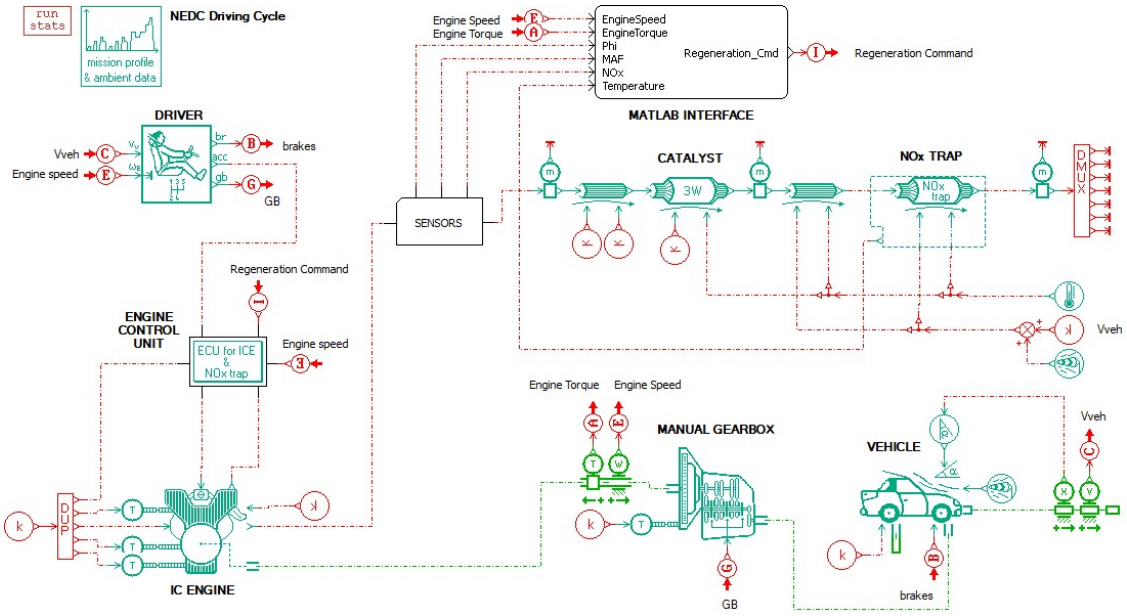

Figure 4.6: Plant scheme for regeneration timing control.

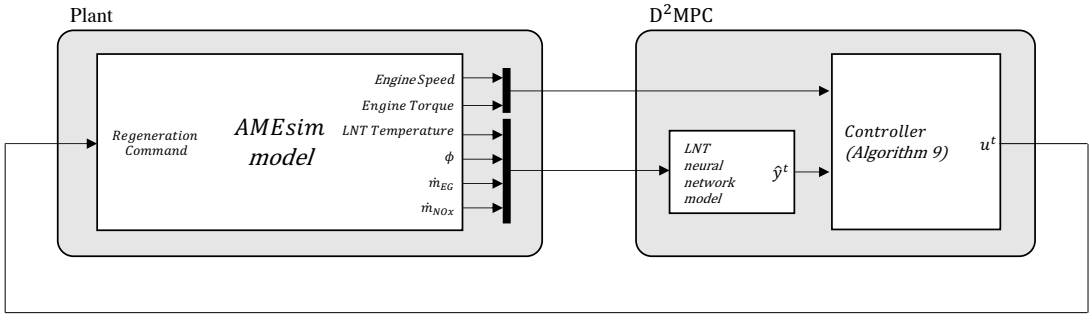

Figure 4.7: D^2-MPC scheme for regeneration timing control.

4.6 Simulation Results

As discussed above, the aim of the regeneration timing control is to minimize the fuel consumption and convert the NO_x trapped inside the catalyst to N_2 as much as possible.

The detailed lean burn engine model with after-treatment system of Section 4.3.2, developed in AMEsim was assumed to be the real plant to control (see Figure 4.6). The D^2-MPC controller was implemented in Matlab®/Simulink. A co-simulation AMEsim/Matlab® was carried out, with the AMEsim model connected in feedback with the controller implemented in Matlab®/Simulink (see Figure 4.7). The NEDC driving cycle was considered for this simulation.

Figure 4.8 shows the performance of the controller for different threshold values of the Algorithm 9 where the threshold value 0.4 shows a good tradeoff between fuel penalty and tailpipe NO_x emissions.

Figure 4.9 shows the regeneration trigger timing, the NO_x stored quantity, the catalyst temperature, and the tailpipe NO_x emissions. The first thing to notice is the accuracy of the model which is very close to the actual NO_x stored quantity in the LNT. The second thing to notice is the considerable amount of NO_x removed from the trap with short regenerations which is an indication of efficient regenerations. From the dynamics of the LNT, we know that when the LNT temperature is low, the regenerations are not efficient, therefore it can be seen that no regenerations were made when the LNT temperature is below $200°C$.

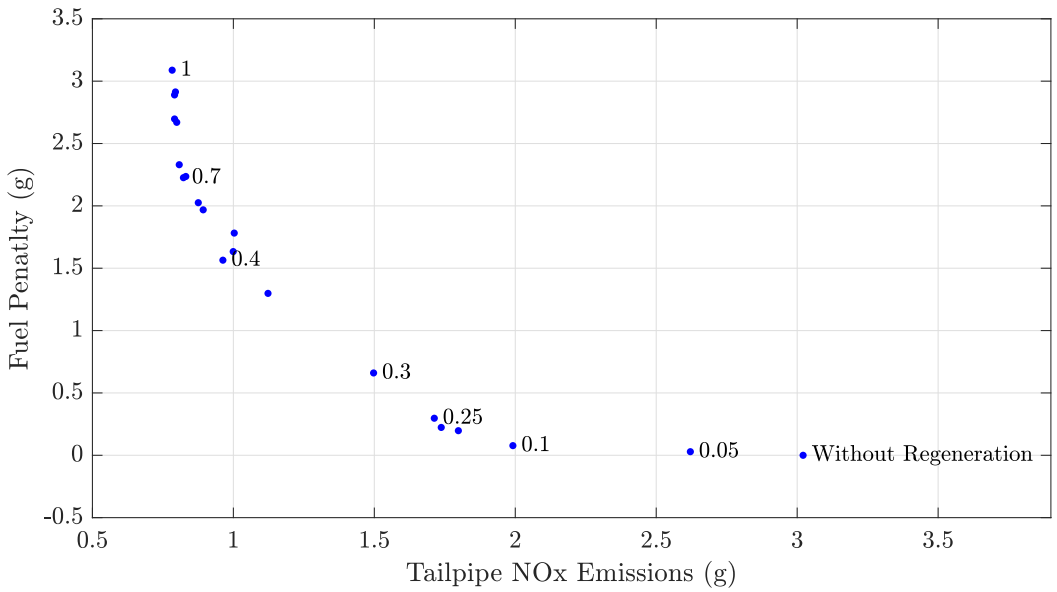

Figure 4.8: D^{2}MPC controller with different threshold values during the NEDC driving cycle.

As discussed in section 4.4.3, the LNT model works in simulation. Therefore, the initial state of the NO_x stored quantity is important for the model simulation. However, because of the dynamics of the LNT, regardless of the initial state, the estimated NO_x stored quantity gets very close to the real value in a short amount of time. Figure 4.10 shows the D^{2}MPC controller with the LNT model starting from a wrong initial state value. If we compare Figure 4.10 with Figure 4.9, we can see the first three regenerations were not efficient because the controller thinks the LNT is nearly full. However, the overall performance of the controller is not much different from the case where the initial state is the true value. As it is shown in Figure 4.11.

Three other controllers were implemented for comparison:

- Ideal MPC: MPC controller, where a perfect knowledge of the plant is assumed so that the model used for prediction and optimization is the exact plant model. Clearly, this is an ideal strategy that can never be applied in a real situation. In our study, this ideal strategy is important to individuate the maximum performance that can be reached.
- Controller 3: MPC controller taken from [27]. This is a nonlinear MPC, with

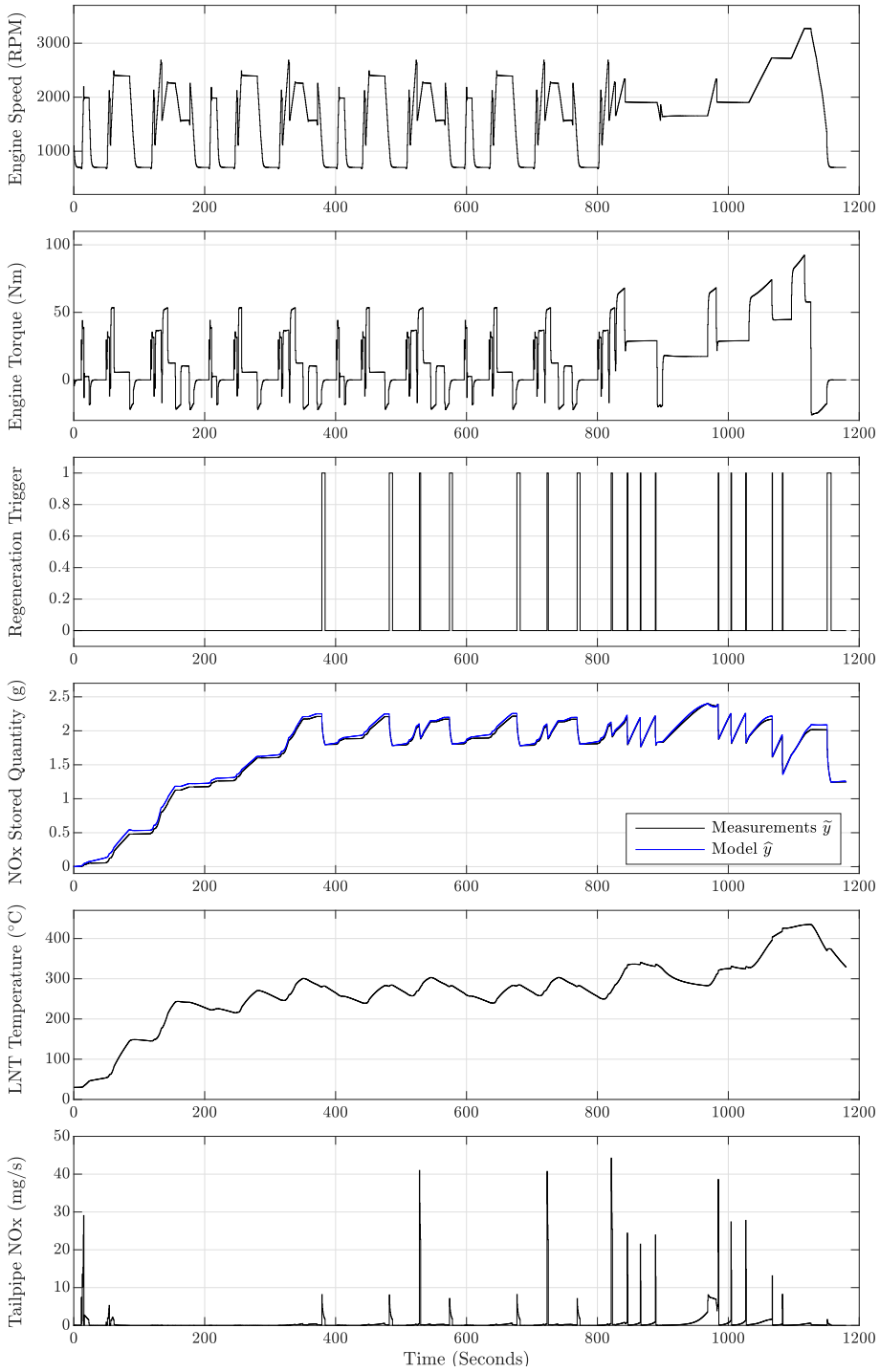

Figure 4.9: AMEsim/Matlab® simulation during the NEDC driving cycle (Fig 4.6) with D^{2}MPC controller.

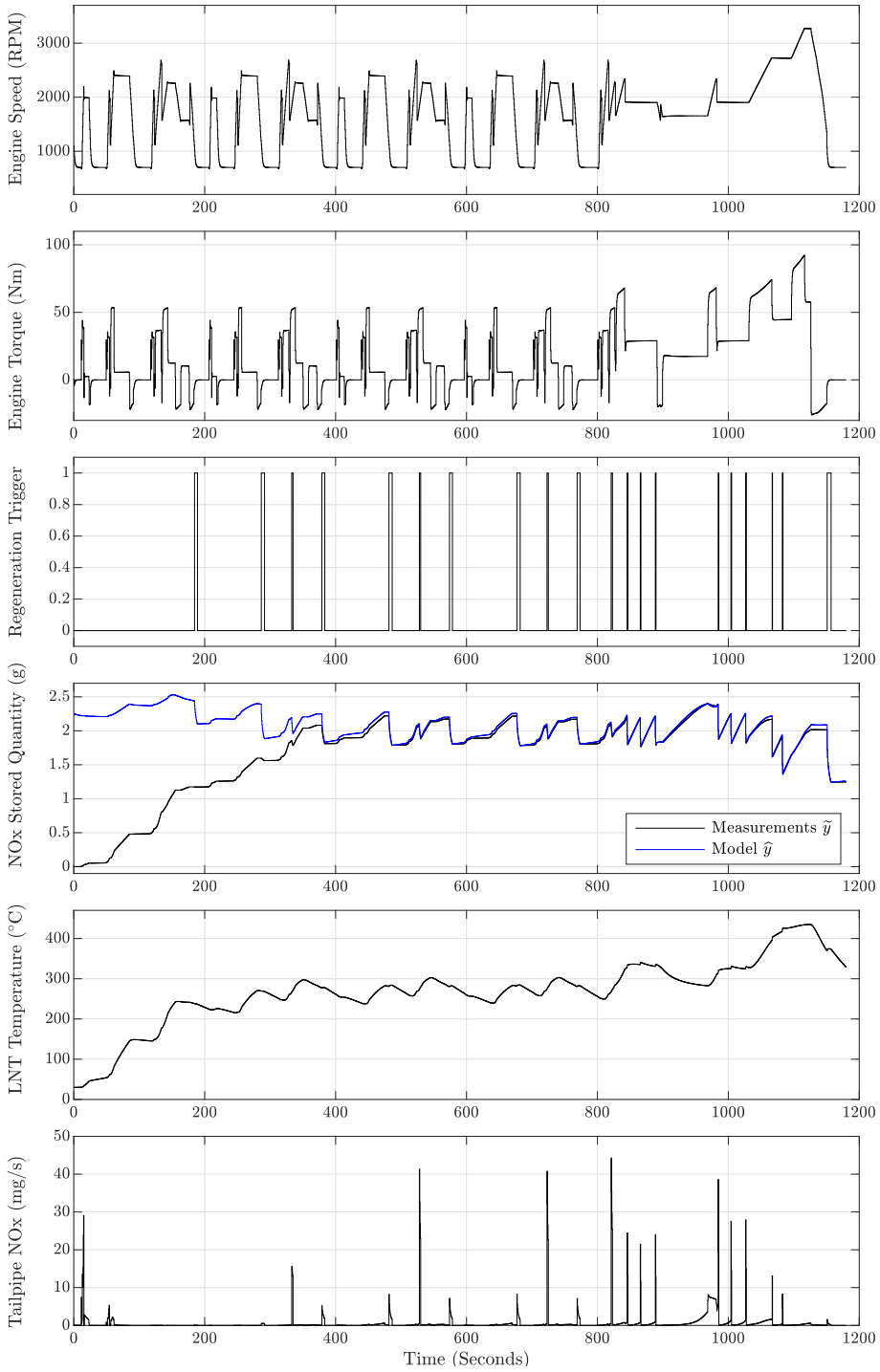

Figure 4.10: AMEsim/Matlab® simulation during the NEDC driving cycle (Fig 4.6) with D^{2}MPC controller starting from a wrong initial NO_x stored quantity.

a 10 second prediction horizon. The cost function is only the fuel penalty and a constraint on the cumulative NO_x emissions and LNT temperature is imposed.

- Controller 4: Simple threshold-based controller. In this strategy, the regeneration starts when the tailpipe NO_x and LNT temperature are higher than a threshold ($NOx \geq 10mg/s$, $T \geq 150°C$).

Figure 4.11 shows the performance of the D^{2}MPC controller compared with the Ideal MPC and also with the D^{2}MPC starting with a random initial state. It is evident that the performance of the Ideal MPC is very close to the D^{2}MPC.

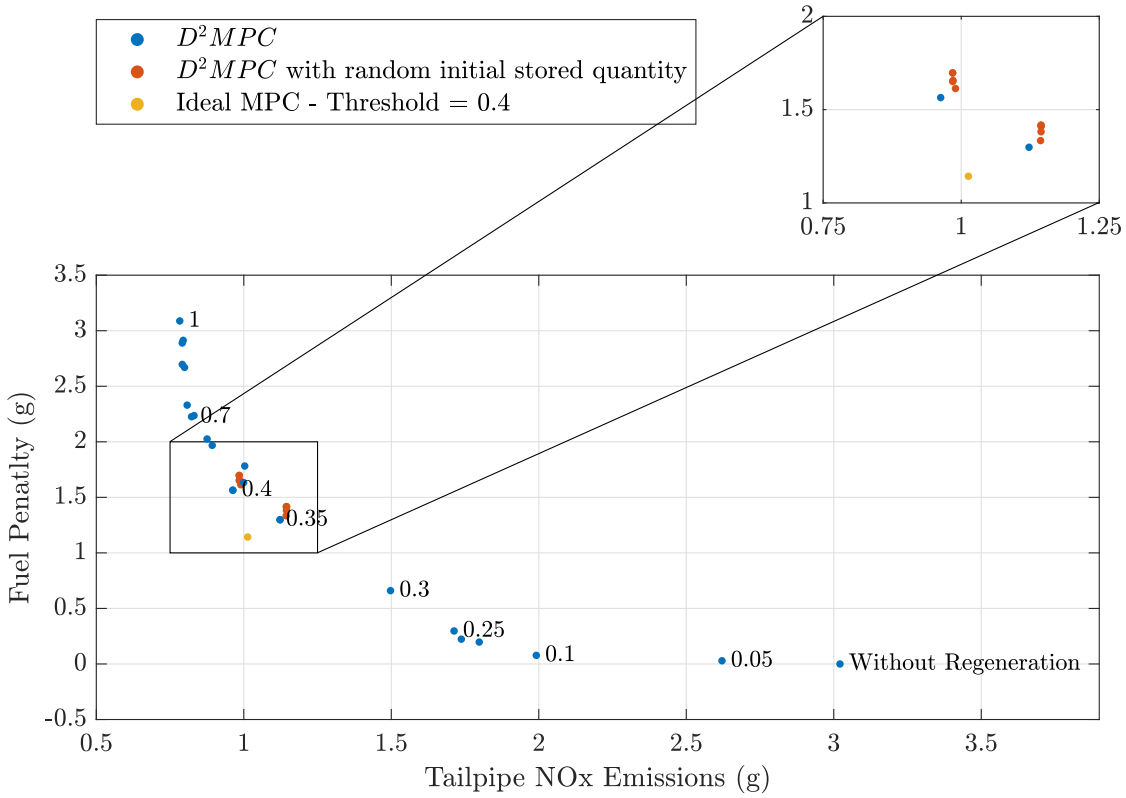

Figure 4.11: Comparison of the Ideal MPC performance with the proposed D^{2}MPC controller.

The results of Table 4.3, indicate that the first two controllers have an almost identical performance. A surprising result is given by Controller 3. Although the objective function consists only of the fuel penalty, this controller gives a higher

fuel consumption with respect to the proposed controllers. This result is due to the fact that the regeneration efficiency is not considered in the cost function and the regenerations continue until the amount of NO_x stored quantity reaches a minimum level, leading to longer regenerations.

Table 4.3: Fuel penalty and NO_x emissions for NEDC driving cycle with cold start.

Controller	Fuel Consumption (g)	Fuel Penalty (g)	Tailpipe NO_x Emissions (g)
Without controller	654.5	0	3.021
D^2-MPC	656.1	1.56	0.962
Ideal MPC	655.6	1.14	1.013
Controller 3	662.0	7.5	1.029
Controller 4	675.5	21	2.728

In summary, the proposed D^2-MPC strategy show very efficient regenerations with a minimum fuel penalty. In particular, the provided values for these two performance indexes are very close to those provided by the ideal strategy, based on the exact model. On the other hand, the other two strategies provide fairly efficient regenerations, at the expense of quite high fuel penalties. We can conclude that the proposed D^2-MPC strategy shows a great performance in terms of fuel consumption and NO_x emission reduction.

4.7 Conclusion

The increasing demand for higher torque, reduced fuel consumption and emissions has led to more complex engine and after-treatment designs with more actuators and sensors which are more difficult to model, calibrate, and control. Considering the expensive operating costs of the engine/after-treatment test benches, and increasing demand for accurate dynamic models, DoE plays a critical role in automotive applications. In this chapter a novel data-driven model predictive control (D^2-MPC) approach for regeneration timing of the LNT has been proposed, allowing to overcome several significant issues of "standard" techniques. In particular, the D^2-MPC approach does not require a physical model of the plant to control but is based on a neural network model, directly identified from experimental data generated by the Set Membership DoE algorithm. The regeneration timing is computed through suitable optimization algorithms, which use the identified models to predict the LNT behavior. In this way, all problems due to the fact that LNTs are

highly complex systems difficult to model are overcome. The D^2-MPC approach was tested in a co-simulation study, where the plant is represented by a detailed LNT model, developed using the well-known commercial tool AMEsim, and the controller is implemented in Matlab®/Simulink.

Chapter 5

Set Membership Fault Detection for Nonlinear Dynamic Systems

5.1 Introduction

In this chapter, an innovative approach to fault detection for nonlinear dynamic systems is proposed, based on the introduced quasi-local set membership identification method in Chapter 2, overcoming some relevant issues proper of the "classical" techniques. The approach is based on the direct identification from experimental data of a suitable filter and related uncertainty bounds. These bounds are used to detect when a change (e.g., a fault) has occurred in the dynamics of the system of interest. The main advantage of the approach compared to the existing methods is that it avoids the utilization of complex modeling and filter design procedures since the filter/observer is directly designed from data. Other advantages are that the approach does not require to choose any threshold (as typically done in many "classical" techniques) and it is not affected by under-modeling problems. An experimental study regarding fault detection for a drone actuator is finally presented to demonstrate the effectiveness of the proposed approach.

Consider a discrete-time nonlinear system in state-space form:

$$\begin{aligned} z^t &= f_o\left(z^{t-1}, u^{t-1}\right) + d^t \\ y^t &= z_i^t \end{aligned} \tag{5.1}$$

where $z^t \in \mathbb{R}^{n_z}$ is the state, $y^t \in \mathbb{R}$ is the output, z_i^t is a component of z^t, $u^t \in \mathbb{R}^{n_u}$ is the input, $d^t \in \mathbb{R}^{n_d}$ is a bounded disturbance and $t = 0,1,2,\ldots$ is the discrete time index. Assume that the input u^t and the state z^t are measured. Note that the assumption of measuring the state is not strictly necessary: the fault detection approach proposed in the following can be applied with minor modifications using an input-output system representation, see Remark 6 below.

A "classical" approach to fault detection is to identify a model of the system (5.1) and to design a filter/observer on the basis of the identified model. The designed filter/observer is then used to generate online a suitable residual signal. The fault is detected when the residual exceeds a given threshold, see e.g. [78, 53, 20, 55, 29, 15, 35, 63, 8, 54]. However, the design of the filter/observer may be hard in the presence of nonlinear and/or uncertain dynamics. Indeed, designing an optimal filter from a nonlinear model is in general not possible, and approximate filters only, such as the extended Kalman filters, can be actually obtained. These kinds of filters may often be inaccurate and not even guarantee the estimation error stability. Moreover, the choice of the threshold may be critical, especially when poor prior information on the system is available. Another relevant issue is that, in real-world applications, the system (5.1) is unknown and only approximate models can be identified from finite data; evaluating the effects of the modeling error on the estimation error of the filter designed from the approximated model is a largely open problem.

Set membership fault detection methods have been introduced to efficiently deal with modeling errors, [1, 56, 60, 3, 58, 69, 70]. These methods have been mainly developed for linear systems, while only a few of them deal with nonlinear systems, [58, 69, 70]. Typically, in set membership methods, a suitable estimation interval is computed online and the fault is detected when one or more measured variables fall outside this interval.

In this chapter, following this set membership philosophy, an innovative approach to fault detection is considered, allowing us to overcome the above issues. The main advantage of this approach compared to the existing methods ("classical" and set membership) is that it avoids the utilization of difficult filter design procedures since the filter/observer is directly designed from data. Other advantages with respect to the "classical" methods are that the approach does not require to choose any threshold and it is not affected by modeling errors since no model is used. A further interesting feature is that the approach is computationally simple, in both the design and implementation phases.

The method proposed in this chapter represents an improvement with respect to the one of [49]. Indeed, in [49], filter design is performed by means of the so-called local nonlinear set membership identification method, where the filter is obtained in the form of a linear combination of given basis functions. In this chapter, a so-called quasi-local method is presented, where no filter parametric form needs to be assumed. The filter is obtained directly from experimental data in a non-parametric closed form, thus not requiring the choice of a suitable set of basis functions. Such a quasi-local approach is similar to the so-called global approach of [39] but leads to the derivation of significantly less conservative uncertainty bounds.

The chapter is organized as follows. In section 5.2 the fault detection problem is formulated in the set membership framework and a summary of the fault detection procedure is given. In section 5.3, the method is tested on a drone propeller in a real experimental setting.

5.2 Nonlinear Set Membership Fault Detection

Suppose that the function f_o in (5.1) is not known but a set of noise corrupted data is available, given by

$$\mathcal{D} = \left\{\tilde{x}^t, \tilde{y}^t\right\}_{t=1}^{T} \tag{5.2}$$

where $\tilde{x}^t \doteq (\tilde{z}^{t-1}, \tilde{u}^{t-1})$. The proposed fault detection approach consists of the following main steps. First, a set membership filter for the system (5.1) is defined from the dataset (5.2) which gives us tight bounding functions $\overline{f}$ and $\underline{f}$, such that

$$\underline{f}\left(\tilde{x}^t\right) \leqslant f_{o,i}\left(\tilde{x}^t\right) \leqslant \overline{f}\left(\tilde{x}^t\right), \ \forall t.$$

Then, a fault detection system F is defined, on the basis of the bounding functions $\overline{f}$ and $\underline{f}$. The inputs of F is $\tilde{x}^t \doteq (\tilde{z}^{t-1}, \tilde{u}^{t-1})$, the outputs are the following:

$$\left.\begin{array}{l} \overline{y}^t \doteq \overline{f}\left(\tilde{x}^t\right) + \varepsilon^t \\ \underline{y}^t \doteq \underline{f}\left(\tilde{x}^t\right) - \varepsilon^t \end{array}\right\} \ k > L. \tag{5.3}$$

where ε^t is a bound on the noise d^t affecting the system. It is shown in Chapter 2 how to construct the functions $\overline{f}$ and $\underline{f}$ and to properly choose the involved parameters (e.g., ε^t). The rationale behind this fault detection scheme can be explained as follows.

Since $\tilde{y}^t = f_{o,i}\left(\tilde{x}^t\right) + d^t$, we have that $\tilde{y}^t \leqslant \overline{y}^t$, $\forall t$. Similarly, it holds that $\tilde{y}^t \geqslant \underline{y}^t$, $\forall t$. It follows that $\tilde{y}^t > \overline{y}^t$ or $\tilde{y}^t < \underline{y}^t$ only if the function f_o has changed, i.e. only if some structural change has occurred in the system (5.1). On the basis of this result, fault detection is performed by checking online if $\tilde{y}^t > \overline{y}^t$ or $\tilde{y}^t < \underline{y}^t$: a fault is detected as soon as one of these two inequalities is satisfied.

Remark 6. If the system state is not measured, the following input-output representation can be considered:

$$\begin{array}{l} y^t = f_o\left(x^t\right) + d^t \\ x^t = \left(y^{t-1}, \ldots, y^{t-n_y}, u^{t-1}, \ldots, u^{t-n_u}\right) \end{array} \tag{5.4}$$

where $y^t \in \mathbb{R}^{n_y}$ is the measured output, $u^t \in \mathbb{R}^{n_u}$ is the measured input and $d^t \in \mathbb{R}^{n_d}$ is an unknown bounded disturbance. Note that the function f_o in (5.4) is different from the one in (5.1). The proposed fault detection approach can be applied considering this representation without significant modifications.

Remark 7. The proposed fault detection approach can be applied to each state

component (or output component, in the case where the input-output representation (5.4) is used), in order to obtain a multi-dimensional fault detection system, allowing us to improve the detection performance with respect to a mono-dimensional case.

5.2.1 Set Membership Fault Detection Procedure

The main steps of the proposed Set Membership fault detection method are now summarized.

Offline operations

1. *Define the measurement dataset $\mathcal{D}$ according to (5.2).*
2. *Estimate the noise bound μ according to Algorithm 3.*
3. *In the case of the local approach, estimate a preliminary approximation f_* according to Algorithm 1 or 2.*
4. *Estimate the Lipschitz parameters according to Algorithm 4. In the case of the global approach, compute $\widehat{\Gamma}$; in the case of the quasi-local approach, compute $\widehat{\gamma}(x)$; in the case of the local approach $\widehat{\Gamma}_\Delta$.*

Online operations

1. *At each time step:*

$$\begin{array}{ll} \textit{If} & \tilde{y}^t > \overline{f}(\tilde{x}^t) + \varepsilon^t \quad \textit{or} \quad \tilde{y}^t < \underline{f}(\tilde{x}^t) - \varepsilon^t \\ \textit{Then} & \textit{Fault} = 1 \\ \textit{Else} & \textit{Fault} = 0 \end{array}$$

2. *In the case of the adaptive algorithm, update the set membership model according to Algorithm 5 if no fault has accrued in the system and the system is not recovering from a fault.*

Regarding the online operations, since the set membership model describes the normal dynamic behavior of the system, it has to be updated when no other

dynamics are involved. In other words, during a fault or immediately after a fault the measurements correspond to an abnormal behavior of the system and therefore they are not suitable for updating the model.

5.3 Example: Fault Detection for a Drone Actuator

In this example, the proposed fault detection algorithms were tested on a real drone actuator, in a laboratory experimental setup. The actuator is composed of three main components: a brushless DC motor, a driver and a propeller. The motor makes the propeller rotate and this rotation produces the required thrust and torque to drive a drone. The torque produced by the motor is given by

$$T = K_t(I - I_0) \tag{5.5}$$

where T is the motor torque, I is the input current, I_0 is the current when there is no load on the motor and K_t is the torque constant of the motor. The voltage across the motor is given by

$$V = R_m I + L_m \frac{\mathrm{d}I}{\mathrm{d}t} + K_e \omega \tag{5.6}$$

where V is the voltage drop across the motor, R_m and L_m are the motor resistance and inductance, respectively, and K_e is the motor speed constant. The motor is attached to a propeller, and therefore we have

$$T = B_m \omega + (J_m + Jp)\frac{\mathrm{d}\omega}{\mathrm{d}t} + T_D \tag{5.7}$$

where B_m is the motor friction, ω is the motor angular speed, J_m and J_p are the motor and propeller moments of inertia, respectively, and T_D is the propeller drag torque, given by

$$T_D = C_p \rho D^5 \omega^2 \tag{5.8}$$

where C_p is the propeller power coefficient, ρ is air density and D is the propeller diameter. The power coefficient C_p is a nonlinear function of the propeller speed, which is difficult to derive from the geometric shape of the propeller [11].

5.3.1 Experimental Setup

A brushless DC motor (RIMFIRE.10) attached to a propeller (APC 10x4.7p) is connected to a driver and a 200 watt power supply. The input command of the driver is a PWM signal with a duty cycle proportional to the voltage across the motor. An encoder is attached to the back of the motor, to measure the angular speed of the propeller. The input command signal and the encoder are connected to a PC running Matlab® through a National Instrument data acquisition device (PCI-6289). Data acquisition and online fault detection were carried out using the Simulink Desktop Real-Time. The drone actuator system is shown in Figure 5.1.

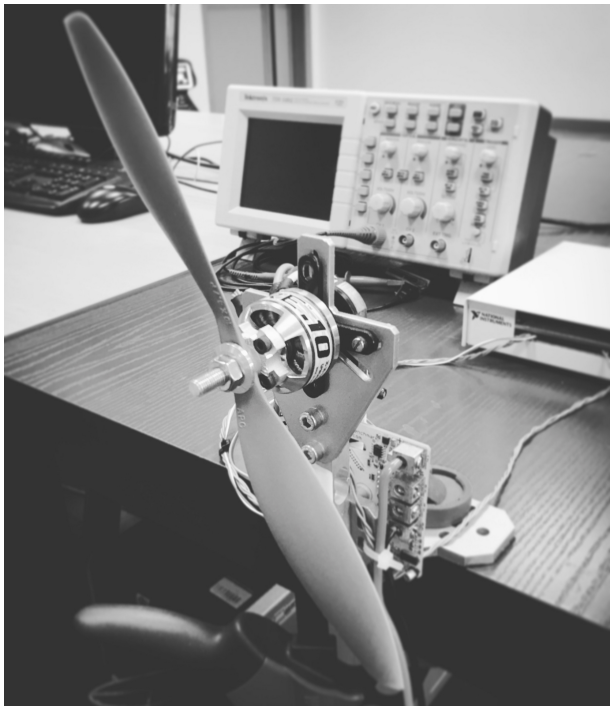

Figure 5.1: Drone Actuator.

5.3.2 Nonlinear Set Membership Fault Detection

In order to identify a model, an experiment was carried out, where an amplitude modulated pseudo random binary sequence (APRBS) command input with a duration of 100 seconds was applied to the actuator. From this experiment, a set of data was collected, using a sampling time of $T_s = 0.05s$. The dataset was divided into an identification set, composed by the first 1000 data and a validation

set, composed by the remaining 1000 data. See Figure 5.2(a). The measurement set was defined according to (5.2) as follows:

$$\begin{aligned} \mathcal{D} &= \left\{\widetilde{x}^t, \widetilde{y}^t\right\}_{t=4}^{1000} \\ \widetilde{x}^t &= [\widetilde{y}^{t-1} \quad \widetilde{y}^{t-2} \quad \widetilde{u}^{t-2} \quad \widetilde{u}^{t-3}] \end{aligned} \tag{5.9}$$

To evaluate the performance of the fault detection algorithm, a second experiment was carried out using another APRBS input command that was not used for identification nor validation. This second experiment had a duration of 30 seconds and during this experiment, in order to introduce a fault scenario, a sheet of paper was placed between the blades, approximately every 3 seconds, for a total of 8 times. In Figure 5.2(b), the fault occurrences are denoted by the circles. During this experiment, the following fault detection algorithms were running online.

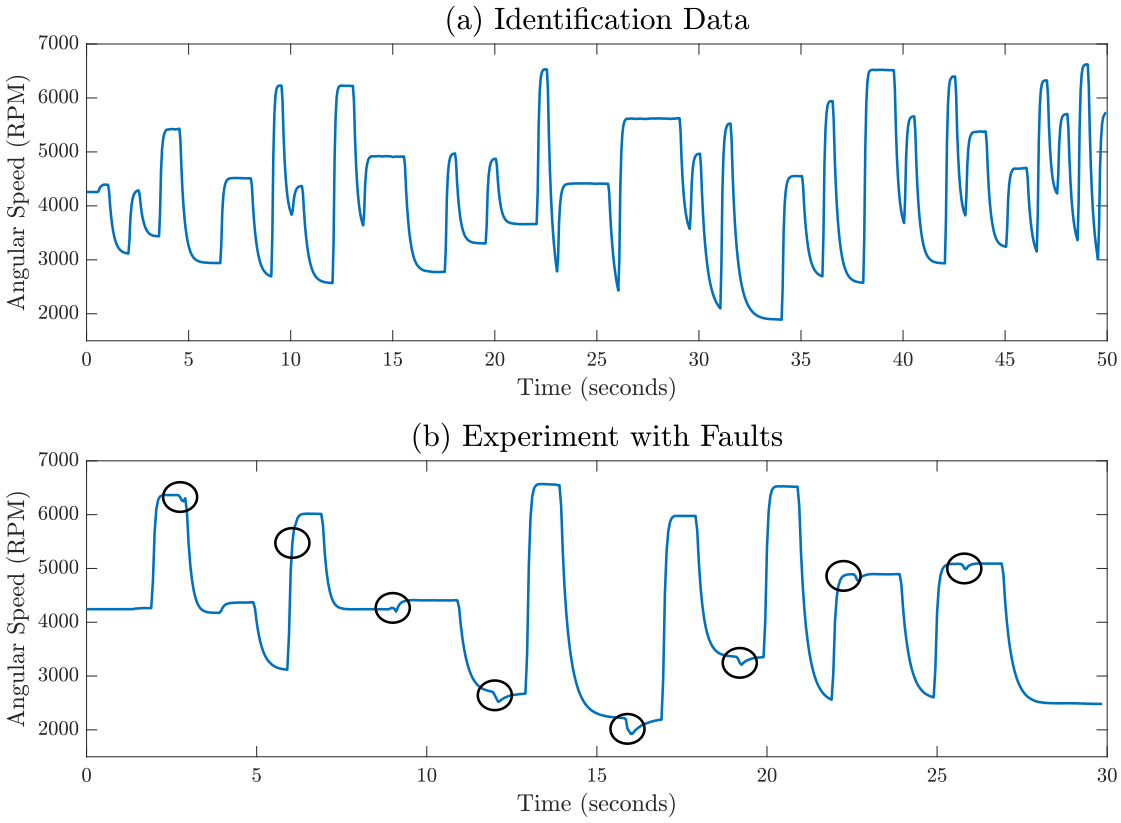

Figure 5.2: (a) First experiment used for identification, (b) second experiment online fault detection test (black circles are where the faults have occurred).

Global Approach

A nonlinear set membership model was obtained assuming a global constant bound on the function gradient according to section 2.3. A constant Lipschitz parameter $\Gamma = 0.7$ and a noise bound $\mu = 15$ were estimated according to Algorithms 3 and 4. The model was tested in simulation on the validation set and the root mean square simulation error (RMSE) was 42 RPM. Then, the fault detection algorithm was applied online, as discussed above. Figure 5.3 shows the model intervals and the bound violations. The model was able to detect seven out of eight faults.

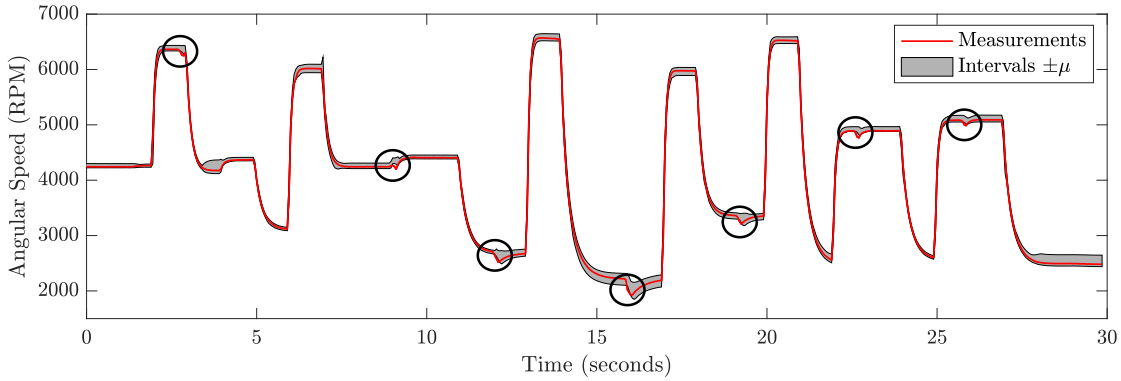

Figure 5.3: Global Approach; Black lines, $\overline{f} + \mu, \underline{f} - \mu$. Red line, $\widetilde{y}$. Circles, bound violation.

Quasi-Local Approach

A nonlinear set membership quasi-local model was obtained according to section 2.5. A quasi-local Lipschitz parameter γ was derived according to Algorithm 4. The model was tested in simulation on the validation set and the RMSE was 30 RPM. Then, the fault detection algorithm was applied online, as discussed above. Figure 5.4 shows the model intervals and the bound violations. The model was able to detect all the eight faults.

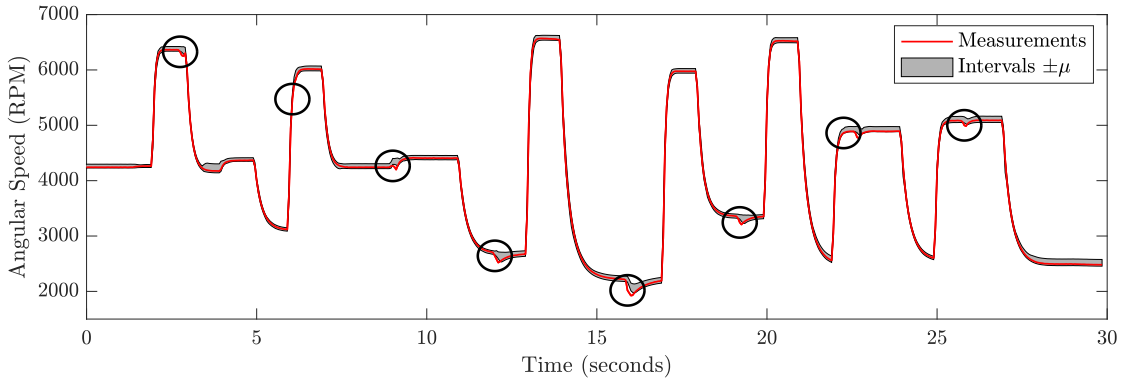

Figure 5.4: Quasi-Local Approach; Black lines, $\overline{f} + \mu, \underline{f} - \mu$. Red line, $\widetilde{y}$. Circles, bound violation.

Local Approach

A preliminary approximation f_* was derived according to Algorithm 1, using polynomial basis functions up to degree 5. No improvements were observed considering higher degrees. The number of basis functions in (2.29) is 81 where, due to ℓ_1 sparsification, only 33 have a non-null coefficient. The nonlinear set membership local model was obtained according to section 2.4. A Lipschitz parameter $\Gamma_\Delta = 0.2$ was derived according to Algorithm 4. The model was tested in simulation on the validation set and the RMSE was 23 RPM. Then, the fault detection algorithm was applied online, as discussed above. Figure 5.5 shows the model intervals and the bound violations. The model was able to detect all eight faults.

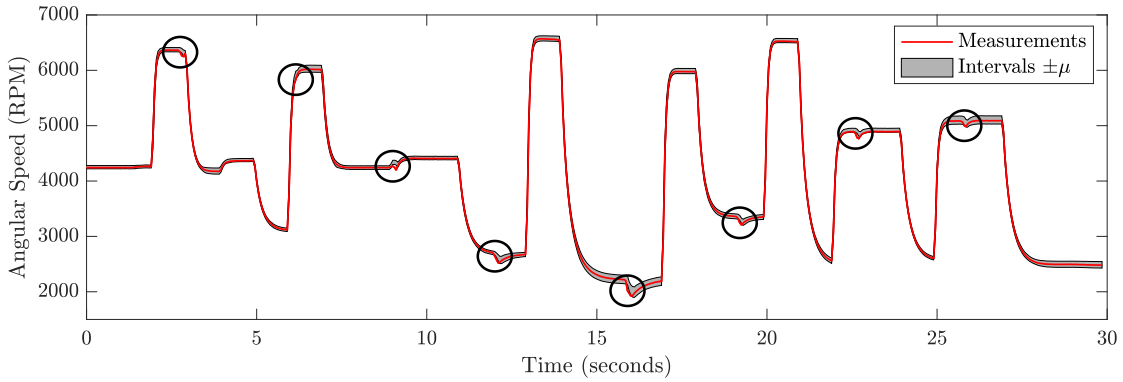

Figure 5.5: Local Approach; Black lines, $\overline{f} + \mu, \underline{f} - \mu$. Red line, $\widetilde{y}$. Circles, bound violation.

5.4 Conclusions

A novel fault detection approach, based on set membership interval estimates, has been presented, allowing us to overcome several problems of the standard techniques. Its effectiveness has been demonstrated in a laboratory study, related to fault detection for a real propeller.

Chapter 6

Discussion and Conclusions

The main goal of the current study was to develop a general systematic methodology for design of experiment for nonlinear systems that can be applied to a wide range of systems and applications.

The first main contribution of this thesis is the proposed quasi-local nonlinear set membership method. Even though nonlinear set membership is a quite powerful method, in some situations a global constant bound on the gradient of the function is too conservative, resulting in high uncertainty bounds. In the proposed quasi-local set membership approach, instead of a global constant bound on the gradient of the function, a quasi-local bound is assumed. Therefore, the uncertainty bounds are less conservative. Also unlike the local nonlinear set membership, this quasi-local approach does not require a preliminary estimate of the function.

The second main contribution of this thesis is a novel DoE algorithm for input-constrained MISO nonlinear systems. As discussed in Chapter 3, a key element to design a proper DoE algorithm is understanding which are the regions of the regressor space where the model is most uncertain. Set membership identification allows us to properly quantify the uncertainty of the identified model in a deterministic manner. Therefore, we formulated the DoE problem in a set membership framework using the proposed quasi-local nonlinear set membership approach. However, knowing where the model is most uncertain is not sufficient. Since the unknown system is dynamic, the DoE algorithm has to be able to generate an input sequence such that the system moves toward those uncertain regions of the regressor space, in order

to take new measurements. For this reason, we propose a novel adaptive Set Membership Predictive Control (SMPC) algorithm to move the system toward the most uncertain regions of the regressor space and take new informative measurements. Finally, a Set Membership DoE (SM-DoE) algorithm for input-constrained MISO nonlinear dynamic systems is proposed which is aimed to minimize the so-called radius of information, a quantity giving the worst-case model error. The proposed SM-DoE algorithm is able to guarantee any desired worst-case error larger than the measurement error in a finite-time experiment. Applications of the proposed method are clearly most useful in areas where experiments are expensive and/or a very accurate model is desired. Two numerical examples and a case study in the automotive field are also presented, showing the effectiveness of the approach and its potential in view of real-world applications.

The third main contribution of this thesis is an innovative approach to fault detection for nonlinear dynamic systems, based on the introduced quasi-local set membership identification method, overcoming some relevant issues proper of the "classical" techniques. The approach is based on the direct identification from experimental data of a suitable filter and related uncertainty bounds. These bounds are used to detect when a change (e.g., a fault) has occurred in the dynamics of the system of interest. The main advantage of the approach compared to the existing methods is that it avoids the utilization of complex modeling and filter design procedures since the filter/observer is directly designed from data. Other advantages are that the approach does not require to choose any threshold (as typically done in many "classical" techniques) and it is not affected by under-modeling problems. The set membership fault detection approach can also be made adaptive which is very useful in systems where the dynamics change over time.

As discussed in Chapter 4, the findings of this study have a number of practical applications. The increasing demand for higher torque, reduced fuel consumption, and emissions has led to more complex engine and after-treatment designs with more actuators and sensors which are more difficult to model, calibrate, and control. Considering the expensive operating costs of the engine/after-treatment test benches, and the increasing demand for accurate dynamic models, DoE plays a critical role in automotive applications.

The most important limitation of the set membership method, in general, is the need of storing the measurement dataset on the memory which could be problematic in systems with high dimension and/or size of the regressor space.

Also, the computation effort of the optimal bounds increases linearly by the size of the measurement dataset. Notwithstanding this limitation, as discussed in Chapter 2, the study suggests that the measurements to be stored only where the error is larger than a value which will result in a reduced size measurement dataset.

Regarding the proposed DoE algorithm, a difficult part is the computation of the set $\mathcal{S}$ which is required by the SMPC algorithm and makes it computationally expensive and hard to implement in fast dynamic systems. For this reason, in Chapter 4, a different cost function for the controller is used which is easy to compute but it doesn't have the theoretical guarantees of Chapter 3.

Despite the practical applications and limitations of the proposed approach that has been discussed so far, I believe this study lays the groundwork for future research on autonomous learning and data-driven control algorithms. There has been a lot of research focusing on learning algorithms from data, where, the data is provided by a user and the computer cannot experiment, collect data, and consequently learn by itself. Experiments are an inseparable part of the learning which us humans do all the time naturally. Imagine riding a bicycle, we instinctively experiment with the bicycle, fall down a couple of times and ultimately, create neural paths and muscle memory to control the bicycle. Now imagine a future that robots need to interact with the environment and perform some control tasks where modeling and designing a controller is not possible by a human user and the robot has to make sense of the environment by itself not only by detecting objects but also by modeling and controlling them autonomously. The robot could run experiments on the system, model, and then create a data-driven controller. The fault detection algorithm can also be integrated into the experiment algorithm or used separately in order to have an understanding of the normal behavior of a system.

Bibliography

[1] Joaquim Armengol et al. “A survey on interval model simulators and their properties related to fault detection.” In: *Annual Reviews in Control* 24 (2000), pp. 31–39.

[2] Andrew R Barron. “Universal approximation bounds for superpositions of a sigmoidal function”. In: *IEEE Transactions on Information theory* 39.3 (1993), pp. 930–945.

[3] Joaquim Blesa, Vicenç Puig, and Jordi Saludes. “Identification for passive robust fault detection using zonotope-based set-membership approaches”. In: *International Journal of Adaptive Control and Signal Processing* 25.9 (2011), pp. 788–812.

[4] Massimo Canale, Lorenzo Fagiano, and Maria Carmela Signorile. “Design of robust predictive control laws using set membership identified models”. In: *Asian Journal of Control* 15.6 (2013), pp. 1714–1722.

[5] Massimo Canale, Lorenzo Fagiano, and Maria Carmela Signorile. “Nonlinear model predictive control from data: a set membership approach”. In: *International Journal of Robust and Nonlinear Control* 24.1 (2014), pp. 123–139.

[6] M. Canova et al. “Control-Oriented Modeling of NO_x Aftertreatment Systems”. In: *SAE Transactions* 116 (2007), pp. 1640–1647.

[7] Jie Chen and Guoxiang Gu. *Control-Oriented System Identification: An H_∞ Approach*. New York: John Wiley & Sons, 2000. ISBN: 978-0471320487.

[8] Jie Chen and Ron J Patton. *Robust model-based fault diagnosis for dynamic systems*. Vol. 3. Springer Science & Business Media New York, 2012. ISBN: 978-1-4615-5149-2.

[9] Michael Deflorian, Florian Klöpper, and Joachim Rückert. “Online dynamic black box modelling and adaptive experiment design in combustion engine calibration”. In: *IFAC Proceedings Volumes* 43.7 (2010), pp. 703–708.

[10] Michael Deflorian and Susanne Zaglauer. “Design of experiments for nonlinear dynamic system identification”. In: *IFAC Proceedings Volumes* 44.1 (2011), pp. 13179–13184.

[11] Robert Deters and Michael Selig. “Static testing of micro propellers”. In: *26th AIAA applied aerodynamics conference*. 2008, p. 6246.

[12] David L Donoho, Michael Elad, and Vladimir N Temlyakov. “Stable recovery of sparse overcomplete representations in the presence of noise”. In: *IEEE Transactions on information theory* 52.1 (2006), pp. 6–18.

[13] Lorenzo Fagiano and Carlo Novara. “Learning a nonlinear controller from data: theory, computation and experimental results”. In: *IEEE Transactions on Automatic Control* 61.7 (2016), pp. 1854–1868.

[14] Valerii Vadimovich Fedorov. *Theory of optimal experiments*. Elsevier, 2013.

[15] R.M.G. Ferrari, T. Parisini, and M. M. Polycarpou. “Distributed Fault Detection and Isolation of Large-Scale Discrete-Time Nonlinear Systems: An Adaptive Approximation Approach”. In: *IEEE Transactions on Automatic Control* 57.2 (2012), pp. 275–290.

[16] Simone Formentin et al. “Active Braking Control System Design: The D ^{2}-IBC Approach”. In: *IEEE/ASME Transactions on Mechatronics* 20.4 (2015), pp. 1573–1584.

[17] Urban Forssell and Lennart Ljung. “Some results on optimal experiment design”. In: *Automatica* 36.5 (2000), pp. 749–756.

[18] Jean-Jacques Fuchs. “Recovery of exact sparse representations in the presence of bounded noise”. In: *IEEE Transactions on Information Theory* 51.10 (2005), pp. 3601–3608.

[19] Zhiming Gao et al. “Lean NO_x trap modeling for vehicle systems simulations”. In: *SAE International Journal of Fuels and Lubricants* 3.2010-01-0882 (2010), pp. 468–485.

[20] J Gertler Janos. *Fault Detection and Diagnosis in Engineering Systems*. New York: Marcel Dekker, 1998.

[21] ST Glad and Lennart Ljung. “Model structure identifiability and persistence of excitation”. In: *29th IEEE Conference on Decision and Control*. IEEE. 1990, pp. 3236–3240.

[22] Graham Clifford Goodwin and Robert L Payne. *Dynamic system identification: experiment design and data analysis*. Vol. 136. Academic press New York, 1977.

[23] Dimitry Gorinevsky. "On the persistency of excitation in radial basis function network identification of nonlinear systems". In: *IEEE Transactions on Neural Networks* 6.5 (1995), pp. 1237–1244.

[24] Matthias Gringard and Andreas Kroll. "On the parametrization of APRBS and multisine test signals for the identification of nonlinear dynamic TS-models". In: 2016, pp. 1–8.

[25] Håkan Hjalmarsson. "From experiment design to closed-loop control". In: *Automatica* 41.3 (2005), pp. 393–438.

[26] Kurt Hornik et al. "Degree of approximation results for feedforward networks approximating unknown mappings and their derivatives". In: *Neural Computation* 6.6 (1994), pp. 1262–1275.

[27] Ming-Feng Hsieh, Junmin Wang, and Marcello Canova. "Two-level nonlinear model predictive control for lean NO_x trap regenerations". In: *Journal of dynamic systems, measurement, and control* 132.4 (2010), p. 041001.

[28] Kenneth Hsu et al. "Parametric and nonparametric curve fitting". In: *Automatica* 42.11 (2006), pp. 1869–1873.

[29] Rolf Isermann. *Fault-Diagnosis Systems: An Introduction from Fault Detection to Fault Tolerance*. Berlin, Germany: Springer, 2006.

[30] Timothy V Johnson. "Review of vehicular emissions trends". In: *SAE International Journal of Engines* 8.2015-01-0993 (2015), pp. 1152–1167.

[31] Ahmed Ketfi-Cherif et al. *Modeling and control of a NO_x trap catalyst*. Tech. rep. SAE Technical Paper, 2000.

[32] Yong-Wha Kim et al. *A phenomenological control oriented lean NO_x trap model*. Tech. rep. SAE Technical Paper, 2003.

[33] Christian A Larsson et al. "Model predictive control with integrated experiment design for output error systems". In: *2013 European Control Conference (ECC)*. IEEE. 2013, pp. 3790–3795.

[34] Anna Lindholm et al. "Detailed kinetic modeling of NO_x storage and reduction with hydrogen as the reducing agent and in the presence of CO_2 and H_2O over a Pt/Ba/Al catalyst". In: *Journal of catalysis* 258.1 (2008), pp. 273–288.

[35] Binfan Liu and Jennie Si. "Fault isolation filter design for linear time-invariant systems". In: *IEEE Transactions on Automatic Control* 42 (1997), pp. 704–707.

[36] Lennart Ljung. *System Identification: Theory for the User*. Upper Saddle River, NJ, USA: Prentice-Hall, Inc., 1986. ISBN: 0-138-81640-9.

[37] *LMS Imagine.Lab Amesim IFP Drive Library 15 User's Guide*. English. Version 15. siemens. 2016. 72 pp.

[38] Mario Milanese and Carlo Novara. "Computation of local radius of information in SM-IBC identification of nonlinear systems". In: *Journal of Complexity* 23 (2007), pp. 937–951. DOI: 10.1016/j.jco.2007.05.004.

[39] Mario Milanese and Carlo Novara. "Set membership identification of nonlinear systems". In: *Automatica* 40.6 (2004), pp. 957–975.

[40] Mario Milanese and Carlo Novara. "Set Membership Prediction of Nonlinear Time Series". In: *IEEE Transactions on Automatic Control* 50.11 (2005), pp. 1655–1669. DOI: 10.1109/TAC.2005.858693.

[41] Mario Milanese and Carlo Novara. "Unified Set Membership theory for identification, prediction and filtering of nonlinear systems". In: *Automatica* 47.10 (2011), pp. 2141–2151.

[42] Mario Milanese and Michele Taragna. "H_∞ set membership identification: A survey". In: *Automatica* 41 (2005), pp. 2019–2032.

[43] Mario Milanese and Antonio Vicino. "Optimal algorithms estimation theory for dynamic systems with set membership uncertainty: an overview". In: *Automatica* 27 (1991), pp. 997–1009.

[44] Mario Milanese et al. *Bounding Approaches to System Identification*. Plenum Press, New York, 1996.

[45] Shinji Nakagawa, Toshio Hori, and Masami Nagano. *A new feedback control of a lean NO_x trap catalyst*. Tech. rep. SAE Technical Paper, 2004.

[46] C. Novara. "Sparse identification of nonlinear functions and parametric Set Membership optimality analysis". In: *American Control Conference*. San Francisco, USA, 2011.

[47] Carlo Novara. "Experiment design in nonlinear set membership identification". In: *American Control Conference*. IEEE. 2007, pp. 1566–1571.

[48] Carlo Novara. "Polynomial model inversion control: numerical tests and applications". In: *arXiv* 1509.01421 (2015).

[49] Carlo Novara. "Sparse set membership identification of nonlinear functions and application to fault detection". In: *International Journal of Adaptive Control and Signal Processing* 30.2 (2016), pp. 206–223.

[50] Carlo Novara et al. "Data-driven design of two degree-of-freedom nonlinear controllers: The D ^{2}-IBC Approach". In: *Automatica* 72 (2016), pp. 19–27.

[51] Carlo Novara et al. "Parametric identification of structured nonlinear systems". In: *Automatica* 47.4 (2011), pp. 711–721.

[52] Carlo Novara et al. "Set Membership inversion and robust control from data of nonlinear systems". In: *International Journal of Robust and Nonlinear Control* 24.18 (2014), pp. 3170–3195. DOI: 10.1002/rnc.3048.

[53] Ron J. Patton, Paul M. Frank, and Robert N. Clarke, eds. *Fault Diagnosis in Dynamic Systems: Theory and Application*. Upper Saddle River, NJ, USA: Prentice-Hall, Inc., 1989. ISBN: 0-13-308263-6.

[54] Ron J Patton, Paul M Frank, and Robert N Clark. *Issues of fault diagnosis for dynamic systems*. Springer-Verlag London, 2000.

[55] C. D. Persis and A. Isidori. "A geometric approach to nonlinear fault detection and isolation". In: *IEEE Transactions on Automatic Control* 46.6 (2001), pp. 853–865.

[56] V. Puig et al. "Passive Robust Fault Detection of Dynamic Processes Using Interval Models". In: *IEEE Transactions on Control Systems Technology* 16.5 (2008), pp. 1083–1089.

[57] Zhihua Qu. *Robust Control of Nonlinear Uncertain Systems*. 1st. New York, NY, USA: John Wiley & Sons, Inc., 1998. ISBN: 0471115894.

[58] T. Raissi, G. Videau, and A. Zolghadri. "Interval observer design for consistency checks of nonlinear continuous-time systems". In: *Automatica* 46.3 (2010), pp. 518–527.

[59] Freeman Randy and Kokotovic Petar V. *Robust Nonlinear Control Design*. Boston: Birkhäuser Basel, 1996.

[60] V. Reppa and A. Tzes. "Fault detection and diagnosis based on parameter set estimation". In: *IET Control Theory and Applications* 5.1 (2010), pp. 69–83.

[61] Cristian R Rojas, James S Welsh, and Graham C Goodwin. "A receding horizon algorithm to generate binary signals with a prescribed autocovariance". In: *2007 American Control Conference*. IEEE. 2007, pp. 122–127.

[62] Maria Carmela Signorile. "Robust control of nonlinear systems from data". PhD thesis. Politecnico di Torino, 2012.

[63] Silvio Simani, Cesare Fantuzzi, and Ron J. Patton. "Model-based fault diagnosis in dynamic systems using identificationtechniques". In: (2003).

[64] Timothy W Simpson, Dennis KJ Lin, and Wei Chen. "Sampling strategies for computer experiments: design and analysis". In: *International Journal of Reliability and Applications* 2.3 (2001), pp. 209–240.

[65] Jonas Sjöberg et al. “Nonlinear Black-box Modeling in System Identification: a Unified Overview”. In: *Automatica* 31 (1995), pp. 1691–1723.

[66] Peter Stoica and T Soderstrom. “A useful input parameterization for optimal experiment design”. In: *IEEE Transactions on Automatic Control* 27.4 (1982), pp. 986–989.

[67] Marko V Tanaskovic. “Application of Set Membership Identification to Controller Design”. PhD thesis. ETH Zurich, 2015.

[68] Marko Tanaskovic, Lorenzo Fagiano, and Manfred Morari. “Worst-case experiment design for constrained MISO systems”. In: *53rd IEEE Conference on Decision and Control*. IEEE. 2014, pp. 999–1004.

[69] S. Tornil-Sin et al. “Robust fault detection of non-linear systems using set-membership state estimation based on constraint satisfaction”. In: *Engineering Applications of Artificial Intelligence* 25.1 (2012), pp. 1–10.

[70] S. Tornil-Sin et al. “Robust Fault Diagnosis of Non Linear Systems Using Interval Constraint Satisfaction and Analytical Redundancy Relations”. In: *IEEE Transactions on Systems, Man, and Cybernetics: Systems* 44.1 (2014), pp. 18–29.

[71] J. F. Traub, G. W. Wasilkowski, and H. Woźniakowski. *Information-based Complexity*. San Diego, CA, USA: Academic Press Professional, Inc., 1988. ISBN: 0-12-697545-0.

[72] J.A. Tropp. “Just relax: convex programming methods for identifying sparse signals in noise”. In: *IEEE Transactions on Information Theory* 52.3 (Mar. 2006), pp. 1030–1051. ISSN: 0018-9448. DOI: 10.1109/TIT.2005.864420.

[73] Michiel Van Nieuwstadt and O Yanakiev. *A diesel lean NO_x trap model for control strategy verification*. Tech. rep. SAE Technical Paper, 2004.

[74] Yanying Wang, Shankar Raman, and Jessy W Grizzle. “Dynamic modeling of a lean NO_x trap for lean burn engine control”. In: *American Control Conference, 1999. Proceedings of the 1999*. Vol. 2. IEEE. 1999, pp. 1208–1212.

[75] Hanlong Yang. *LNT NO_x Storage Modeling and Estimation via NARX*. Tech. rep. SAE Technical Paper, 2010.

[76] Susanne Zaglauer. “Bayesian design of experiments for nonlinear dynamic system identification”. In: *Proceedings of the 5th International ICST Conference on Simulation Tools and Techniques*. ICST (Institute for Computer Sciences, Social-Informatics and ... 2012, pp. 85–92.

[77] Martin B Zarrop. *Optimal experiment design for dynamic system identification*. Vol. 21. Springer, 1979.

[78] X. Zhang, M.M. Polycarpou, and T. Parisini. "A robust detection and isolation scheme for abrupt and incipient faults in nonlinear systems". In: *IEEE Transactions on Automatic Control* 47.4 (2002), pp. 576–593.